71-12,157

HUANG, Frank Tsung-chien, 1941-
IONOSPHERIC PARAMETERS DEDUCED FROM
LANGMUIR PROBE MEASUREMENTS.

University of Maryland, Ph.D., 1970
Aerospace Studies

University Microfilms, A XEROX Company, Ann Arbor, Michigan

IONOSPHERIC PARAMETERS DEDUCED FROM LANGMUIR PROBE MEASUREMENTS

by

Frank Tsung-chien Huang

June 1970

Dissertation submitted to the Faculty of the
Graduate School of the University
of Maryland in partial fulfillment of
the requirements for the degree of
Doctor of Philosophy
1970

copy 1

APPROVAL SHEET

Title of Thesis: Ionospheric Parameters Deduced from Langmuir Probe Measurements

Name of Candidate: Frank Tsung-chien Huang
Doctor of Philosophy, 1970

Thesis and Abstract Approved:

Richard T. Bettinger
Assistant Professor of Physics
Department of Physics and Astronomy

Date Approved: June 25, 1970

ABSTRACT

Title of Thesis: Ionospheric Parameters Deduced from Langmuir
Probe Measurements

Frank Tsung-chien Huang, Doctor of Philosophy, 1970

Thesis directed by: R. T. Bettinger, Assistant Professor of Physics

We have obtained charged particle densities and temperatures in the "normal" daytime ionosphere above Wallops Island, Virginia. These are the results of two rocket-borne spherical Langmuir probe experiments conducted in the altitude range of 100 to 240 kilometers.

The flights were contrasted mainly by different probe sizes to investigate the behavior of plasma sheaths. We have also incorporated the effects of contact potential variation (patch effect) over the probe surface, probe velocity, and vehicle potential in our interpretation of the data. Reasonable ion temperatures are obtained only if the above effects are considered. Our analysis also show that if the patch effect is neglected, the electron density and temperature would be overestimated, although this error is small in the latter case.

We have found that electron densities range from approximately $.8 \times 10^5$/cc. to 4.0×10^5/cc. The electron temperature vary from 700 to 2000 degrees Kelvin while the ion temperature lie in the interval between 400 and 700 degrees Kelvin.

ACKNOWLEDGEMENTS

I would like to express my deep and sincere gratitude to my advisor, Dr. Richard T. Bettinger, not only for the invaluable guidance, ideas, and advice he has given me throughout these years, but also for the design and development of this experiment.

Thanks is due also to Dean Jordan, Elwood Barnes, Milton Grimsley, and George Tilton for their roles in the construction and testing of the payload. My appreciation is also extended to my collegue, Jerome Bohse, and my brother, Philip, for their enlightening and helpful suggestions and to Dave Nelson for supplying me with the portion of the computer program which read the data.

Finally, by chronological order, I thank Mrs. Janis Kinsman whose efficiency and patience in typing and organization have facilitated matters to a high degree.

This project was supported by the National Aeronautics and Space Administration Grant NGR 21-002-057. The computer time for this project was supported by National Aeronuatics and Space Administration Grant NsG-398 to the Computer Science Center of the University of Maryland.

TABLE OF CONTENTS

TABLE OF CONTENTS (Continued)

LIST OF FIGURES

LIST OF FIGURES (Continued)

LIST OF TABLES

CHAPTER I

The Ionosphere

A. Introduction

The ionosphere is that part of the earth's upper atmosphere which extends from approximately 60 kilometers up to the magnetospheric boundary (magnetopause). The base of the ionosphere may be marked as that region where the atoms and molecules have become sufficiently ionized to affect radio wave propagation while the upper boundary, the magnetopause, is the transition region where dominance of particle motions shifts from the geomagnetic field to the solar wind. In the sunside of the earth, the magnetosphere boundary occurs at roughly ten earth radii. It has not been ascertained as to exactly how far the magnetosphere extends in the dark side, although it is surmised that this may be at least several hundred earth radii.

The source of ionization is solar electro-magnetic radiation and cosmic rays, the latter having the most relative influence in the lower ionosphere, at night and at high latitudes. In particular, we are concerned with measurements of mid-latitude, daytime, ion and electron densities and temperatures in the range of 100 to 240 km.

The amount of ionization which occurs is determined by the balance of production and loss rates per unit volume. In our region of interest the dominant means of producing ions and electrons are direct photoionization and charge interchange between neutrals and ions. These may be symbolically represented as

$$X + h\nu \rightarrow X^+ + e \tag{1.1}$$

and

$$X^+ + YZ \rightarrow XY^+ + Z \tag{1.2}$$

respectively, where e denotes an electron; X, Y, and Z are neutral atoms or molecules; the superscript + denotes singly ionized states; and hν stands for the ionizing radiation. The processes mainly responsible for loss of ionization in the altitude range of our measurements are ion-atom interchange followed by dissociative recombination:

$$\begin{aligned} X^+ + YZ &\rightarrow XY^+ + Z \\ XY^+ + e &\rightarrow X^* + Y^* \end{aligned} \tag{1.3}$$

with the asterik denoting possible excited states. There are other competing processes such as radiative recombination, three body recombination and loss by transport, but these are important only at other altitude ranges. Specifically, the major neutral constituents in our region of interest are oxygen (O), nitrogen (N_2), and diatomic oxygen (O_2), while the main ions are O^+, NO^+, and O_2^+. It is supposed that N_2^+ ions are neutralized quickly enough so that its density is relatively small, and NO^+ and perhaps O_2^+ result primarily from charge transfer (Equation 1.2). The photoionization process is performed by wavelengths less than 1027 Angstroms, which include the extreme ultraviolet radiation and x-rays, among which portions of the continuum and several line radiation are most important.

As the radiation penetrates into the ionosphere, it becomes attenuated with decreasing altitude. On the other hand, the amount of ionizable material increases with decreasing altitude. For a given wavelength and netural species, these offsetting processes will produce a maximum of ionization rate (per unit volume) at some height. Although the loss rate is also height dependent and adds to the complexity, there will still be at least one maximum in the charged density profile. In addition, because of diffussive separation of the neutral particles (above 100 km), different wavelengths will be absorbed with varying proportions as a function of altitude. This contributes to a series of "layers" of charge density, and was first explained by Chapman. Measurements have shown that there actually exists five main layers and are symbolized by the C,D,E, F1 and F2 regions. In Figure 1.1 we have a sketch of the gross features of the ionized regions (the C layer, which lies just beneath the D layer, is not shown), and we see that our measurements, which are from 100 to 240 km, extend from the base of the E layer into the F1 region.

In regard to electron temperature, the energy source is attributed to relatively energetic (compared to the ambient) electrons. Exactly how this "high energy tail" is formed is open to conjecture. Nevertheless, these electrons lose their energy to ambient ions and electrons via the coulomb interaction and to neutrals by elastic and/or inelastic collisions. This process is inefficient enough so that there is a temperature differential between electrons and neutrals in the manner shown in Figure (1.2). Up to roughly 250 km, the thermal contact between ions and neutrals is good enough so that their temperatures are nearly equal as are the temperatures of the different ions. As the altitude is increased, the ion-neutral thermal contact becomes less effective while the ion-electron contact becomes more so, and it is expected that at great heights the ion and electron temperatures approach one another. In Figure (1.2) we have reproduced Delgarno's[1]

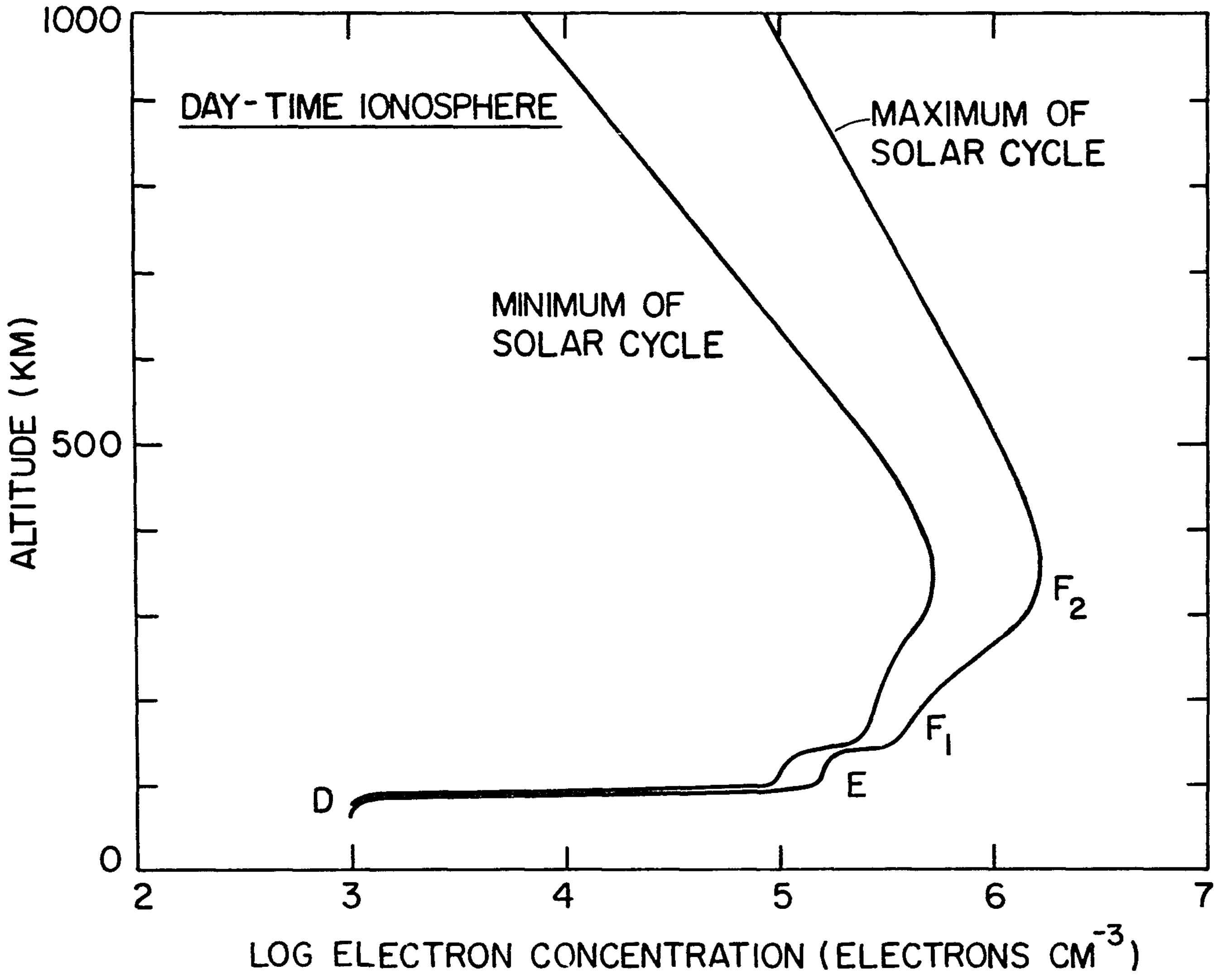

DAY-TIME IONOSPHERE
MINIMUM OF SOLAR CYCLE
MAXIMUM OF SOLAR CYCLE
D
E
F_1
F_2
1000
500
0
ALTITUDE (KM)
2
3
4
5
6
7
LOG ELECTRON CONCENTRATION (ELECTRONS CM^{-3})

Fig. 1.1

results, where he has compared his calculations with measurements of ion and electron temperatures made by Evans[2].

A knowledge of densities and temperatures ultimately reflect on the physical processes involved. There are, as yet, multiple problems confronting attempts to explain much of ionospheric phenomena. A need for better knowledge of reaction rates and cross-sections and mathematical difficulties have inhibited progress toweard a more complete understanding. In addition, solar, diurnal and seasonal variations, plus various anomolies have in many respects rendered some investigations somewhat phenomenological in nature. Surveys of the various a aspects of ionospheric studies along with references may be found in some recent texts[3,4,5].

B. Ionospheric Measurements

The measurement of ionospheric parameters using rockets, satellites and ground based sounders have provided an appreciable amount of data especially in the last decade. A variety of probes, analyzers, spectrometers, and propagation equipment have provided data on both neutrals and charged particles, which at times give overlapping information. This is not considered redundant, but rather points to the need for cross checking various measurements.

Electrostatic, or Langmuir probes had already been used in laboratory experiments for several decades before their use in the ionosphere. The interpretation of data is based on Mott-Smith and Langmuir's theory[6], first set down in 1926. Although some refinements have been included since then, there remain complications in data analysis, and we will consider these in the following chapters. First, we will describe the experiment, which was originated by Bettinger[7].

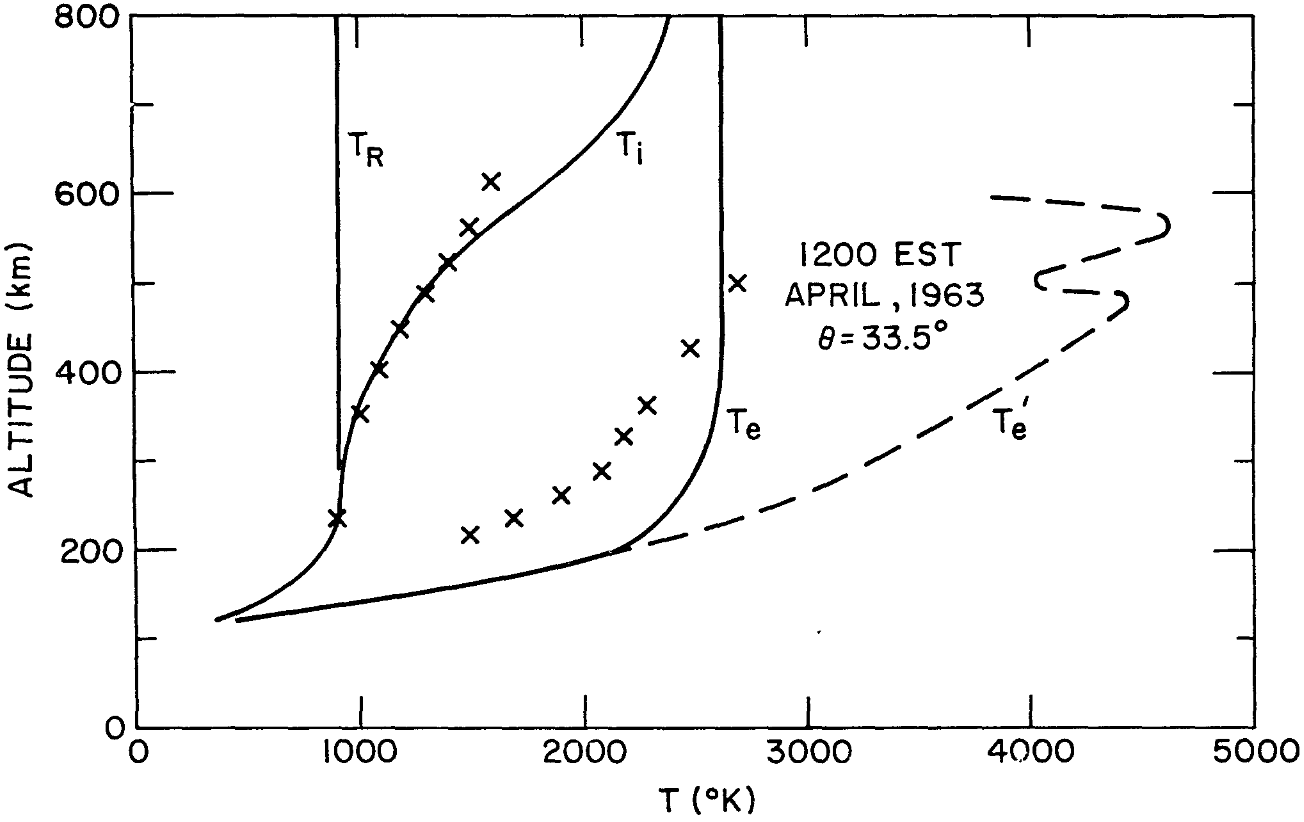

Fig. 1.2 PROFILES OF ELECTRON, ION AND NEUTRAL TEMP. (T_n) T_e' is the theoretical electron temperature with thermal conduction ignored. T_e is the temperature when conduction is considered and T_i is the ion temperature. The measured electron and ion temperatures (Evans, reference 2) are indicated by X. [After reference 1]

CHAPTER II

The Experiment

A. Purpose and Introduction

The idea behind the use of Langmuir probes for measuring the parameters of charged particles in a plasma is to immerse a collector (conducting surface) in the plasma and monitor the current collected by the conductor, or probe. Mott-Smith and Langmuir[6] were first to derive the expressions for this current as a function of the probe to plasma potential: i.e., the volt-ampere characteristics. These expressions, which also contains the charged particle temperatures and densities, are then used in conjunction with experimental data to obtain plasma parameters.

The situation which arises when a body is at some potential difference from that of the plasma is to cause the plasma to react in such a manner so that the field due to the collector is shielded from the rest of the plasma. This is accomplished by a build-up of space charge, or sheath, in the neighborhood of the probe. Langmuir's theory was formulated by using the approximation that the sheath has a well defined boundary or edge. That is, although the potential only approaches the plasma potential asymptotically it is assumed that there is a definite point where the plasma potential is reached and that the velocity distribution and the density at this point-- the sheath edge-- has the values of the neutral undisturbed plasma. In addition, if collisions are negligible inside the sheath, then one can calculate which particle trajectories originating at the sheath edge will reach the probe without solving the space charge problem.

In practice, the problems become more involved, including many auxiliary complications. Among these is the determination of the probe to plasma potential. The situation we have is that the probe is attached to the rocket payload and the applied potential on the probe is relative to the vehicle surface. At equilibrium, because of the greater mobility of the electrons (versus that of the ions), the vehicle itself will be at some negative potential with respect to the plasma. Another quantity which is needed is the sheath size since this determines the amount of current available to the probe.

In addition, the effects of electron reflection at the probe surface and the contact potential variation over the probe surface must be accounted for. Thus, we are in the position of having data which consists of volt-ampere curves to which many parameters are to be fitted and from which we would like to extract the plasma parameters of temperature and density of the charged particles.

We will discuss the above and related problems in more detail in Chapter III.

B. Description

In this experiment, the probes were cast into the ionosphere by two rocket flights at Wallops Island, Virginia. Each carried, in addition to a spherical Langmuir probe, a number of thermal equalization probes and a pulse probe. We will henceforth refer to these flights by their NASA flight numbers, 14.298 and 18.12. A more detailed description of the payload, probe configuration and pulse probe results for flight 18.12 has been reported on earlier[8].

In Table 2.1 we have listed the particulars of the Langmuir probes for the two flights. Although both of these probes were spheres, they were divided into hemispheres so that only the current collected by that hemisphere opposite to the electrical leads were measured as shown in Figure 2.1. Both were also constructed with ABS plastic cores with an undercoat of nickel and an outercoat of rhodium. The differences between the probes lie mainly in their respective sizes and unavoidable microscopic differences in their surface structures. The probe aboard Flight 18.12 had a radius of 0.25 inches and the altitude range of the measurements was from approximately 120 to 240 kilometers, while the corresponding numbers for Flight 14.298 are 0.05 inches and 100 to 160 kilometers. The probe placement and configurations are shown in Figures 2.2 to 2.5. Basically, the pulse probe protruded from the top of the payload section in both flights, while four arms extended perpendicularly (after deployment) from the vehicle. In Flight 18.12, each arm (36 inches long) contained a thermal equalization (TEP) probe and the Langmuir probe was located 10 inches below, 17 inches from the rocket body. In Flight 14.298, there was one less TEP whose place was taken by the Langmuir probe, and the arms were about 40 inches in length. The rocket proper consisted of two stages (Nike-Tomahawk for 18.12; Nike-Apache for 14.298) and the booster stage was jettisoned after burnout. At liftoff, the arms were held flush with the rocket body and the pulse probes were protected by nose cones. Before deployment of the probes, the rockets were despun to a rate of 1.01 revolutions per second for 18.12 and 1.56 revolutions per second for 14.298.

The applied potential on the probe was swept in the form of a

TABLE 2.1

LOCATION: WALLOPS ISLAND, VIRGINIA (37.8°N, 75.5°W)

Vehicle Type:	NASA 18.12 Nike-Tomahawk	NASA 14.298 Nike-Apache
Launch Date:	3-30-67	11-16-67
Launch Time (UT):	19^h09^m	18^h14^m
Apogee (km.):	239	164
Langmuir Probe Radius (in.):	0.25	.05
†K_p	2	2
†A_p	11	9
†Pr.Rz	130	119

K_p = three-hour planetary geomagnetic activity index
Q = one of the ten selected geomagnetically quiet day for month
A_p = linear daily geomagnetic activity index
Pr.Rz = provisional sunspot number

†obtained from data published in the Journal of Geophysical Research (J.V. Lincoln)

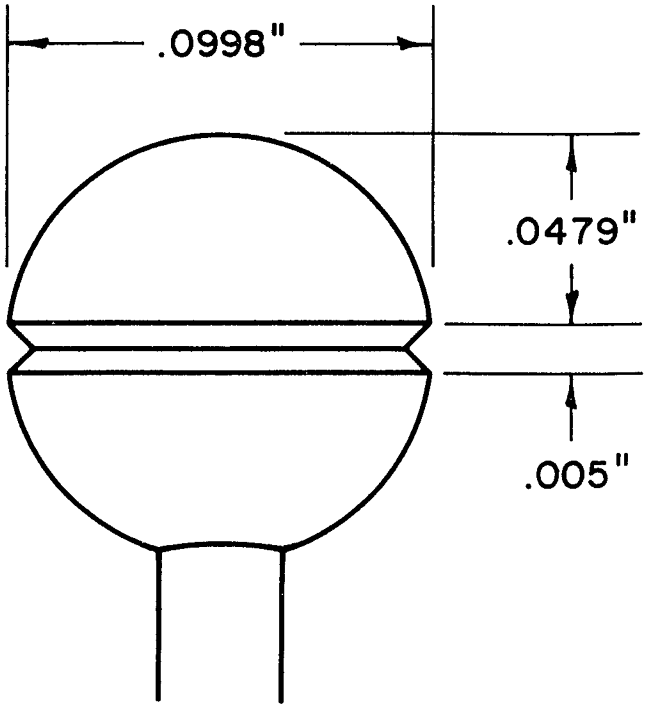

Fig. 2.1 FLIGHT 14.298 – LANGMUIR PROBE

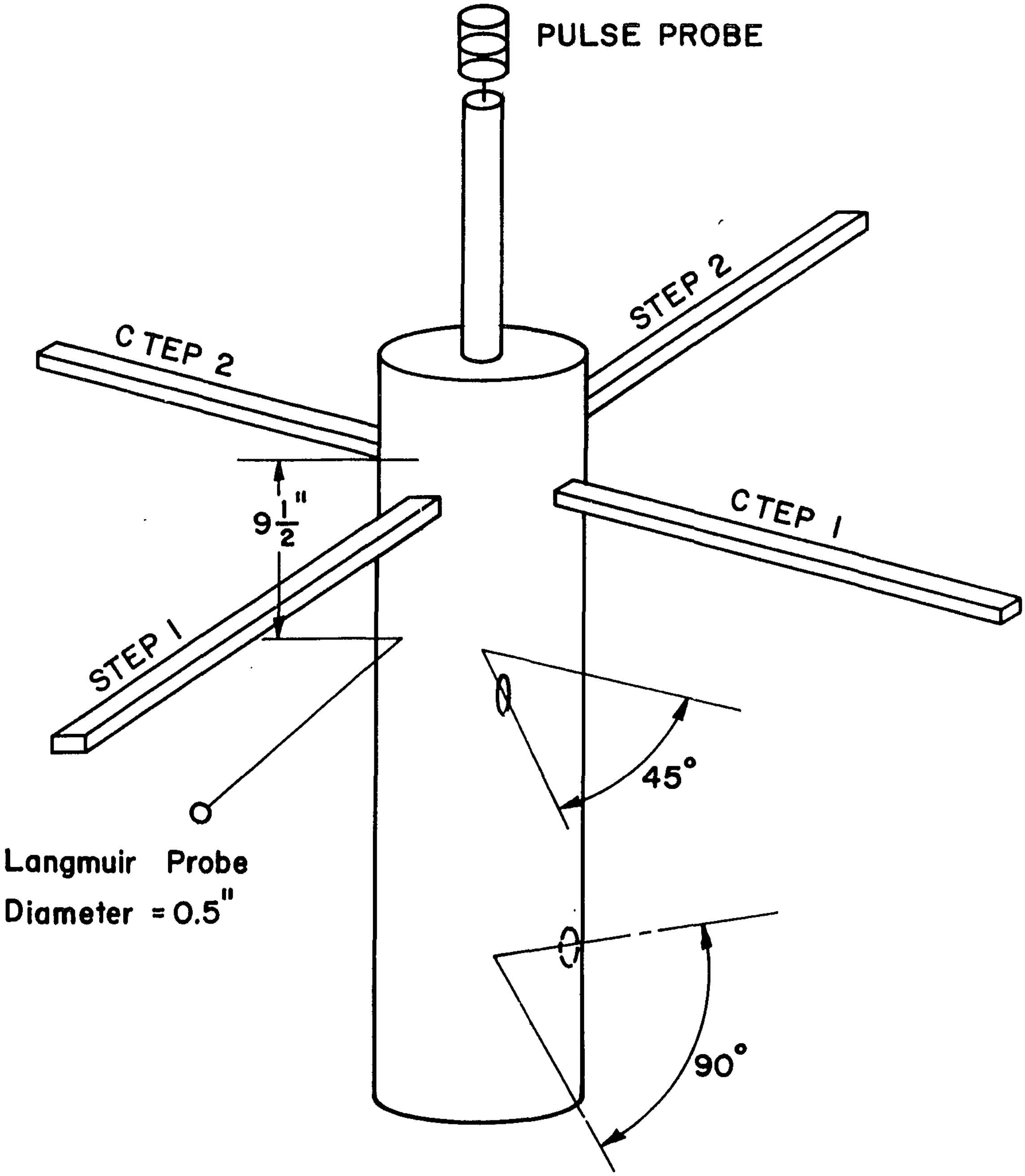

Fig. 2.2 N/T 18.12 PAYLOAD SECTION

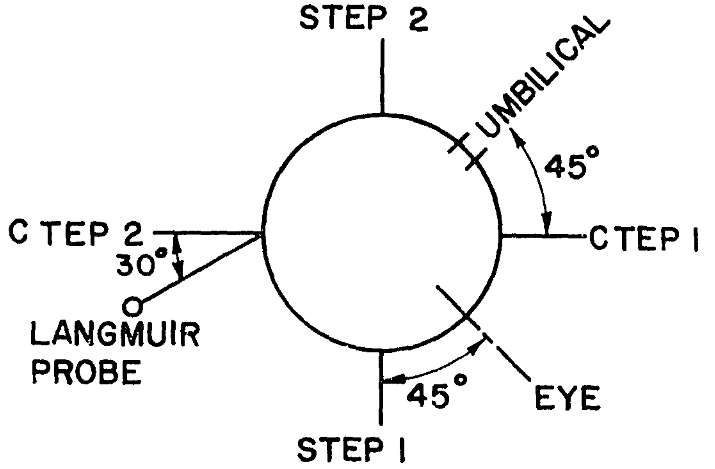

C TEP & STEP'S are orthogonal

TOP VIEW

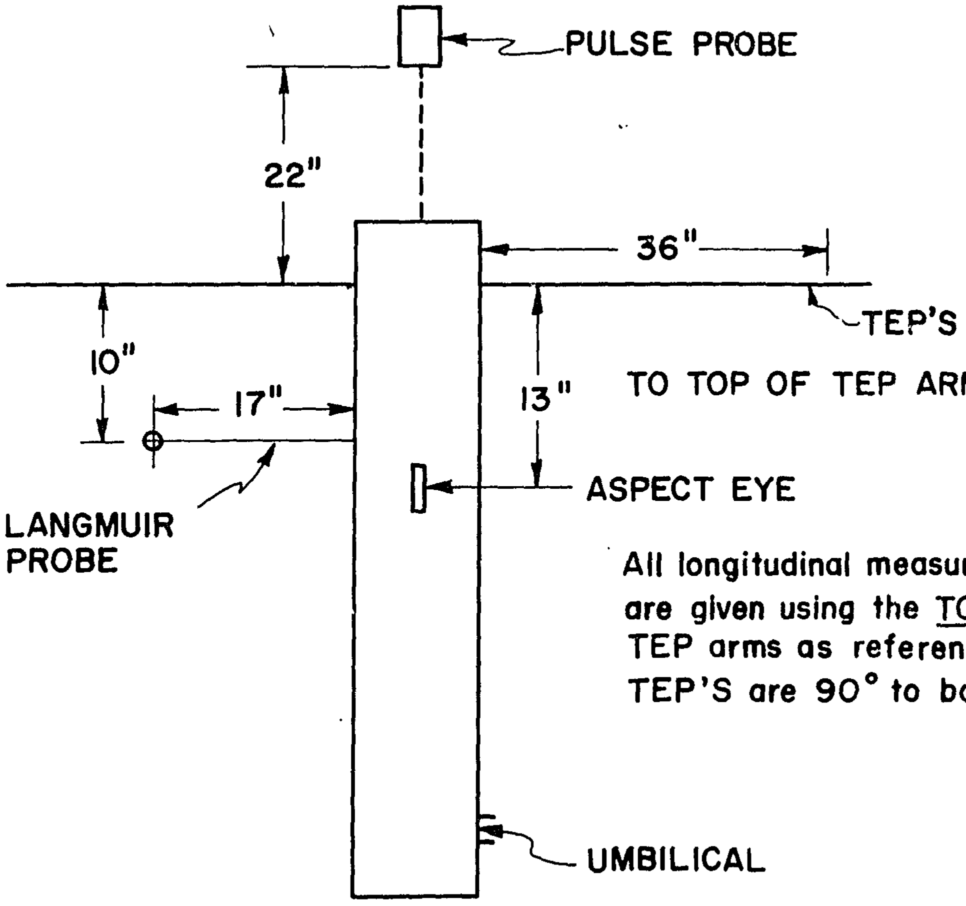

TO TOP OF TEP ARMS

All longitudinal measurements are given using the TOP of the TEP arms as reference plane. TEP'S are 90° to body.

SIDE VIEW

Fig. 2.3 N/T 18.12 PAYLOAD SECTION

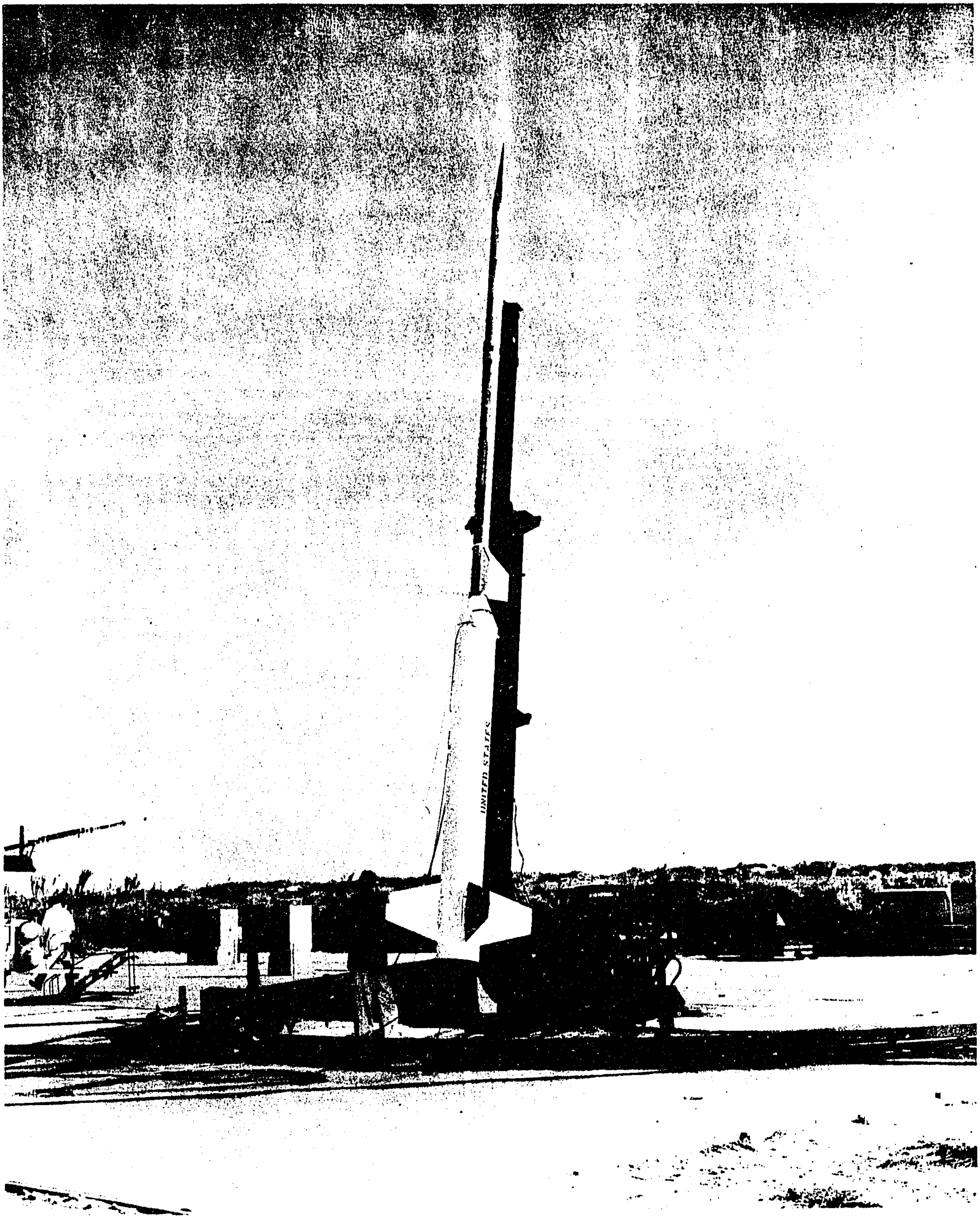

Figure 2.4 NIKE-APACHE (NASA 14.298)

15

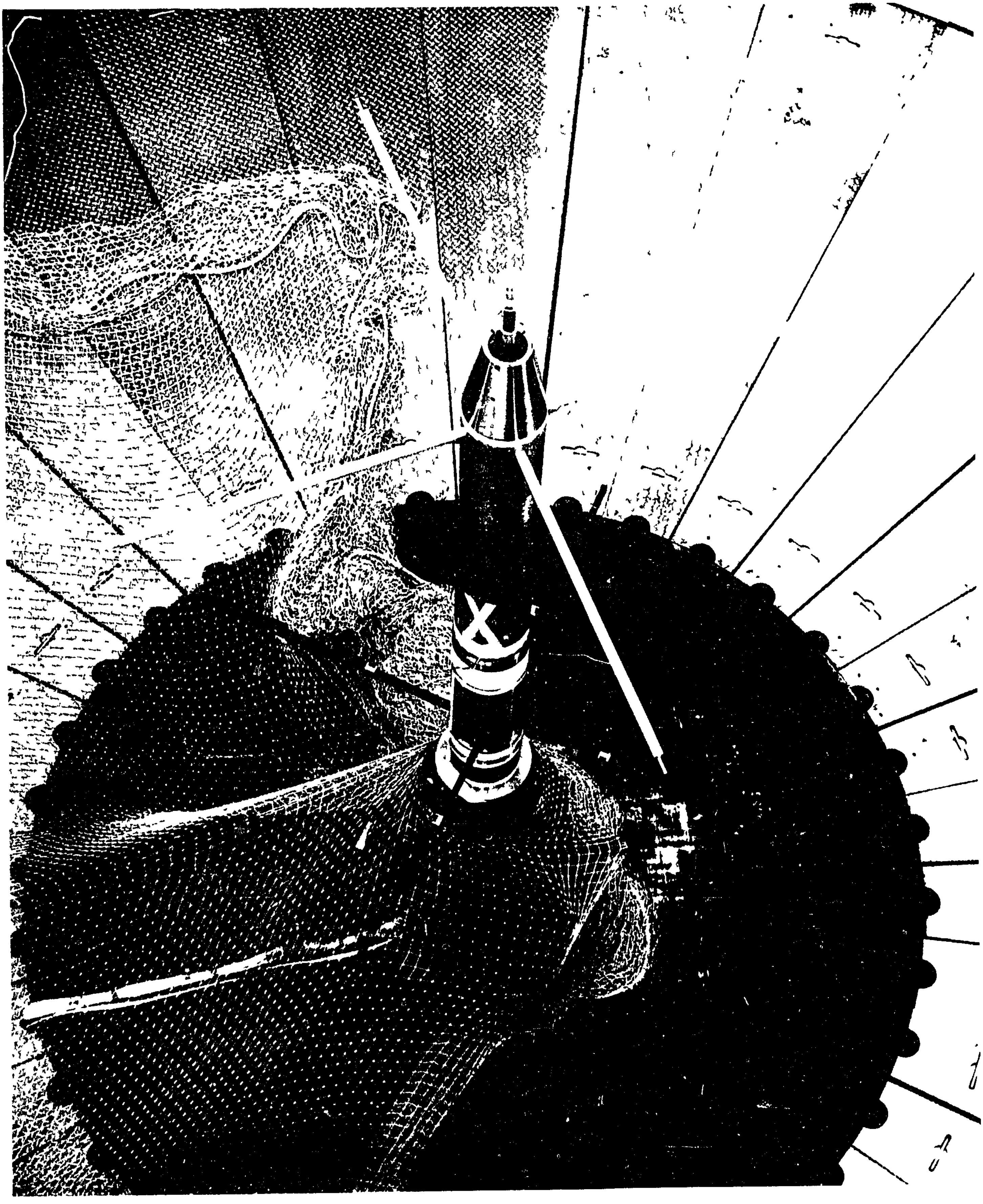

Figure 2.5 PAYLOAD SECTION (NASA 18.12)

symmetric sawtooth at a rate of nearly one cycle per second with limiting values of about -4 to +13 volts. An electrometer with different ranges of sensitivity measured the collected current. Since the current was expected to vary over several orders of magnitude during the potential sweep, the electrometer sensitivity was periodically and successively changed over five ranges and was synchronized with the maximum and minimum of the sweep. That is, on successive sweeps, the electrometer sensitivity is increased in steps of one order of magnitude. When the most sensitive range is reached, the cycle is made to repeat again. Figure (2.6) shows a visual recording taken during the Flight 18.12 giving simultaneous drawings of the sweep (bottom portion) and the collected current (top). The change in electrometer sensitivity can be seen with the electrometer saturating at the higher sensitivities.

The output from the different sources are amplified and each fed to voltage controlled oscillators. These are combined and transmitted to the receiving station where the signals are recorded on one magnetic tape. This analogue data was then demultiplexed by a series of Airpax discriminators and simultaneously converted to digital form. An Epsco Datrac unit was used for digitizing, which was done cyclically at a rate of approximately 12.5 thousand times per second. In our setup, every other channel contained data of the current, and every tenth channel involved the sweep potential. There was also a "time" channel which generated numbers that progressed in regular intervals as a check on the digitizing process.

The output of the digitizer was in turn recorded, via a buffer,

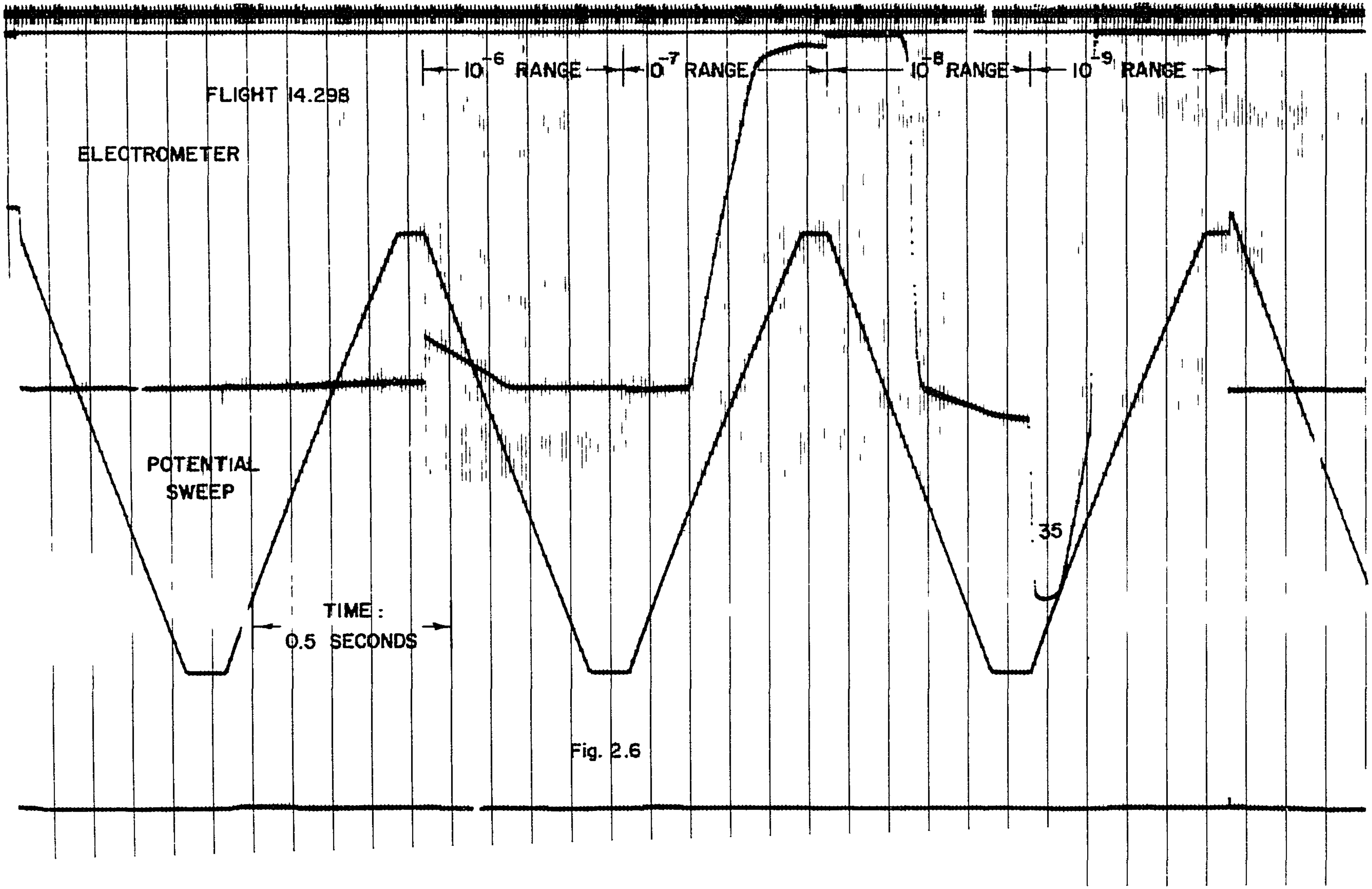
FLIGHT 14.298
ELECTROMETER
10^{-6} RANGE
10^{-7} RANGE
10^{-8} RANGE
10^{-9} RANGE
POTENTIAL SWEEP
TIME : 0.5 SECONDS
35

Fig. 2.6

on magnetic tape using a Control Data 163 tape unit. This was in binary form with twelve bit words. The conversion to physical units was made from pre-flight calibrations in the case of the current and in-flight calibration for the potential sweep.

Finally, the tapes were rewritten into smaller records so that selected portions of data could be loaded into a computer (IBM 7094) for analysis. A discussion of the computer programs can be found in Chapter IV.

CHAPTER III

Probe Theory

A. The Mott-Smith Langmuir (MSL) Equations

As we have noted in Chapter II, the foundation of electrostatic probe theory was first formulated by Langmuir and Mott-Smith. We will briefly consider their development, examining only those aspects which are particularly pertinent to us.

Although a probe which is at a potential V relative to the plasma disturbs the plasma locally, it is possible to-- by using energy and angular momentum considerations, without solving the space charge problem--find an expression for the current the surface of the probe under the following assumptions:

1) The distribution functions of the charged particles at the sheath edge is known.

2) The mean free path is large enough so that the trajectories of the charged particles inside the sheath are unaffected by collisions.

3) The behavior of the potential inside the sheath is such that the total potential change across the sheath will uniquely determine which particle trajectories will reach the probe surface. (See p.21)

Let us consider a spherical coordinate system with a spherical probe at the origin and the following notations:

r = probe radius

a = sheath radius

r' = radial coordinate of the particle with $r \leq r' \leq a$

$u_{r'}$ = radial velocity of a particle at r'

e = magnitude of the electronic charge

u = radial velocity at a

$q_{r'}$ = total tangential velocity at r'

q = total tangential velocity at a

V = potential of probe relative to the plasma

m = mass of the particle

k = Boltzman's constant

T = the temperature of the particles in ^{o}K

N = number density of the electrons

= number density of all positive ions

$A = 2\pi r^2$ = area of hemispherical probe

$\psi = \frac{eV}{kT}$

In a steady state, the net current across the sheath surface will be the same as that reaching the probe. Therefore, we can find the current to the probe by calculating the total drift current through the sheath, counting only those particles whose trajectories will reach the probe surface. From Assumption (2), these can be selected by incoming energy and angular momentum conservation alone. For singly charged particles, we have

$$\begin{aligned} \tfrac{1}{2}m(u_r^2 + q_r^2) &= \tfrac{1}{2}m(u^2 + q^2) + eV \\ rq_r &= aq \end{aligned} \tag{3.1}$$

where V is positive if the probe attracts the particles and negative if the probe repels them. Therefore,

$$u_r^2 = u^2 - \left(\frac{a^2}{r^2} - 1\right) q^2 + \frac{2eV}{m} \tag{3.2}$$

and

$$u^2 = u_r^2 + \left(1 - \frac{r^2}{a^2}\right) q_r^2 - \frac{2eV}{m} \tag{3.3}$$

A particle at the sheath edge with radial velocity u will reach the probe only if in Equations (3.2) and (3.3), u, $u_r^2 > 0$.

As Mott-Smith and Langmuir[6] pointed out, the condition that $u_r^2 > 0$ is not sufficient to insure that a particle orbit will cross the probe surface: $u_{r'}^2$ must also be >0 for all values of r' between the probe and sheath edge. This will be a restraint on the potential variation inside the sheath. Thus, adopting Equation (3.2), we have

$$u_{r'}^2 = u^2 - \left(\frac{a^2}{r'^2} - 1\right) q^2 + \frac{2eV_{r'}}{m} \tag{3.5}$$

When particles are attracted to the probe (i.e., V > 0), it can be shown by using angular momentum conservation and the condition $u_{r'}^2 > 0$, that $V_{r'}$ must be such that

$$V_{r'} > \frac{r^2}{r'^2} \, \frac{a^2 - r'^2}{a^2 - r^2} \, V \tag{3.6}$$

In the case where $V < 0$, it is only necessary that V_r, be monotonic.

In order to find the current reaching the probe surface, we assume that the ionospheric velocity distribution is Maxwellian; i.e., if we denote this by $f(u,q)$, then

$$f(u,q) = \frac{1}{\sqrt{2\pi}} \left(\frac{m}{kT}\right)^{3/2} q\exp\left[\left(-\frac{m}{2kT}\right)\left(u^2 + q^2\right)\right] \quad . \tag{3.7}$$

Therefore, the ambient drift current per unit area is

$$I_o = Ne\sqrt{\frac{kT}{2\pi m}} \quad , \tag{3.8}$$

and the current reaching the spherical probe is

$$i = 4\pi Nea^2 \int_{o,u_1}^{\infty} du \int_{o}^{q_1} u\, f(q,u)dq \tag{3.9}$$

where

$$u_1^2 = -\frac{2eV}{m} \tag{3.10}$$

is used in the limit of the integral (3.9) when $V < 0$, and

$$q_1^2 = \frac{r^2}{a^2 - r^2}\left(u^2 + \frac{2eV}{m}\right) \quad .$$

Equations (3.9) and (3.10) are determined by (3.1), (3.2), and (3.3). Upon evaluating (3.9) we have

$$i = 4\pi a^2 I_o \left[1 - \frac{a^2 - r^2}{a^2} \exp\left(- \frac{\psi r^2}{a^2 - r^2}\right)\right] , \quad \psi > 0 \tag{3.13}$$

and

$$i = 4\pi r^2 I_o \exp(\psi) , \qquad \psi < 0 \tag{3.14}$$

where $\psi \equiv \frac{eV}{kT}$. Equations (3.13) and (3.14) are the Mott-Smith Langmuir equations for a spherical probe. We shall refer to (3.13) and (3.14) as the accelerating and retarding cases respectively. These equations, and their counterparts for other probe geometries are taken as the basis for interpretation of probe data. Equation (3.14) can be used with more facility, since besides requiring only that the potential variation in the sheath be monotonic, it is also independent of the sheath size. We will consider the sheath size and condition (3.6) for the potential variation in reference to equation (3.13) later in this section.

These last two equations can also be arrived at by directly using the distribution function at the probe surface, and will be useful when we consider reflections of electrons from the probe. By using conservation of current, Langmuir[6] found that if f'(u,q) is the distribution at the probe, then

$$f'(u,q) = \exp\left(\frac{eV}{kT}\right) f(u,q) \tag{3.15}$$

with the following restrictions: In the case where V<0, only particles with u>0 exist (q is always positive by its nature). For V>0, there is an excluded region in u-q space, centered about the origin, bounded by the curve

$$u_r^2 + \left(1 - \frac{r^2}{a^2}\right) q_r{}^2 - \frac{2eV}{m} = 0 \tag{3.16}$$

This condition is obtained from equation (3.3) by setting u = 0. The current reaching the probe is then

$$i = 4\pi r^2 Ne \int uf'(u,q)dudq \tag{3.17}$$

Where the limits of integration is over all allowed values of u and q. If $\psi > 0$, then

$$i = 4\pi r^2 Ne \int uqB\exp\left(\frac{eV}{kT}\right) \exp\left(-\beta(q^2 + u^2)\right) dudq \tag{3.18}$$

where $$B = \frac{1}{\sqrt{2\pi}}\left(\frac{m}{kT}\right)^{3/2}, \quad \beta = \frac{m}{2kT}, \quad b = 1 - \frac{r^2}{a^2}$$

$$q_1^2 = \frac{2eV}{mb}, \quad \gamma = \frac{2e}{m}, \quad \alpha = \frac{e}{kT} \tag{3.19}$$

We evaluate this integral by integrating over regions I and II separately as shown in Figure 3.1. Thus,

$$i = NeB4\pi r^2 \exp(\alpha V)\left\{\int_0^{q_1} qdq \int_{\sqrt{\frac{2eV}{m} - b\,q^2}}^{\infty} u\, e^{-\beta(u^2 + q^2)} + \int_{q_1}^{\infty} dq \int_0^{\infty} duuqe^{-\beta(u^2 + q^2)}\right\} \tag{3.20}$$

$$= 4\pi a^2 I_o \left[1 - \frac{a^2 - r^2}{a^2} \exp\left(- \frac{\psi r^2}{a^2 - r^2}\right)\right] \tag{3.21}$$

which is the same as equation (3.13). If $\psi < 0$, things are simpler, and

$$i = 4\pi r^2 NeB\exp(\alpha V) \int_0^{\infty} dq \int_0^{\infty} uduqe^{-\beta(u^2 + q^2)} \tag{3.22}$$

$$= 4\pi r^2 I_o \exp(\psi)$$

and is the same as equation (3.14).

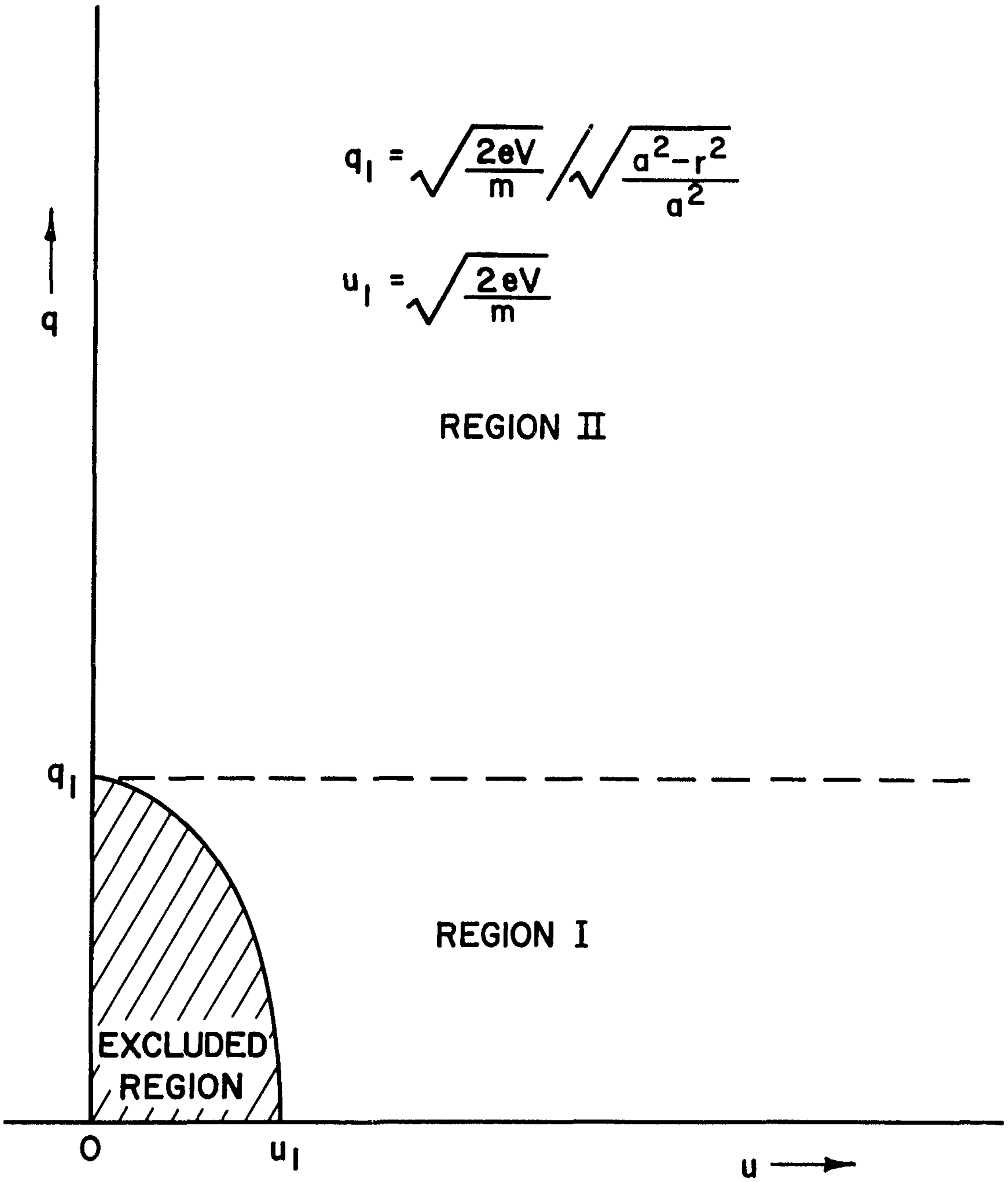

Fig. 3.1 VELOCITY DISTRIBUTION AT r, a = SHEATH RADIUS

We see then, that under the assumptions listed at the beginning of this chapter, it is possible to obtain rather tractable expressions for the current reaching the probe, as first derived by Langmuir[6]. It was also Langmuir[9] who first pointed out that the assumption of a finite sheath with effective shielding may, depending on the circumstances, need modification.

Let us first consider the case for accelerated currents. In order for equation (3.21) to be utilized, the behavior of the potential must satisfy equation (3.6). In addition, the potential at the sheath edge must be zero--or nearly zero, so that the distribution function is known. Ideally, however, the potential only asymtotically approaches zero and we here examine what effects this may have on equations (3.21) and (3.22)

If the probe radius is of the order of a Debye length or less, condition (3.6) is obeyed up to some distance from the probe. The transition from sheath to plasma regions may logically be taken at the point where quasi-neutrality becomes satisfied[9,10,11]. Unfortunately, the potential at this point may still be relatively important. In particular, let us consider the situation where electrons are repelled and ions are attracted to the probe. Langmuir and Tonks[9], Bohm, Burhop and Massey[10], and Allen, Boyd, and Reynolds[11] have shown that when quasi-neutrality is first satisfied, the potential is $\sim kT_e/2e$, where T_e is the electron temperature. Qualitatively, it can be seen that quasi-neutrality would be violated rapidly (proceeding in the direction approaching the probe) since the electron density varies as $\exp(-eV/kT_e)$ and becomes quickly negligible for $eV/kT_e \gtrsim \frac{1}{2}$. Bohm[12] has also shown that this is the criterion for the existence of a stable sheath. If electrons are attracted to the probe instead, then T_i (the ion temperature) is substituted for T_e. Therefore, if T_e is much larger than T_i, then at the sheath edge, the shielding is much more complete when the potential is positive (attracting electrons), whereas a significant field penetrates into the plasma region when ions are accelerated to the probe. Therefore, in the latter case, as Chen[13] has noted, ions would have gained substantial speeds (relative to their undisturbed state) upon reaching the sheath edge, and their velocity distribution would then be unknown. On the other hand if we take the sheath edge to be farther from the probe so that the potential is more nearly zero, then Equation (3.6) is no longer satisfied. The above criteria for the potential at the sheath edge can be shown more rigorously for a monoenergetic distribution, and as noted in reference 13, although the requirement is less stringent for a Maxwellian distribution, no analogous simple expression can be found.

In our situation, (ionosphere, 100 to 250 km) it is expected that the electron temperature may be from two to three times the ion temperature. Thus, when electron accelerated currents are measured, Langmuir's equation (3.21) is expected to be satisfactory. When ion currents are collected, however, because of less effective screening, it is expected that there will be some enhancement in the volt-ampere curve. Because of the complexity of the situation, it is necessary to rely on numerical solutions of Poisson's equation when more quantitative analysis is needed, and has been done by Bernstein and Rabinowitz[14], Al'pert, Gurevich and Pitaevskii[15], and Laframboise[16]. Generally, these results evidently bear out the above analysis on the sheath problem, although in the numerical calculations there was no need to make the distinction between the sheath and plasma regions. For example, there is evident agreement for electron accelerated currents, when $T_e > T_i$, with Langmuir's equation (3.21) for large sheaths. Also, there seems to be little change when the ion and electron temperatures are equal. If the ratio of T_i to T_e is < 1 and ions are collected, then the current is enhanced over the case when T_i is equal to T_e. For $T_e \simeq 2T_i$, this enhancement may be of the order of 20%. Unfortunately, of course, a direct use of numerical calculations in analyzing data would involve trial comparisons with theoretical curves evaluated over a wide range of plasma parameters.

In our case, we will adopt the results of Bettinger and Walker[17], who have numerically derived an expression relating the probe radius and the sheath thickness for equal ion and electron temperatures. This was done in such a way that Langmuir's equation (3.21) would be consistent with the numerical calculations. Their result shows that if s is the sheath thickness and ρ is the probe radius (both in units of Debye lengths), then

$$s = .83\rho^{1/3}\psi^{\frac{1}{2}} \tag{3.23}$$

where the Debye length $h \equiv \left(\frac{\varepsilon_o k}{e^2}\right)^{\frac{1}{2}} \left(\frac{T}{N}\right)^{\frac{1}{2}} = 69.1 \left(\frac{T}{N}\right)^{\frac{1}{2}}$ meters, ε_0 is the permitivity of free space, and N is expressed in number per cubic meter.

We will expect that this, in conjunction with (3.21) we will give the electron accelerated current, and that the ion current would be somewhat larger than (3.21) when the analogous ionic values are used.

Substituting equation (3.23) in (3.21) we then have for $\psi > 0$

$$i = 4\pi r^2 I_o \left[\left(\frac{s}{\rho} \right)^2 + \frac{2s}{\rho} + 1 - \left[\left(\frac{s}{\rho} \right)^2 + \frac{2s}{\rho} \right] \exp\left(- \frac{\rho^2 \psi}{s^2 + 2s\rho} \right) \right] \tag{3.24}$$

$$= 4\pi r^2 I_o \left[1 + \left(\frac{.689\psi}{\rho^{4/3}} + \frac{1.66\psi^{\frac{1}{2}}}{\rho^{2/3}} \right) \left[1 - \exp\left(\frac{\psi}{\frac{.689\psi}{\rho^{4/3}} + \frac{1.66\psi^{\frac{1}{2}}}{\rho^{2/3}}} \right) \right] \right] \tag{3.25}$$

Hence, if we know the current reaching the probe and the probe to plasma potential, we have an indirect measurement of N and T through the expression for I_o. In practice, however, this current is not the same as that collected by the probe and measured by the electrometer because of surface effects at the probe. It is this, and other related problems we will consider in the rest of this chapter.

B. Effects of the Non-uniformity of the Probe Surface

The fact that except for single crystal surfaces which are free from impurities there exists variations in the work function as a function of position on the surface is well known and have been reviewed at length by Herring and Nichols[18] among others. Early interest in this so called "patch effect" which has among its causes surface dipole layers, impurities, and imperfections, was in relation to thermonic emission studies. The problem of emission is essentially inverse to that of collection, and although there exists a close connection between the two, the literature on this considers conditions which differ from ours in terms of space charge and collector-emittor geometry.

Haas and Thomas[19,20] have directly measured the distributional nature of various polycrystals under different surface conditions. Their technique consisted of shooting a thin electron beam (approximately 2 to 5 microns in diameter) at the surface to be investigated. This was small enough to scan each patch independently. According to the Schottky image theory[18] the incoming electrons will see a potential near the surface which is dependent on the patch potentials. Therefore, the amount of current collected by a particular patch will give a measure of its work function relative to the other patches. In this way Haas has obtained work function distributions for various surfaces. Generally, although there exist asymmetries it is found that the distribution is essentially Gaussian in nature, and that if one uses an equivalent, pure Gaussian distribution, the emission characteristics would not differ by more than 5% from that of the real distribution for temperatures between 1250° - 2000° K[19].

In the same manner, the change of distribution as a function of adsorbed gases and applied fields was investigated. The results indicated that although the mean potential changed, the distribution function about this mean did not differ significantly from its previous state.

Heil[21] has made numerical calculations of electron trajectories under the influence of patch fields to investigate the effect of channeling. This is the process in which particles which would normally (by energy considerations) be reflected by a given patch are instead deflected into a less retarding patch field and is subsequently collected. In cases where there exists an applied field much larger than the patch fields, channeling effects were found to be negligible. This result is supported experimentally by Haas[20], where, as mentioned above it was possible to obtain an electron beam thin enough so that patches may be studied singly. The plots of current verses applied retarding voltages for individual patches show that channeling may be neglected for large applied fields.

When the applied field is relatively weak, Heil's calculations reveal the result that a significant portion of particles are deflected into the potential "valleys" of the patch fields where they may undergo oscillations and are finally collected. We will not consider this in more detail since the situation under which Heil's calculations are made is restrictive in terms of the periodicity of the patch distribution, the patch potential variations, and the geometry.

C. A Model for the effect of Patches

In order to have something definite, we consider the following model:

(1) The distribution of the patch work functions about the mean is a Gaussian, and the standard deviation remains constant with time. That is, if the applied probe to plasma potential is V, then the probability that a given patch has a deviation from V between ϕ and $\phi + d\phi$ is

$$p(\phi) = \frac{1}{\sigma\sqrt{2\pi}} \left[\exp\left(- \frac{\phi^2}{2\sigma^2} \right) \right] d\phi \tag{3.26}$$

where σ is the standard deviation, and therefore the potential distribution at the probe surface is distributed in the same manner.

(2) As we go outward from the probe surface, the electric field is a superposition of the patch and applied fields, and at some distance from the surface, the patch potentials approach zero and the total potential no longer shows the nature of the patches.

How quickly the patch applied potentials decay depends on the size and arrangments of the patches, the radius of curvature of the probe, and the space charge. Qualitatively, the rate of decay of the patch potentials is primarily determined by geometric factors. For a geometric arrangement of patches which is periodic, Herring and Nichols[18] have shown that the patch potentials die off exponentially at a distance large compared to the periodicity of the patches if the radius of curvature of the surface is also large compared to this periodicity. In practice, since purely periodic patches are not realized, the patch potentials would decrease at a slower rate; and if the radius of curvature is not much larger than the periodicity, then the patch potentials may vary as slowly as the reciprocal of the distance from the probe[18].

Let r' be the radial coordinate and $\chi(r')$ be the behavior of the potential (patch plus applied) as a function of r'. In addition, let Δr be the distance from the surface of the probe where the patch fields become negligible. At this point, $\chi(r')$ will be somewhat less (in absolute value) than the mean potential at the probe (V) by a value

ΔV. Since we have adopted the convention that $V < 0$ for the retarding case, ΔV is also negative when $V < 0$. Figure 3.2 shows a sketch of the relevant terms, where r is the probe radius, a is the sheath radius and $r_s \equiv r + \Delta r$. Earlier (p.20) we had seen that the distribution function at the probe surface may be found from the distribution at the sheath edge. The distribution at r_s can be found in the same manner. Let us first consider the retarding case. At r_s, the distribution is still Maxwellian, but is reduced by a factor $e^{\alpha V_s}$, where $V_s = V - \Delta V$. When a particle is less than Δr from the probe surface, it becomes influenced by the patch fields. We assume that when this exists we may use equations (3.22) and (3.25) on a probablistic basis with respect to the patch potentials. For convenience, let us for the present, reference the potential to the value at r_s, since we know the distribution there. If we define

$$I_1(\sigma,\Delta V,\ T,\ N) \equiv \int_{-\infty}^{-\Delta V} \exp(\alpha\Delta V + \alpha\phi)p(\phi)d\phi \ = \tfrac{1}{2}\exp\left(\alpha\Delta V + \frac{\alpha^2\sigma^2}{2}\right)\left[1 - \mathrm{erf}\left(\frac{\alpha\sigma}{\sqrt{2}} + \frac{\Delta V}{\sigma\sqrt{2}}\right)\right]$$

$$I_2(\sigma,\Delta V,\ T,\ N) \equiv \int_{-\Delta V}^{\infty} \left[1 + \left(\frac{.689(\alpha\Delta V + \alpha\phi)}{\rho^{4/3}} + \frac{1.66(\alpha\ \Delta V + \alpha\phi)^{\frac{1}{2}}}{\rho^{2/3}}\right)\left\{1 - \exp\left[-\frac{\alpha\Delta V + \alpha\phi}{\frac{.689(\alpha\Delta V + \alpha\phi)}{\rho^{4/3}} + \frac{1.66(\alpha\Delta V + \alpha\phi)^{\frac{1}{2}}}{\rho^{\ 2/3}}}\right]\right\}\right] p(\phi)d\phi \qquad (3.27)$$

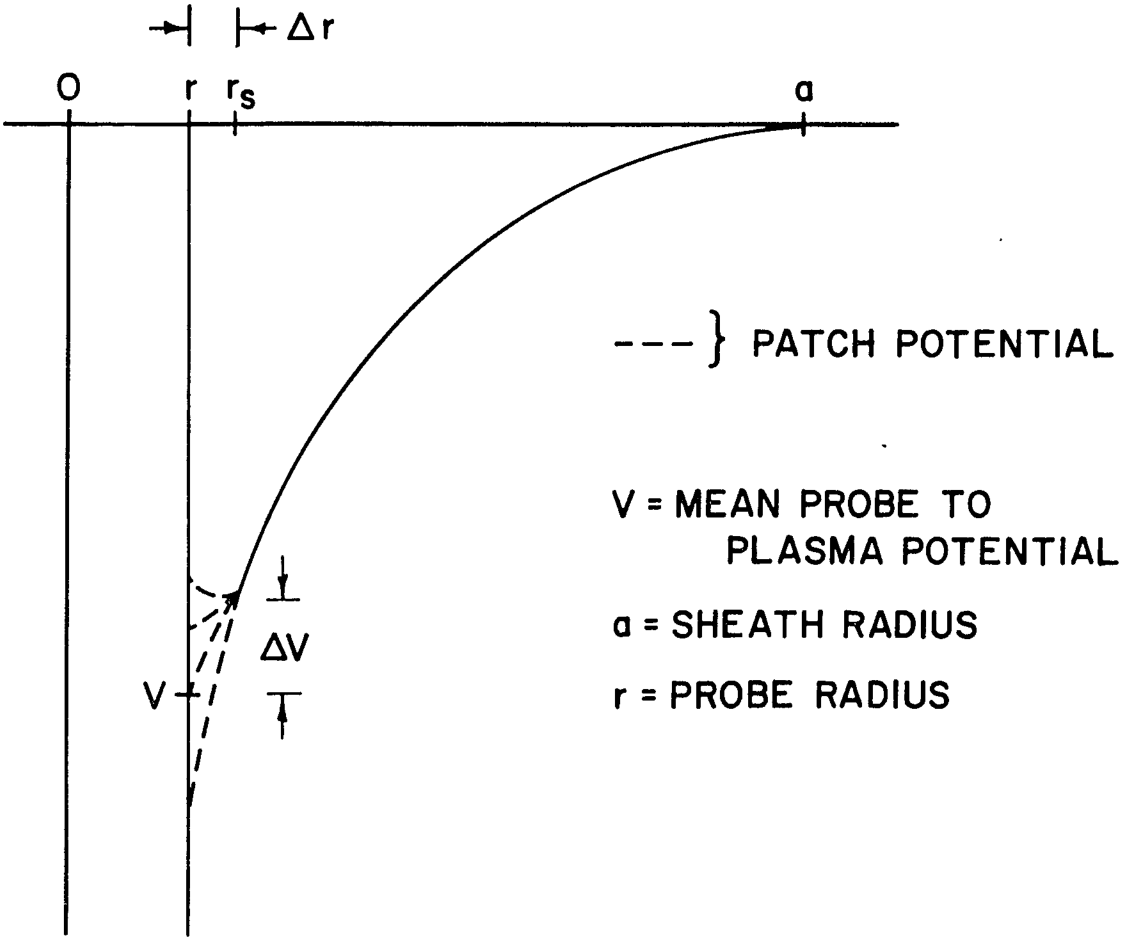

Fig. 3.2 GROSS SKETCH OF POTENTIAL VARIATION vs. RADIAL COORDINATE

and

$$W(\sigma,\Delta V,T,N) \equiv I_1(\sigma,\Delta V, T, N) + I_2(\sigma,\Delta V, T, N) \quad . \tag{3.28}$$

The current reaching the probe is then

$$i = AI_oW(\sigma,\Delta V, T, N)e^{\alpha(V - \Delta V)} \tag{3.29}$$

where A is the area of the probe.

We must still determine σ and ΔV, and these will be found emperically from the data in Section 4.D.

In the accelerating case, the situation is similar except now V is positive. That is, the potential increases monotically as we proceed towards the probe form the sheath edge up to r_s, and may then either increase or decrease. It can be shown that, unlike the retarding case, the current depends only on the net potential change from the sheath edge. We do this by first finding the distribution at r_s, and from this, the distribution at the probe surface. Following equations (3.15) and (3.16), the distribution at r_s is a truncated Maxwellian, i.e., there is a portion in velocity space centered about the origin that is excluded by the condition,

$$u_s^2 + \left(1 - \frac{r_s^2}{a^2}\right) q_s^2 - \frac{2eV_s}{m} > 0 \tag{3.31}$$

Letting the subscript r denote the evaluation at r we also have

$$u_r^2 + q_r^2 = u_s^2 + q_s^2 + \frac{2e(V_{rp} - V_s)}{m} \tag{3.32}$$

where V_{rp} is the potential of the patch in question. Therefore, from (3.31) we get

$$u_r^2 + q_r^2 > q_s^2 \frac{r_s^2}{a^2} + \frac{2eV_s}{m} + \frac{2e(V_{rp} - V_s)}{m} \tag{3.33}$$

In addition, we have from angular momentum conservation, $rq_r = r_s q_s$, and therefore

$$u_r^2 + q_r^2 \left(1 - \frac{r^2}{a^2} \right) - \frac{2eV_{rp}}{m} > 0 \tag{3.34}$$

determines the allowed velocity components at the surface of the patch under consideration. This is the same condition as (3.16), and we can take for the current (when $V > 0$) to be

$$i = AI_o W(\sigma,V,T,N) \tag{3.35}$$

We can consider the gross effect of patches by comparing equations (3.29) and (3.35) with (3.14) and (3.13) respectively. For retarding applied potentials ($V < 0$) equation (3.29) is larger than equation (3.14) by a factor $W(\sigma,\Delta V)\ \exp(-\alpha\Delta V)$, where $\Delta V < 0$. When V is zero, (3.35) is still larger than (3.14). This is because the more attracting patches pull in some particles which otherwise would not reach the probe and this more than offsets the effect of the repelling patches. In the accelerating case ($V > 0$), if V is large enough ($\gtrsim$ 1 volt) so that nearly all the patches are positive, I_1 in equation (3.27) goes to zero, while the effect of patches in I_2 average out since equation (3.25) is, for all practical purposes, linear. In this case, (3.35) agrees with (3.13).

In using the expression (3.28) for $W(\sigma,V)$ and V near zero we have two probable sources of error. On the one hand, I_1 (equation 3.27, with $W = I_1 + I_2$) would likely underestimate the current to the negative patches since we have not included channeling effects, while I_2 would overestimate the current to the positive patches.

C. Electron Reflection

By definition, the reflection coefficient of electrons at a surface is the ratio of the reflected current to the incident current. Unfortunately, this depends on the specific nature and condition of the surface in terms of lattice structure and contaminents, and quantitative calculations have generally been limited to simplified models[18,22]. The interactions through which electrons can be returned from a surface include those with applied and patch fields, and with the atoms, electrons and lattice proper. We have already considered the first of these in the last two sections via the volt-ampere characteristics and we will here examine the reflection coefficient of electrons by the last mentioned processes.

In view of the above mentioned complexities, and considering the differences in specific conditions, we can only interpret the qualitative behavior of our measurements in terms of laboratory experiments.

Fowler and Farnsworth[23] have measured the reflection coefficient under varied conditions, as have others[22,24, 25]. In principle, the current incident on the target is measured in conjunction with the returned current. It is found that there are some general properties common to the reflection coefficient under different conditions and targets[23]. As a function of incident energy, the reflection is $\leq .05$ at zero energy, rises to a local maximum near 3 ev., with a further increase at higher energies. There seems to be general agreement that the finite value at zero energy may be caused by uncertainties in the contact potential difference between emitter and target, the energy spread of the incident electrons, and patch effects. Although the mathematical and physical complexities obviate a quantitative explanation of the reflection coefficient, the increase from zero energy is variously attributed to interactions with atoms and adsorbed gases, impurities and Bragg reflection[18,23,24,25]. Above ~1 ev incident energy, the reflection coefficient varies slowly enough so that an energy spread of a few tenths of an ev is tolerable.

As we have seen in Section A of this chapter, the velocity distribution at the probe surface depends on the probe to plasma potential. As Langmuir has pointed out, for retarding potentials, we can see from equation (3.15) that the average reflection coefficient will be constant with V. In the case where V is positive, (p.20) there is an excluded region in velocity space depending on V.

If we set b = 1 in equation (3.19) and transform to polar coordinates in u - q space, we have, from equation (3.20), the incident current

$$i_{inc} = NeB4\pi r^2 e^{\alpha V} \int_{q_1}^{\infty} v^3 dv \int_{o}^{\pi/2} d\Theta \sin\Theta \cos\Theta e^{-\beta v^2} \qquad (3.36)$$

where

$$v^2 = q^2 + u^2,\ v\sin\Theta = q,\ v\cos\Theta = u,\ q_1 = \sqrt{\frac{2eV}{m}},\ V > 0 \qquad (3.37)$$

The average reflection coefficient, $\bar{R}$, is then

$$\bar{R} = \frac{\int_{q_1}^{\infty} v^3 dv R(V) e^{-\beta v^2}}{\int_{q_1}^{\infty} v^3 dv e^{-\beta v^2}} \qquad (3.38)$$

where R(v) is the reflection coefficient for incident velocity v. We now let

$$\varepsilon = \frac{mv^2}{2}$$

and obtain

$$\bar{R} = \frac{\int_{eV}^{\infty} d\varepsilon \; \varepsilon \; R(\varepsilon) e^{-\varepsilon/kT} \; d\varepsilon}{\int_{eV}^{\infty} d\varepsilon \; \varepsilon \; e^{-\varepsilon/kT}} \tag{3.39}$$

Therefore,

$$\frac{d\bar{R}}{dV} = e[R(eV) - \bar{R}(v)] \; \frac{eV \; e^{\frac{-eV}{kT}}}{\int_{eV}^{\infty} \varepsilon \; e^{-\varepsilon/kt} \; d\varepsilon} \tag{3.40}$$

and

$$\frac{d\bar{R}}{dV} = [R(eV) - \bar{R}(v)] \; \frac{eV}{kT} \; \frac{1}{\left(\frac{kT}{e} + V\right)} \tag{3.41}$$

Since (except possibly for V less than a few tenths of a volt) $\frac{d\bar{R}}{dV}$ is small, the percentage difference between R(eV) and $\bar{R}$(v) will also be small as will be the effect of setting b = 1 in equation (3.18). Therefore, although there is an energy spread in the incident electron current for our case, the resulting reflection ceofficient would not be significantly different from the situation where the electrons are monoenergetic.

We will measure the electron coefficient from the electron accelerating portion of the volt-ampere curve by using equation (3.5). If i is the theoretical current from (3.35) and i_{exp} is the measured current, then the reflection coefficient is

$$R = 1 - \frac{i_{exp}}{i} \tag{3.35a}$$

CHAPTER IV

Data Analysis

A. Introduction

As mentioned earlier, the telemetered data from the payload is digitzied and recorded on magnetic tape. These give, in relative units, the total current as a function of the applied potential on the probe relative to the vehicle (rocket) surface. As a convention, we will, in the graphs, plot increasing electron current with increasing ordinate axes. The symbols will remain the same as in the previous chapter with the subscripts e and i standing for electron and ion respectively.

In Figure 4.1, we have drawn an unscaled graph of the total current--i.e., the sum of the electron and ion currents as a function of the probe to plasma potential. In order to get a clearer prospective, we have shown some anticipatory properties which will be explained in the following sections. The dashed curve is found from equations (3.13), (3.25), and (3.14) while the solid curve corresponds to equation (3.29). In particular, segment AB of the curve represents the part in the acceleration region where the total current is due almost entirely to ions. The portions CD and C'D' show that region where, although ions are still attracted to and electrons repelled from the probe, the ratio of mean electron to ion velocities is large enough so that the electron current alone approximates the total current. A more exact measure of the electron current in this region is obtained by extrapolating the section AB to the point F and subtracting the

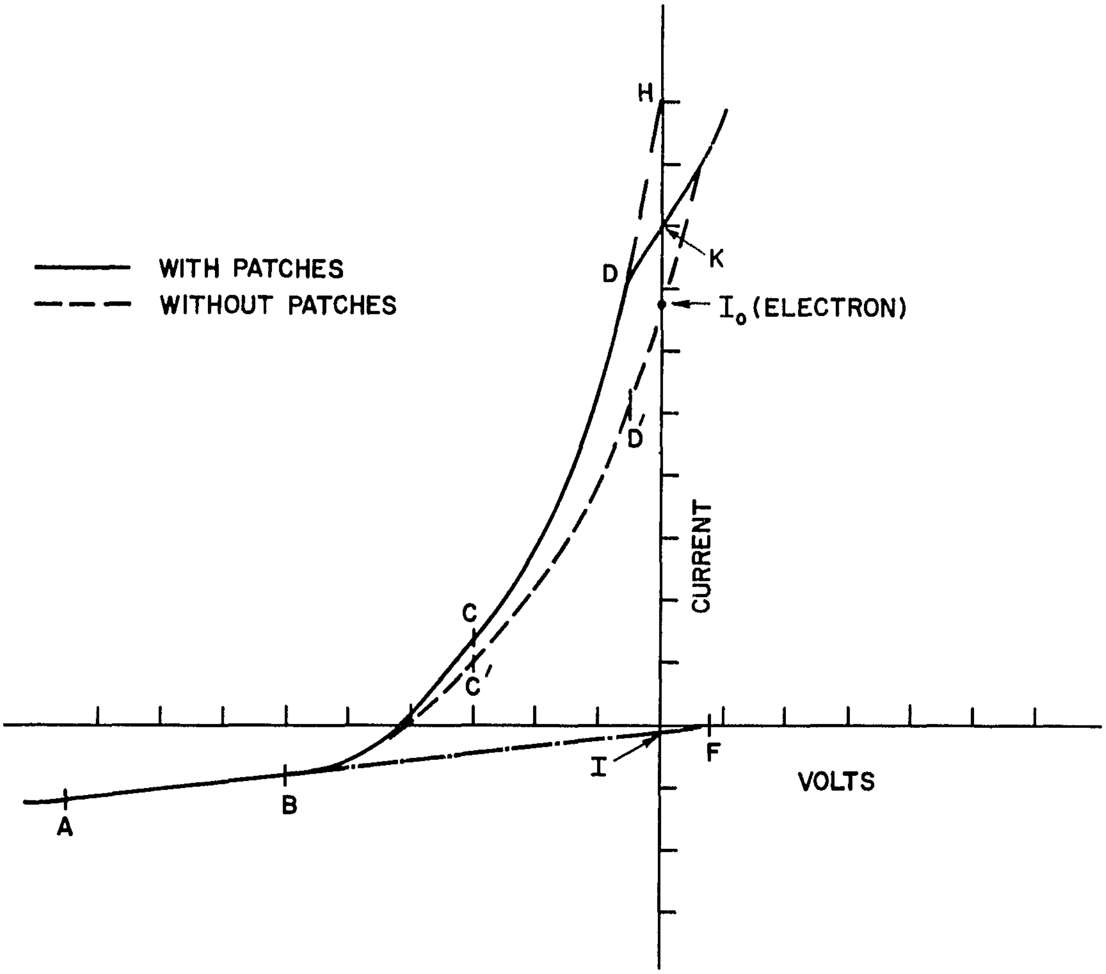

Fig. 4.1 SKETCH OF LANGMUIR PROBE CHARACTERISTIC : CURRENT vs PROBE TO PLASMA POTENTIAL

segment BF from CD and C'D'. We thus get curves which correspond to equations (3.29) (which shows the enhancement due to the effect of patches), and (3.14) respectively. As we approach zero potential, the part of the curve DK shows the premature departure from the exponential which again is a consequence of the presence of patches, while the ion retarding region is essentially entirely obscured by the electron current.

B. The Ion Accelerating Region

Bettinger[26] has suggested that ionic parameters may be obtained by using the slope of the volt-ampere curve for large ion accelerating potentials (segment AB, Figure 4.1). In this way, uncertainties due to emission of electrons from the probe and due to the probe to plasma potential are minimized. The problem of Auger ejection of electrons can be treated in the same manner as reflection of electrons through a electron yield coefficient. Although we have not found measurements on rhodium, the literature of experiments of other metal surfaces suggest that the variation of the yield coefficient as a function of incident ion energy is small enough that we may neglect this mechanism.

There is, however, an additional complication when considering the ion curves. Until now we have considered an ambient distribution which is Maxwellian in velocity. Unlike the electron case, however, the velocity of the probe is comparable to that of the ions. Therefore, it is necessary to calculate the volt-ampere curves using an ambient distribution which has a superimposed drift on the Maxwellian. Shea[28] and Smiddy and Stuart[27] have derived this characteristic:

$$i = 4\pi r^2 \frac{I_o}{2c} \Bigg[\frac{a^2}{r^2} \Bigg(\frac{\sqrt{\pi}}{2} (1 + 2c^2)\ \mathrm{erf}(c) + c\exp(-c^2) \Bigg) - \frac{a^2 - r^2}{r^2} \Bigg(\frac{\sqrt{\pi}}{2} (\tfrac{1}{2} + c^2 - x^2)$$

$$\cdot\ (\mathrm{erf}(x + c) - \mathrm{erf}(x - c)) + \tfrac{1}{2}(x + c)\exp[-(x - c)^2]$$

$$- \tfrac{1}{2}(x - c)\exp[-(x + c)^2] \Bigg) \Bigg] \tag{4.1}$$

where

$$u_o = \text{velocity of probe},\ v_o = \sqrt{\frac{2kT_i}{m_i}},\ c = \frac{u_o}{v_o} \tag{4.2}$$

and

$$x^2 \equiv \frac{r^2}{a^2 - r^2}\ \psi \quad . \tag{4.3}$$

If we now define

$$F(\rho,\psi) \equiv \frac{a^2 - r^2}{r^2} \tag{4.4}$$

then by equation (3.23)

$$F(\rho,\psi) = \frac{.689\psi}{\rho^{4/3}} + \frac{1.66\psi^{\frac{1}{2}}}{\rho^{2/3}} \quad \text{and} \quad x^2 = \frac{\psi}{F(\rho,\psi)} \tag{4.5}$$

Following Shea[28] we expand the term which is multiplied by $\frac{a^2 - r^2}{r^2}$ in equation (4.1) in a Taylor series in x. Since this is an even function of x, only the even powers exist and the leading terms for the Volt-Ampere characteristic are, (letting $I_1 = \sqrt{\frac{\pi}{2}}\,(1 + 2c^2)\mathrm{erf}(c) + c\,\exp(-c^2)$)

$$i = AI_o\,\frac{1}{2c}\,[I_1 + F\,(\sqrt{\pi})\mathrm{erf}(c)x^2 - ce^{-c^2}\,x^4 + e^{-c^2}\,\frac{(60c - 40c^3)}{180}\,x^6 - \ldots] \tag{4.6}$$

$$= AI_o\,[\frac{I}{2c}1 + \frac{\sqrt{\pi}}{2}\,\frac{\mathrm{erf}(c)}{c}\,\psi - \frac{e^{-c^2}}{2}\,x^2\psi + e^{-c^2}\,\frac{(60c - 40c^3)}{360\,c}\,x^4\psi - \ldots.] \tag{4.7}$$

If c is large, only the first two terms in (4.7) need be retained, and the Volt-Ampere curve in the deep accelerating region is for all practical purposes, linear. For Flight 14.298, ρ is of the order .2 and over the range of probe potentials which the measurements are made (-1 to -3 volts), $x \lesssim .4$, if $T \simeq 1000$. Therefore, in this case the higher order terms in x may (for c ≳2), be neglected. In Flight 18.12 ρ and x are both near unity, and more terms must be retained in the expansion unless c ≳ 3. However, (again for V between -1 and -3 volts) x^2 and x^4 are constant (∿ 1) to within a few percent and (4.7) is therefore also linear to within a few percent. This approximation facilitates the use of the slopes of the ion curves and the advantages we had mentioned earlier. It also gives the simplification that the effect of patches is averaged out. We therefore have

$$\frac{di}{dV} \cong AI_o \frac{e}{kT_i} \left[\frac{\sqrt{\pi}}{2} \frac{\mathrm{erf}(c)}{c} - \frac{e^{-c^2} x^2}{2} + e^{-c^2} \frac{(60 - 40c^2)}{360} x^4 - \ldots \right] \tag{4.8}$$

The unknowns in the above equation involve the ion temperature T_i, the percentage ion composition of the different species, and the total ion density.

To be complete, we note that, the measured ion currents (and slopes) involve the sum over the partial currents (and slopes) of the different ions:

$$\frac{di}{dV} = \sum_j \left(\frac{di}{dV}\right)_j \tag{4.9}$$

We can eliminate one unknown, the total ion density, if we know the electron density and assume charge neutrality.

In order to interpret our measurements in terms of the preceeding equations, we have made polynomial curve fits to the data. These curves are determined by the usual least-square criterion. That is, we numerically obtain the coefficients $\{a_n\}$ such that the mean square deviation of the data with respect to the polynomial

$$i_{exp} = \sum_{m=o}^{N} a_m V_{pv}^m \tag{4.9}$$

is minimized. Here, i_{exp} is taken as the measured current and V_{pv} is the applied probe potential relative to the vehicle. V_{pv} will differ from the probe to plasma potential by the vehicle to plasma potential, V_{vpl}, which we will assume to be constant within a given curve. Thus, to obtain i_{exp} as a function of the probe to plasma potential, we must adjust the coefficients in equation (4.9) to account for vehicle potential.

In Flight 18.12 (larger probe), the ion curves show small, but systematic 2nd and 3rd order terms in the polynomial fit, while the ion sections of Flight 14.298 exhibits no non-linear terms. This is consistent with the sheat sizes (equation 3.22) which we have used.

Since equation (4.1) is for all practical purposes linear, we have neglected the effect of patches, which averages out.

C. The Vehicle Potential

In view of the previous section and the fact that we will eventually need the probe to plasma potential, it is necessary to obtain the vehicle potential relative to the plasma. We can get a measure of this from the point F in Figure (4.1). This point is found by numerically extrapolating the portion AB in Figure (4.1) until it intersects zero current.

At F, the probe to plasma potential is $\lesssim$ 0.1 volt. We can see this from an estimate of the ambient ion current (point I in Figure 4.1) and the slope of the extrapolated ion curve near I. Although the ion current at plasma potential is completely obscured by the electron current, we can estimate the ratio of the electron to ion ambient currents and therefore obtain a maximum ion drift current at plasma potential. From our calculated coefficients (equation 4.9) we can then find the potential at F to within a few hundredths of a volt.

D. The Electron Curve

1) The Retarding Region: Electron Temperatures

The electron current in the deep retarding region (segment CD, Figure 4.1) is obtained by substracting segment BI from the total current and corresponds to equation (3.29). Figure 4.2 shows a representative data curve corresponding to this region, plotted (in arbitrary units) on a semi-log scale. If we evaluate the logarithmic derivative of equation (3.29) with respect to V, we obtain

$$\frac{\frac{di}{dV}}{i} = \left\{ \frac{1}{W(\sigma,\Delta V,T_e,N_e)} \frac{dW(\sigma,\Delta V,T_e,N_e)}{d(\Delta V)} - \alpha \right] \frac{d(\Delta V)}{dV} + \alpha \qquad (4.10)$$

where $\alpha = \frac{e}{kT_e}$.

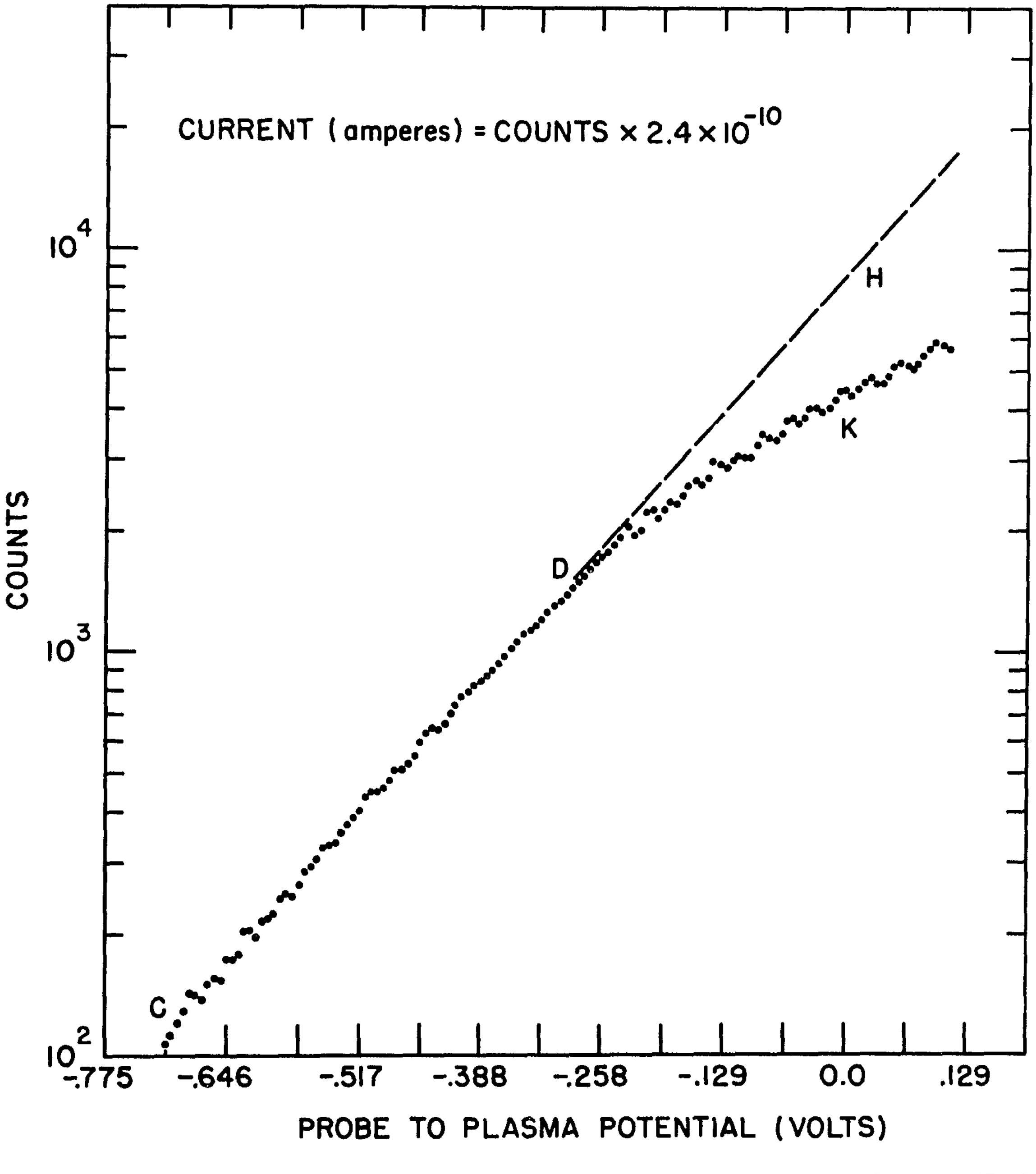

Fig. 4.2. FLIGHT 18.12, LANGMUIR PROBE CURVE NO. 49 PLOT OF COUNTS VS. PROBE TO PLASMA POTENTIAL.

The portion CD of Figure 4.2 shows a nearly constant logarithmic derivative. For reasonable values of T_e, σ, and ΔV, our calculations show that the difference of the terms in the brackets of (4.10) is roughly 10 to 15 percent of α. Since the data show a constant logarithmic slope, then in (4.10), $\frac{d(\Delta V)}{dV}$ must be small or nearly independent of V. In that latter case, V_s must be approximately proportional to V (since $\Delta V = V - V_s$), where V_s is the value of the potential at r_s (see Figure 3.2). An upper bound for r_s can be found by noting that at distances from the probe surface much larger than the geometric "periodicty" of the patches, the patch potentials must be negligible[18]. Measurements[19] have shown that the size of patches is of the order of 10 microns. Therefore, r_s is at most, say, 500 microns (the diameter of the smaller probe). Now, near the surface (within a Debye length) of the probe, the potential varies less slowly than $1/r'^2$ [15, 13], where r' is the radial coordinate. Therefore, at worst, $\frac{V_s}{V} \gtrsim \frac{1}{4}$, if we take $r_s \simeq$ the probe radius. Then from equation (4.10), $\frac{di}{dV}/i = \alpha = \frac{e}{kT_e}$ within 10 percent, which is a conservative estimate. From this, we obtain T_e. In our numerical analysis, a linear least-squares fit is made to the natural log of the data to obtain the slope. Since the log is not a linear function, different values of the current were weighted appropriately[29], although for practical purposes this precaution turned out to be unnecessary.

2) Electron Density

Once the electron temperature is known, we can obtain the electron density N_e from the electron current density I_o;

$$I_o = N_e \cdot e\sqrt{\frac{kT_e}{2\pi m_e}} \tag{4.11}$$

We may find I_o by examing equation (3.29) in conjunction with the data. We again refer to Figure 4.2, noting that the curve breaks from an exponential behavior at point D. This variation is taken to be due to a stronger dependence of ΔV on V in the portion DK of the graph. It is expected that at D, the corresponding value of V approaches that of the standard deviation of the patches. We will assume that for this and values of V nearer to zero, the potential at r_s (see Section 3.B) is small enough so that the main effect of V is in determining the mean value of the patch potential distribution over the probe surface. Our expression for the current in the portion DK of Figure 4.2 is then

$$i = AI_o W(\sigma, V) \quad . \tag{4.11a}$$

Mathematically, this is equivalent to assuming that in equation (3.29) ΔV is approximately V in this section of the Volt-Ampere curve. The ratio of K to D will give us a measure for σ, the standard deviation of the patch distribution. Although the multiplicative factor I_o cancels in this ratio, there is still an implicit dependence of this ratio on N_e through the expression for ρ, (equation 3.23).

In order to find σ and N_e, we have, from (4.11a),

$$AI_o = AN_e e\sqrt{\frac{kT_e}{2\pi m_e}} = \frac{K}{W(\sigma,0)} \tag{4.12}$$

Also, from (4.11a)

$$D = AI_o W(\sigma, V_D) \tag{4.13}$$

where, again, K and D are found from the data (see Figure 4.2), and V_D is the value of V corresponding to D. Therefore,

$$\frac{K}{D} = \frac{W(\sigma,0)}{W(\sigma,V_D)} \quad . \tag{4.14}$$

We then perform a double iteration on σ and N_e until equations (4.12) and (4.14) are simultaneously satisfied. We will assume here (zero probe to plasma potential) the reflection coefficient is negligible. We have mentioned in Section 3.D that in laboratory experiments, there is evidence that the reflection coefficient does in fact approach zero with zero incident electron energy. The situation here differs in that there is a spread of ∿ .2ev in energy and that patch effects exist. However, the slope of the reflection coefficients is small so that we may neglect reflections.

3. The Electron Acceleration Region

As the probe to plasma potential becomes increasingly positive, the reflection of electrons from the probe becomes larger. As discussed in Section 3.D., the probe, in this case, accelerates electrons towards it, and upon reaching the probe, the particles have a minimum total energy of eV, where V is the probe to plasma potential.

This reflection coefficient is found by calculating the expected current reaching the probe and dividing it into the measured current (see Section 3.D).

E. Data Processing and Numerical Calculations

The data reduction and numerical calculations essentially consists of a series of computer programs which perform the operations outlined in the previous sections of this chapter. These programs are listed at the end of this dissertation. We shall refer to the programs by number, and any subroutines which may exist by name. These were written in Fortran IV language, with the exception of the subroutine (written in macro-assembly language--MAP) which read and stored in computer memory the data from the magnetic tapes. This facilitated the transformation of twelve bit words (which were recorded on the tapes during the digitization process) to thirty-six bit words which the computer reads.

Program I consists of a main program and the five subroutines READ, ORDER, XFIT, YFIT, AND XZERO. Subroutine READ is the aforementioned MAP program and loads the data, while subroutine ORDER was used as a check against errors in the digitizing process and possible imperfections in the magnetic tapes. In Chapter II, we had seen that the conversion of analogue to digital data was performed on the different channels of information successively and cyclically, each channel carrying different types of information. It was found that at times, although this occurred rarely, a channel would be inadvertantly skipped, with the consequence that the computer would then misinterpret the data. As we mentioned previously, one of the channels contained readings from a "clock" which gave numbers that progressed in a regular and known rate. The channel immediately preceeding this time reading was also fixed so that the last bit of each word remained an even interger. Basically, subroutine ORDER tested these conditions. If the restraints were not satisfied, the corresponding words were set to zero and the computer was programmed to discount these readings.

The decks XFIT and YFIT are respectively those programs which performed the least square polynomial fits to the ion and sweep (probe to vehicle potential) data, and to the logarithm of the electron retarding section. The process of fitting these curves essentially amounts to the solution of a set of simultaneous equations in the coefficients of the polynomials to be obtained (equation 4.9)[29].

Thus, in the main deck of Program I, the data is loaded and scanned for inconsistencies. The routine XFIT is then called to make a linear fit to the sweep potential and a polynomial fit (of order three for Flight 18.12 and order one for 14.298) to the ion section. These two choices on the order of the polynomials were dictated by trial runs, i.e., by simply trying different orders of polynomials to determine if there existed any systematic non-linear terms in the ion currents.

The curves fitted to the ion section is then extrapolated to zero current. The remainder of Program I numerically evaluates the steps for the electron retarding region described in Section D of the chapter.

After each of the curve fits, the standard deviation of the data from the corresponding values of the curve was calculated. The fitting procedure was then repeated, with any data having a deviation larger than ten standard deviations regarded as spurious and consequently ignored. The end results of this program are then the ion slopes, the electron temperatures, and the vehicle potential.

Program II executes the double iteration procedure outlined in Section D.2 of this chapter. The input data consisted of the values of K and D as in Figure 4.2, the electron temperature, and estimates of the initial values of the ambient drift current (i.e., the density) and the standard deviation of the patch distribution, σ. Let us denote the right hand side of equation (4.14) by KD (σ, N_e). The iteration in sigma was then carried out by the expression

$$\sigma = \sigma - \frac{[KD(\sigma,N_e) - K/D]}{\left\langle \frac{d}{d\sigma} [KD(\sigma,N_e) - K/D] \right\rangle} \tag{4.16}$$

where the brackets <> denotes the average of the expression inside. Actually, we need only an estimate of the expression in the brackets. Convergence is insured if the absolute value of the derivative of (4.16) with respect to σ is less than one. The calculation in (4.16) was repeated until σ changed by less than .001. This value was then substituted in (4.12) and a new value of N_e was found. The whole process was in turn repeated until N_e changed by less than one half of one percent. The subroutine INTEG of this program was used to evalute KD(σ,N_e) and follows the Newton Coates method[30]. In the limits of the integral, infinity was replaced by two (volts) and the step size was one hundredth of a volt. These values were empirically chosen to give three place accuracy in the final results for N_e.

The initial values of N_e and σ were obtained by first considering the case where ratio of the sheath to probe radius approached infinity. In this limit equation (3.20) becomes

$$i \xrightarrow[\frac{a}{r} >> 1]{} 4\pi r^{2} I_{o} \left(1 + \frac{eV}{kT}\right) \tag{4.17}$$

and the corresponding expression for (3.27) is

$$W(\sigma, V) \longrightarrow \tfrac{1}{2}\exp\left(\alpha V + \frac{\alpha^{2}\sigma^{2}}{2}\right) \left[1 - \mathrm{erf}\left(\frac{\alpha \cdot \sigma}{\sqrt{2}} + \frac{V}{\sqrt{2}\sigma}\right)\right] + \tfrac{1}{2}(1 + \alpha V)\left[1 + \mathrm{erf}\left(\frac{V}{\sigma\sqrt{2}}\right)\right]$$

$$+ \frac{\alpha\sigma}{\sqrt{2\pi}} \exp -\left(\frac{V^{2}}{2\sigma^{2}}\right) \, . \tag{4.18}$$

We see that here the ratio K/D is independent of N_e and we can consequently obtain σ. We also obtained an approximation of the bracket expression in (4.16) in this way. Program III was used to find the electron reflection coefficient in the accelerating region. Having obtained the electron temperature and density from the previous programs we then used equations (3.29) and (3.35) to evaluate the expected current reaching the probe surface. If we divide the measured electron current (accelerating region) by this calculated current, we have $(1 - \bar{R})$ where $\bar{R}$ is the reflection coefficient averaged over the incident energies as in Section 3.D. In order to save computing time, we note that in the large accelerating regions the current is very nearly linear as a function of potentials. Therefore, in the program when $V > 2$, we have substituted equation (3.25) for equation (3.35). It can be seen in the graphs for reflection coefficients (Chapter V) that the continuity is quite good at 2 volts.

The last program listed merely calculates the derivative of equation (4.1) and prints a table of values of the ion slope for a range of ion temperatures. A partial slope is found for atomic masses of 16 and 32 and then summed. It can also be seen that we have used the electron Debye length even in the case for the ion currents. The reason for this is explained in Section 3.A and 5.B. Finally, we mention that since equation (4.1) is very linear, we have neglected the effect of patches which average out and the slope was evaluated for V equals 2.

In summary, we briefly review the steps in finding the electron temperature, electron density, ion temperature and electron reflection coefficient:

1) The electron temperature is obtained from the electron retarding region using equation (4.10) where we have neglected the terms in the brackets as previously explained.

2) The electron density is obtained from the ambient drift current as explained in Section 4 D.2, where the ambient current is the measured current at plasma potential. This potential is found by the extrapolation of the ion current to zero value.

3) The ion temperature is found from the derivative of equation (4.1) with respect to V and then comparing this with the measured ion slope. The required ion density is found from the electron density (using charge neutrality).

4) The electron reflection coefficient is found from the electron accelerating region by finding the ratio of the measured current to the calculated current (equations 3.35 and 3.35a)

We see then, that the electron density is measured from the current at zero potential and is used in calculations in both the electron and ion accelerating regions. This correlation between the different portions of a curve will serve as a sensitive consistency criterion for the resulting ionospheric parameters, and we will see in the next chapter that the results show good internal consistency in the above sense.

CHAPTER V

Results and Discussion

A. Introduction

We will present the results, where it facilitates matters, with respect to curve numbers which progress with the amount of time into the flights. In Tables 5.1 and 5.2 we have listed (for each flight) results for altitudes, electron density, electron temperature, Debye length, and the standard deviation of patches with the curve numbers. Where numbers are missing, it is due to the occurrence of in-flight calibration, and in a few cases due to imperfections of the magnetic tapes on which the data was stored. Results for the last portion (descent) of flight 18.12 are also not presented in that, for reasons uncertain to us, the data went awry. We will discuss this furthur in section 5B.4.

There have also been some adjustments made on several curves in reference to the location of zero potential with respect to the volt-ampere curves. In Section 4.C, we explained that this point was estimated from an extrapolation of the ion accelerating region of the curves. Near flight apogee, we expect that the curves will be similar since this case the altitude change is small and consequently so are the change in plasma parameters. In particular, the electron reflection coefficients should be nearly constant from curve to curve. It was on this basis and the constancy of the patch distribution that the zero potential point was adjusted. The portion of "anomalous" curves [illegible] ~~were~~ approximately one quarter of the total. We note here that although the adjustments were small in terms of potential (of the order of 0.1 volt) it is important because the value of the ambient current

Table 5.1

Flight 14.298

Curve #	Altitude (km)	Electron Temperature (10^{3o}K)	Electron Density (x 10^{11})/cubic meter	Debye Length (x 10^{-2}m)	σ, Standard Deviation of Patches
1	102.6	1.33	.81	.885	.357
3	-----	----	----	----	----
5	116.6	1.06	1.12	.672	.357
7	----	----	----	----	----
9	126.5	1.43	1.00	.826	.367
11	131.5	1.13	1.09	.713	.375
13	-----	----	----	----	----
15	140.8	1.38	1.23	.732	.361
17	-----	----	----	----	----
19	147.5	1.46	1.16	.775	.353
21	150.9	1.40	1.16	.759	.360
23	153.7	1.43	1.33	.716	.32
25	156.2	1.47	1.07	.810	.347
27	-----	----	----	----	----
29	-----	----	----	----	----
31	160.1	1.58	1.34	.75	.374
33	162.8	1.52	1.19	.781	.375
35	163.6	1.66	1.26	.793	.373
37	-----	----	----	----	----
39	164.2	1.60	1.51	.711	.363
41	164.	1.55	1.11	.817	.345
43	163.4	1.61	1.24	.787	.362
45	162.4	1.48	1.29	.740	.346
47	-----	----	----	----	----
49	159.6	1.48	1.15	.784	.361
51	157	1.48	1.14	.787	.364
53	155	1.56	1.06	.838	.354
55	-----	----	----	----	----
57	-----	----	----	----	----
59	147	1.26	.846	.843	.364
61	143	1.28	.973	.793	.38
63	139	1.36	.86	.747	.37
65	134	1.27	.80	.871	.346
67	-----	----	-----	----	----
69	124	1.15	.76	.850	.36
71	119	1.13	.78	.832	.37
73	112	1.09	1.03	.711	.38
75					

Table 5.2

Flight 18.12

Curve #	Altitude (km)	Electron Temperature (10^{3o}K)	Electron Density (x 10^{11})/cubic meter	Debye Length (x 10^{-2}m)	σ, Standard Deviation of Patches
1	120.4	.71	1.133	.547	.22
3	-----	----	-----	----	----
5	136.2	.78	1.99	.433	.23
7	-----	----	----	----	----
9	150.6	1.10	2.2	.489	.24
11	157	1.148	3.06	.423	.23
13	164	1.31	2.76	.476	.25
15	170.4	1.44	2.74	.501	.239
17	176.5	1.68	2.75	.54	.229
19	-----	----	----	----	----
21	-----	----	----	----	----
23	192.9	1.87	2.56	.591	.236
25	-----	----	----	----	----
27	202.4	1.92	3.02	.551	.236
29	-----	----	----	----	----
31	210.9	1.95	3.01	.556	.236
33	-----	----	----	----	----
35	218.2	1.99	2.67	.597	.236
37	221.3	1.97	3.16	.546	.235
39	-----	----	----	----	----
41	227.0	1.91	3.55	.568	.249
43	-----	----	----	----	----
45	231.7	2.11	3.27	.555	.25
47	-----	----	----	----	----
49	235.3	1.94	3.67	.502	.254
51	237	2.05	3.63	.519	.20
53	238	2.02	3.48	.526	.249
55	238.5	1.97	3.71	.503	.26
57	239	2.01	3.68	.511	.24
59	239.4	1.99	3.47	.523	.259
61	-----	----	----	----	----
63	238	2.06	3.31	.545	.248
65	-----	----	----	----	----
67	237.5	2.14	3.38	.55	.26
69	-----	----	----	----	----
71	235	2.08	3.19	.558	.23
73	233	2.08	3.24	.554	.267
75	231	2.13	2.70	.614	.258

is very sensitive to the potential. At lower altitudes, the criterion used was the constancy of the patch distribution alone since the reflection coefficient might have been subject to change as a consequence of probe surface contaminants. A possible cause of these fluctuations is that the probes were hemispherical and for ion collection, there is expected to be some dependency on probe aspect. At flight apogee, the probe velocity is about half the mean ion velocity and this effect should be small, as can be seen by expanding equation (4.1) in terms of c, the ratio of the probe to ion velocity. At lower altitudes c becomes progressively larger and reaches a value which is several times unity. However, at least for ascent, the probe is perpendicular to the rocket axis and the aspect of the probe (relative to the velocity vector) is also expected to have a minimal effect and we may still use spherical geometry, but with half the probe area.

B. Results

1) Electron Temperatures (T_e)

In Figures 5.1 and 5.2 we have plotted the electron temperature profiles for each flight. As noted earlier, it is the electron temperature results which are subject to the least uncertainties in data analysis. We have seen that they may be obtained in a way which is independent of vehicle potential, sheath size, patch effects and reflection coefficients. For flight 18.12, we have as shown in Figure 5.3 compared the electron temperatures with those measured by a pulse probe carried on the same flight.[8] Except for a few curves at low altitudes, the agreement is good. Figures 5.1 and 5.2 also contain the ion temperature measurements and we will discuss this more fully in Section 5.B3.

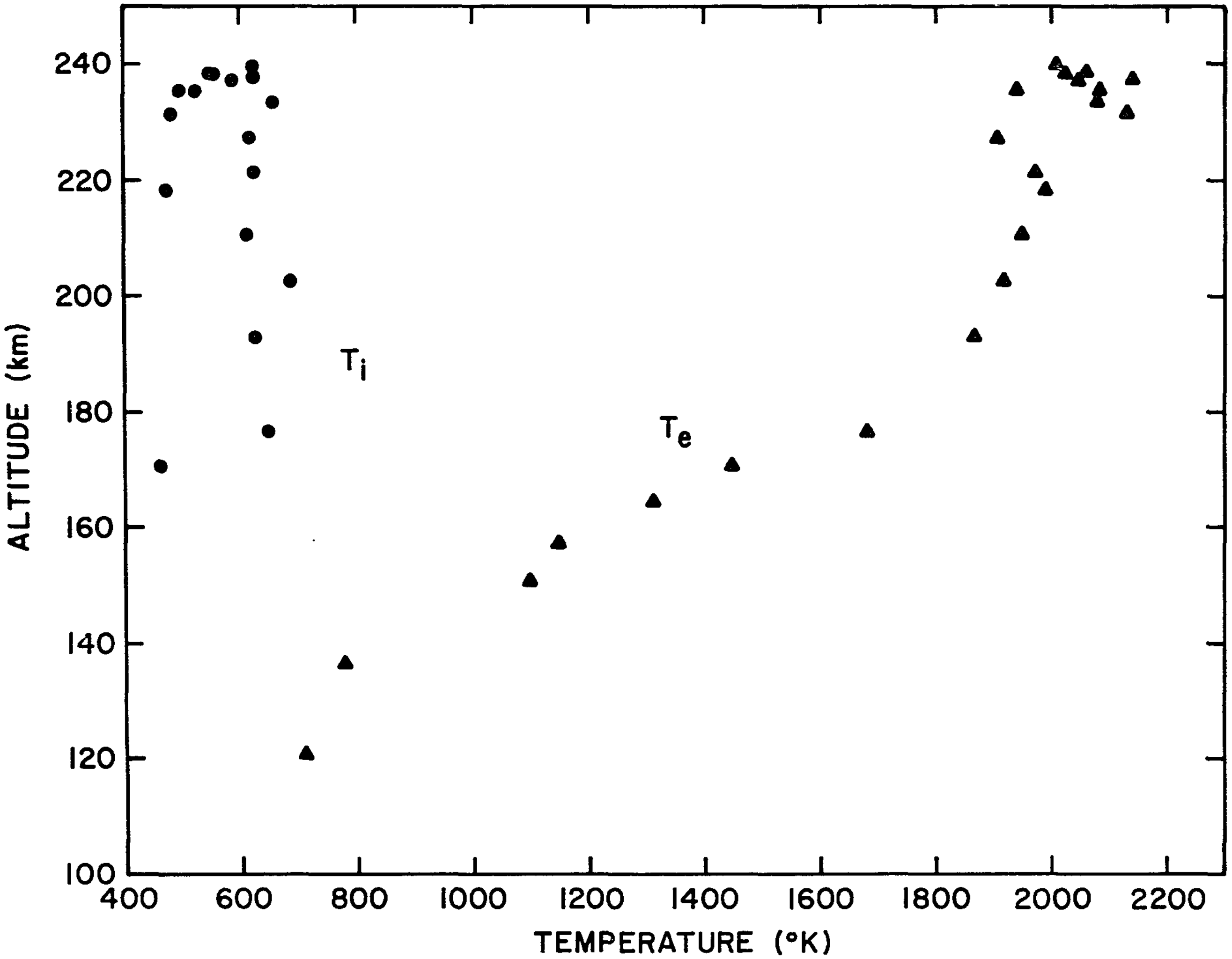

Fig. 5.1 ALTITUDE VS. ION TEMPERATURE (T_i) AND ELECTRON TEMPERATURE (T_e). FLIGHT 18.12

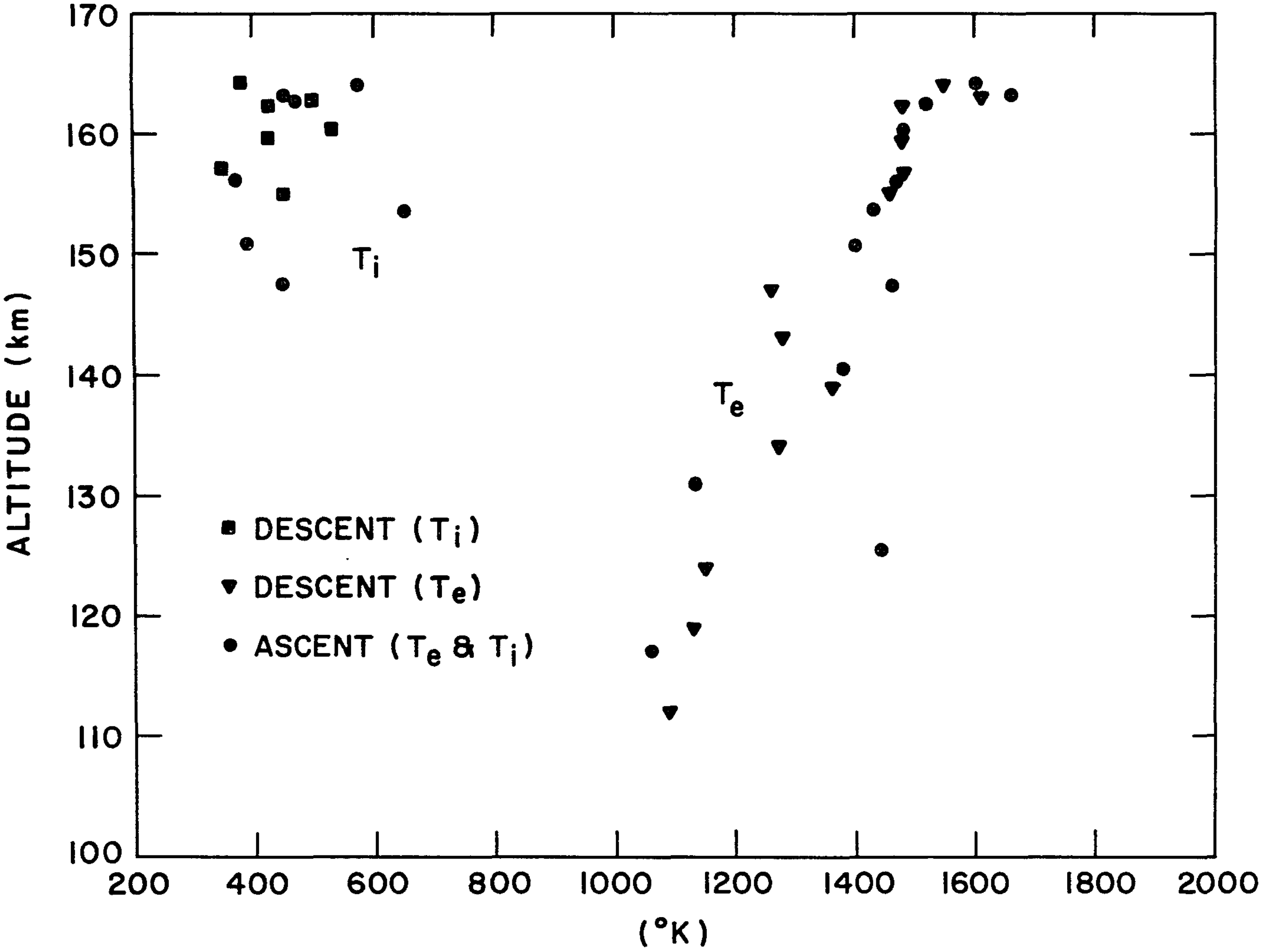

Fig. 5.2. ALTITUDE VS. ION TEMPERATURE (T_i) AND ELECTRON TEMPERATURE (T_e). FLIGHT 14.298

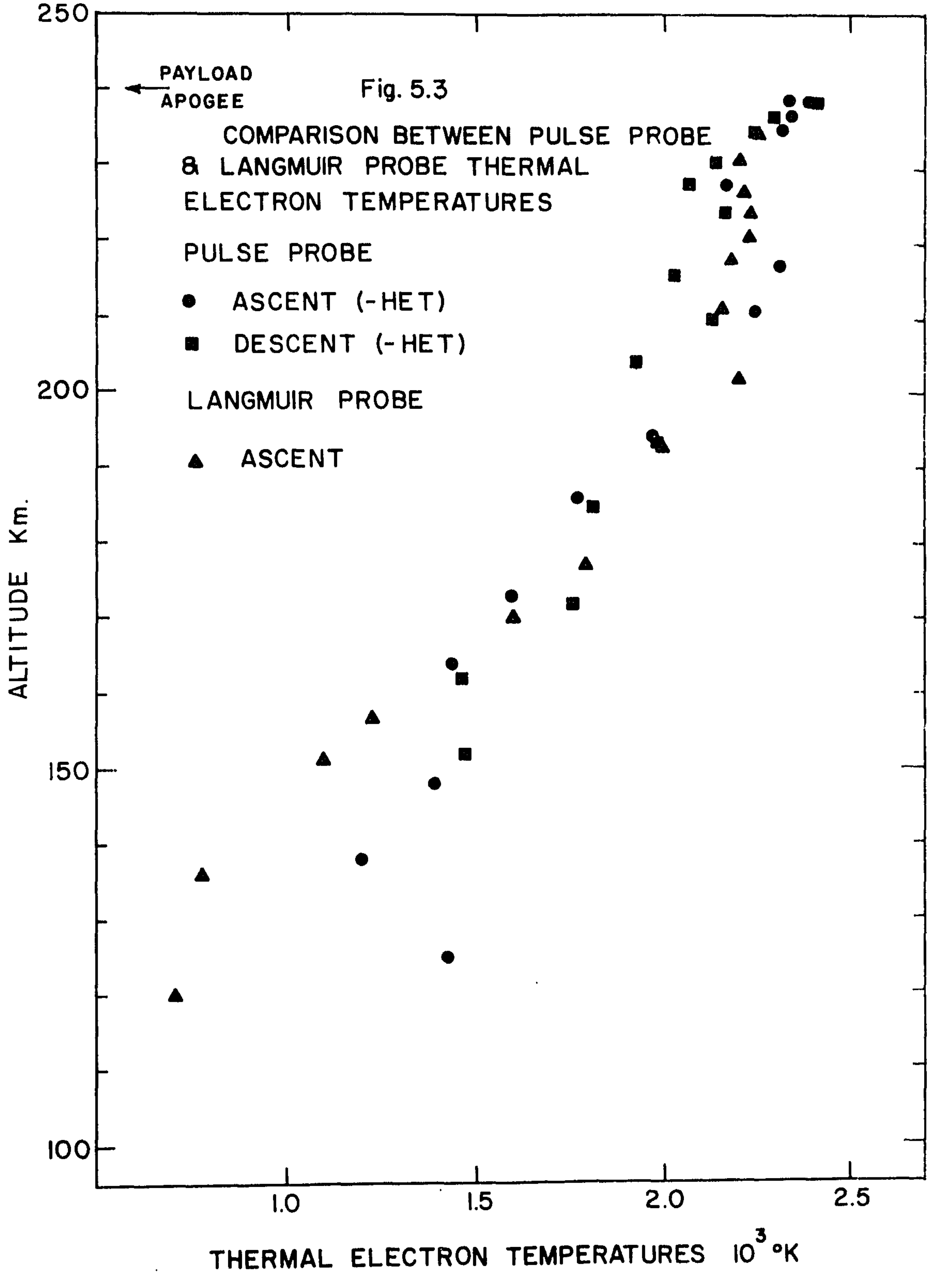

Fig.5.3 FLIGHT 18.12

2) Electron Densities (N_e)

Figures 5.4 and 5.5 give the electron density profiles plotted simultaneously with the ionosonde measurements taken at the same time and location and supplied to us by J. W. Wright and L. Wescott.[31] For both flights, it is apparent that the densities from our measurements are, especially at high altitudes, appreciably lower than the ionosonde results. We may rule out photoelectron emission from the probe as a cause of this discrepancy since there was no substantial dependence of the probe data on the aspect. That is, since the spin rate of the rocket is larger than the probe potential sweep rate, and since the probe was hemispherical, any substantial modulation which occurs when the probe aspect changes would be noticed within a given volt-ampere curve.

Ionosonde measurements are based on the reflection of radio waves by the collective behavior of the electrons and can be conveniently expressed in terms of refractive indices. When these waves traverse through a plasma in a magnetic field, there are two independent modes of propagation- called the ordinary and extraordinary waves- with their respective refractive indices. Reflection occurs when these indices become zero. Since the functional dependence of the indices on density are known, the point of reflection will give a measure of this density. For example, when the frequency of the ordinary wave equals the plasma frequency, then reflection takes place. Ideally, a wave of a given frequency is transmitted and the delay time in its return is measured. This would then give both the height and its corresponding density. However, this height, called the virtual height, differs from the real height since the group velocity of the signal is in turn dependent on the density of the plasma through which it travels. In addition, the true height at some starting point must be known. Formally, one must invert the equation

$$H(f) = \int_{o}^{h_r} n(f,N_e)dh \qquad (5.1)$$

where f is the frequency of the wave, H(f) is the virtual height, $n(f,N_e)$ is the group refractive index and h_r is the real height at reflection. An unambiguous inversion of equation (5.1) is possible only if the density varies monotonically with altitude. Generally, it is assumed that the density is monotonic in the analysis of ionosonde data. This assumption will lead to an overestimation in density if valleys exist in the density profile. For example, in the presence of valleys, the group refractive n(f,N(h)) would be overestimated and would lead to an underestimation of the real height h in equation (5.1).

As a check on our own results, we can compare the densities, found from the measured current at the plasma potential, with results from other sections of the volt-ampere curve. By using the property of charge neutrality, we use the electron densities in the calculation of ion temperatures. These results will then reflect on the accuracy of the electron densities. In addition, for the first (and also the last) few curves of each flight, the ratio of the probe to mean ion velocity is large enough so that we need retain only the first term in Equation 4.8. For ion temperatures of several hundred degrees, the ion slope is then nearly independent of T_i and we are unable to obtain T_i for low altitudes. However, we may instead use Equation 4.8 as an alternate means to find N_e (the electron density) for low altitudes. To accomplish this (as well as to find T_i at higher altitudes) it is necessary to know the percentage ion composition, and we rely on the data of Taylor and Brinton[32] for this estimate. An additional uncertainty arises in that their data was taken several years earlier, although the location was identical. Roughly we expect that the percentage error in finding N_e by equation (4.8) is of the same order as that of the percentage ion compositon. Specifically, the dominant ions are O^+, O_2^+, and NO^+ with atomic masses of 16, 32, and 30 respectively. For simplicity, we have neglected the mass difference between O_2^+ and NO^+ since this is within our range of error. Letting n_e stand for the ion density found here from the ion slope, we can compare n_e with N_e:

Flight 14.298

Curve Number	Altitude (km.)	$N_e(10^{11}$/cubic meter)	$n_e(10^{11}$/cubic meter)
1	103	.81	.82
5	117	1.12	1.06
9	126	1.00	.81
11	131	1.09	1.11
65	134	.80	..83
69	124	.76	.85
71	119	.78	.74
73	112	1.03	1.25

Flight 18.12

Curve Number	Altitude (km.)	$N_e(10^{11}$/cubic meter)	$n_e(10^{11}$/cubic meter)
1	120	1.13	.95
5	136	1.99	1.29
9	150	2.2	2.47

At these low altitudes, the ions are nearly all NO^+ and O_2^+. For intermediate heights (up to roughly 150 km) the amount of O^+ may be up to perhaps 15 percent. In this region, the O_2^+ slope is still very nearly independent of T_i (for $T_i < 1000^oK$), and any change in the

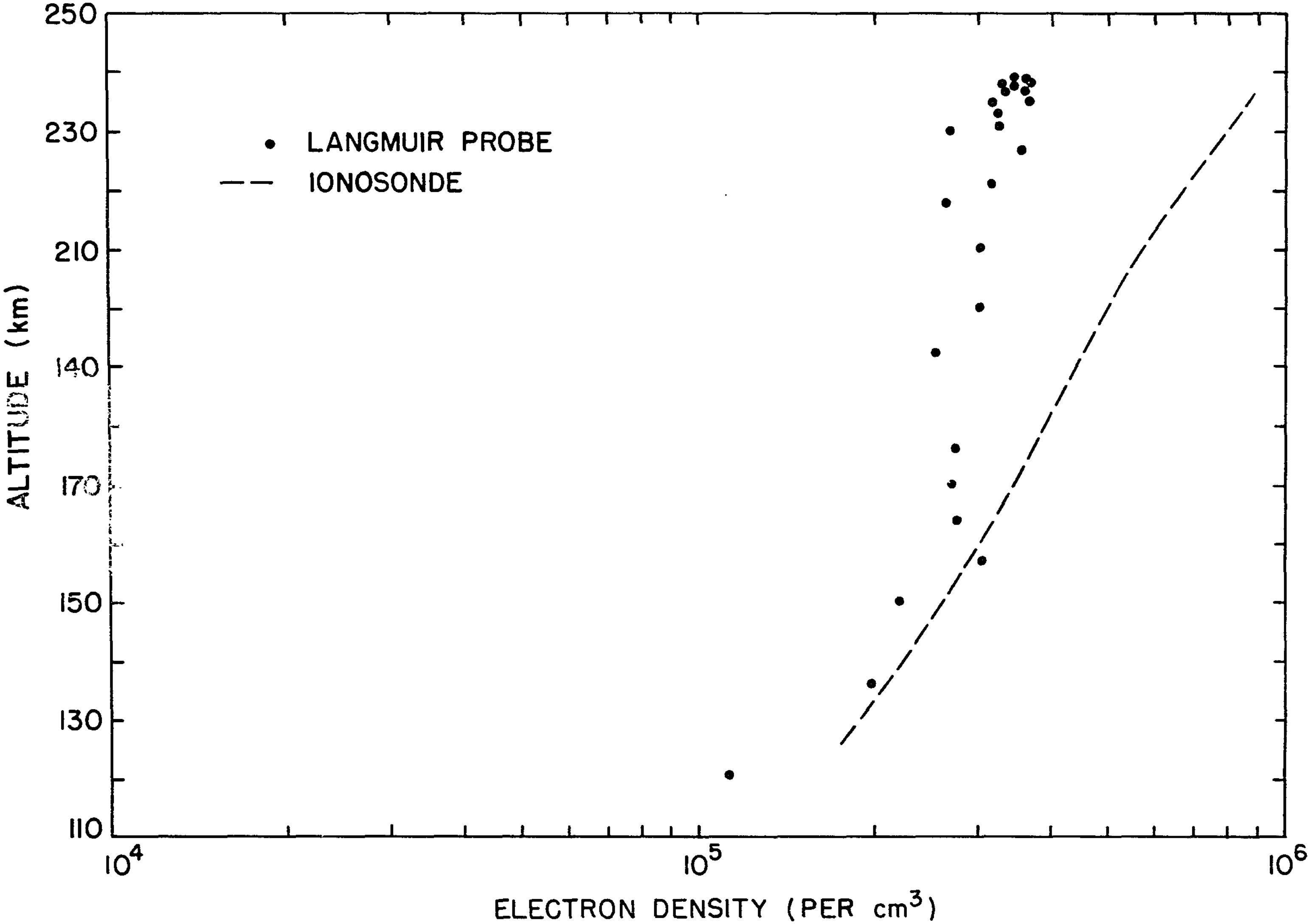

Fig. 5.4 ELECTRON DENSITY, FLIGHT 18.12

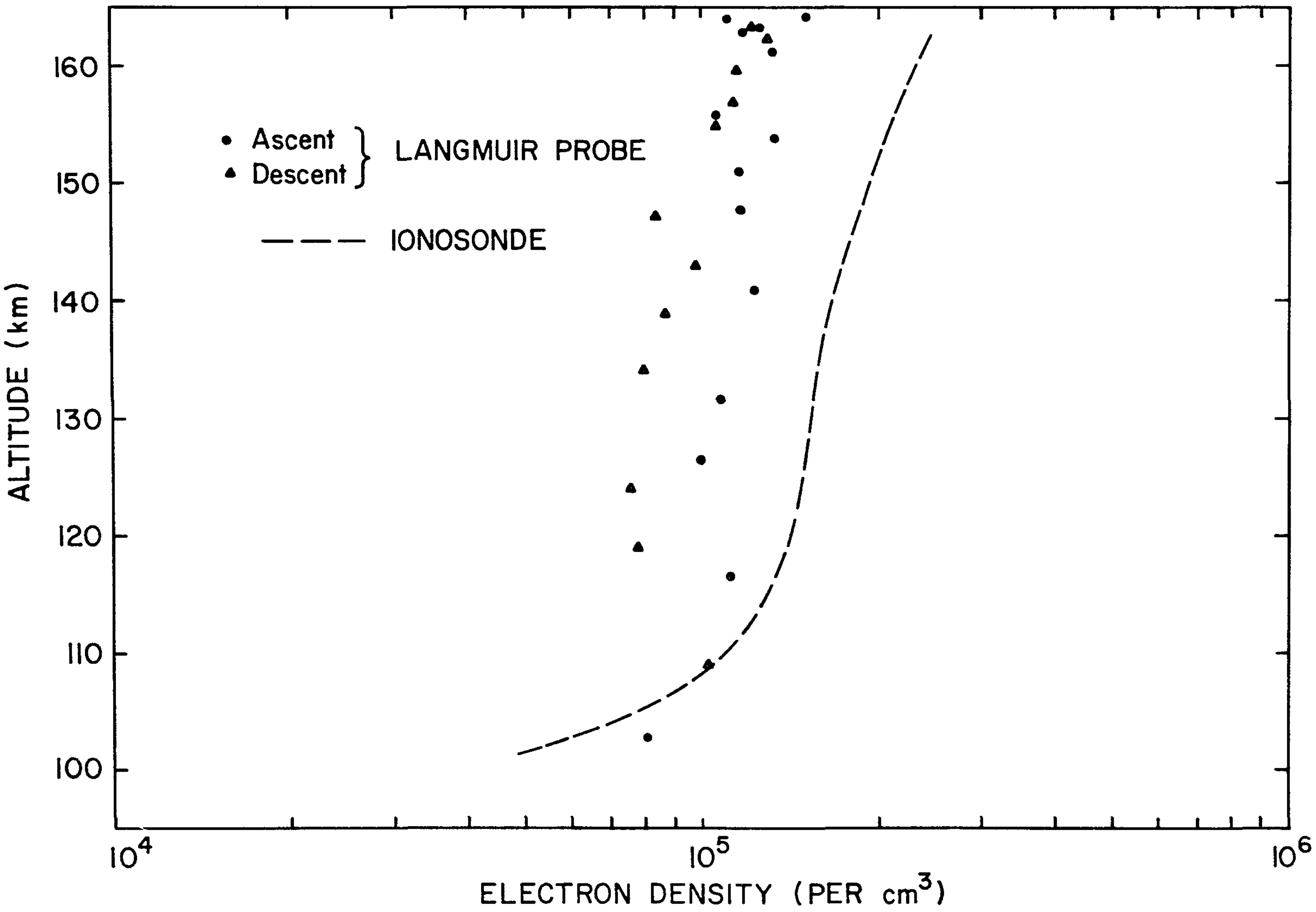

Fig. 5.5 ELECTRON DENSITY, FLIGHT 14.298

total ion slope (with respect to the probe to plasma potential) as a function of T_i is due mostly to the 0^+ current, and it is therefore especially important to have a more exact knowledge of the percentage of 0^+. Since the portion of 0^+ is small, the dependence of the total ion slope on T_i is still weak, although this situation is not as extreme as the situation at the lowest altitudes.

With one exception, (which may have been caused by fluctuations in ion composition), n_e and N_e differ by less than 15 to 20 percent. At high altitude, we may check the densities against the measured current in the electron accelerating region instead. In Section 5 B.4, we will see that for these curves, the reflection coefficient for $V \lesssim 3$ volts is near zero. Figures 5.7a and 5.7b show this fluctuation around zero. Translated into terms of density, this uncertainty is also generally less than 15 to 20 percent. Furthermore, as we shall see in the next section, these densities provide very reasonable ion temperatures, whereas if ionosonde densities are used to calculate T_i, the results would be well over $1000^\circ K$ and would be considerably larger than expected.

3) Ion Temperatures (T_i)

The ion temperature results, for the higher altitudes of each flight are given in Figures 5.1 and 5.2 along with the T_e profiles. In contrast to the density results, we have no simultaneous, independent measurements with which to compare.

To date, there is still a dearth of direct measurements of ion temperatures and the most complete results have been obtained from incoherent backscatter experiments. Keeping in mind geographical, seasonal, and diurnal variations we compare this with the incoherent radar backscatter measurements made by Evans[33] at the Millstone Hill station in Massachusetts. The average daytime T_i profile by Evans show that in the altitude range of from 150 to 250 km., T_i is between $500^{\circ}K$ and $700^{\circ}K$. We can also consider measurements of netural temperatures by Spencer, et al[34] at Wallops Island. Generally, the neutral temperature also shows a slow variation with height, and is in the neighborhood of $800^{\circ}K$.

In incoherent backscatter experiments, as with ionosondes, radio waves are transmitted to the ionosphere and the return is monitored. However, the incoherent backscatter is based on Thomson scattering caused by the statistical fluctuations in the ion and electron densities. In practice, a wave of frequency well above the penetration frequency of the ionosphere is transmitted. The resulting backscatter (caused by density fluctuations) shows a Doppler frequency broadening. Since the Doppler broadening is caused by the thermal motions of the particle, a proper spectral analysis will give the particle temperatures.

It has been shown that[35,36] if the transmitted wavelength is much larger than the ionospheric Debye length, the spectral width of the Doppler broadening is controlled by ionic motions instead of electron velocities. This is because in the presence of charge separation, electric fields are set up to restore neutrality and a plasma is able to do this over distances larger than the order of a Debye length. Since electrons have a much smaller mass, the electron density fluctuations are coupled to that of the ions. This correlation can be "seen" only by wavelengths much larger than the Debye length. For example, if the transmitted wavelength is much smaller than the Debye length, the scattering is by "free" electrons and the return frequency spectrum shows a simple Gaussian distribution (due to the Maxwellian velocity distribution of electrons) centered around the transmitted frequency. In the long wavelength case, the equations are much more complex, and it can be shown[35,36] that the Doppler broadening is controlled mainly by ion motions. However, the exact shape of the return spectrum is still dependent on the electron temperature, and both T_e and T_i can be found. A major problem associated with this method is that the scattering is very weak and high powered systems are needed. For this reason and the fact that the spectral width of the transmitted pulse must be small, long pulses are needed. Consequently, the height resolution is of the order of 15 to 75 km[33]. If continuous waves are used, the height must be determined geometrically which leads to approximately the same amount of uncertainty.

In our own results, we may expect that we underestimated T_i slightly. The reason is that in utilizing the sheath relation (3.23) in conjunction with the derivative (with respect to the probe potential) of equation (4.1), we used the electron Debye length. Near the end of Section 3.A, it was mentioned that, since $T_i < T_e$, the screening is less effective when electrons (the more energetic particles) are repelled. Therefore, the effective sheath size would be somewhat larger than for the electron collecting case, thus causing an enhancement of ion current. Because T_e is only 2 or 3 times T_i, this should not make our results too long, more than 10 to 20%.

Our ion temperatures are within 50 to 100 degrees Kelvin of that measured by the incoherent backscatter results of Evans[33] for daytime, late summer and early winter conditions. The agreement is certainly within the uncertainties of the measurement processes, and is additionally encouraging in that, at least for our range of altitudes, Evans has found no substantial seasonal variations of daytime ion temperatures[33]. A more detailed and conclusive comparison would require a statistical analysis and therefore also more data.

There is one noteworthy discrepancy between Figure 5.1, 5.2 and the backscatter results. In theory, it is expected that near heights of 100km., the thermal coupling between particles is good enough so that their temperatures are close to one another. As Evans[33] has noted, this is borne out by the backscatter data, bit is not confirmed by the results of Spencer, et al.[34], who find that the electron temperatures are always clearly larger than neutral temperatures. In this point, our results seem conflicting. In Figure 5.1, if we extrapolate T_e and T_i downward, it can be seen that the temperatures may well converge, while in Figure 5.2 (Flight 14.298), it is evident that there is no convergence.

4) Electron Reflection Coefficient (R)

In Figures 5.6 and 5.7, we have presented the electron reflection coefficient (in the accelerating region) as a function of probe to plasma potential. Two plots are given representing initial curves and the remaining curves respectively. That is, in both flights, the reflection coefficients, R, are initially as shown by Figure 5.6. As the flight progressed, there was a general systematic decrease so that after several curves, R has taken the form as shown in Figure 5.7,

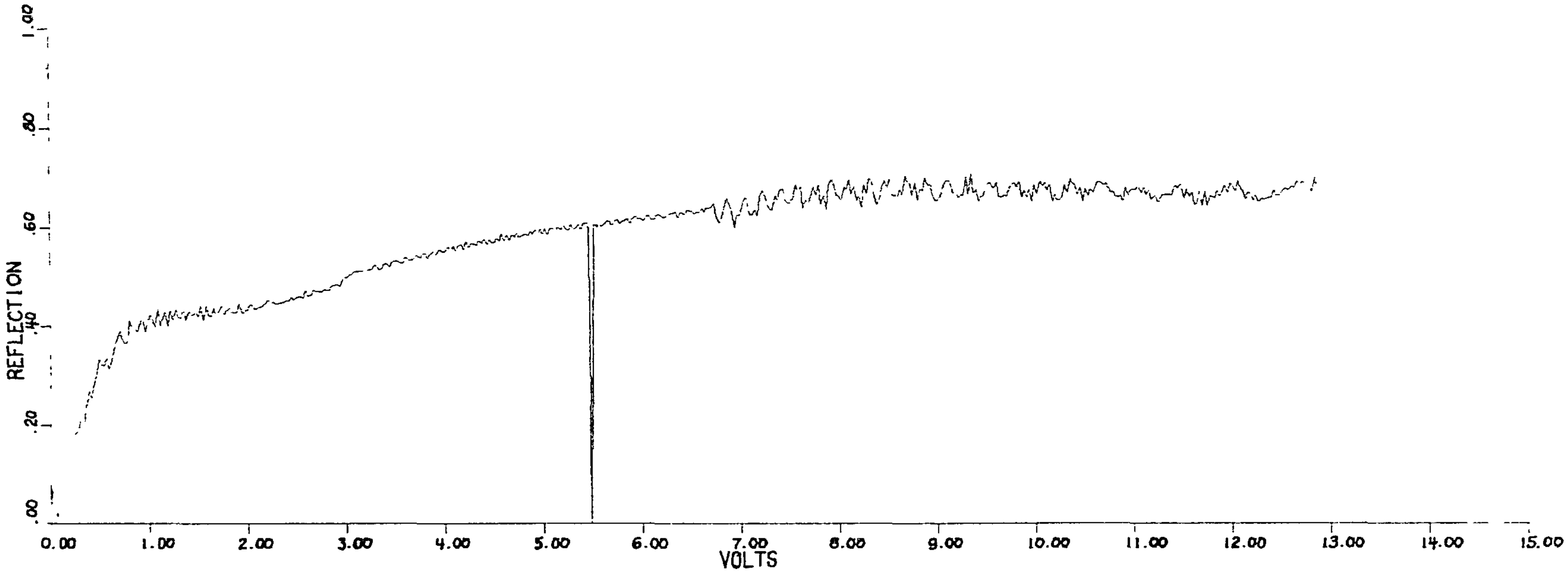

Fig. 5.6 : ELECTRON REFLECTION COEFFICIENT vs. PROBE TO PLASMA POTENTIAL
FLIGHT 18.12 CURVE NO. 1

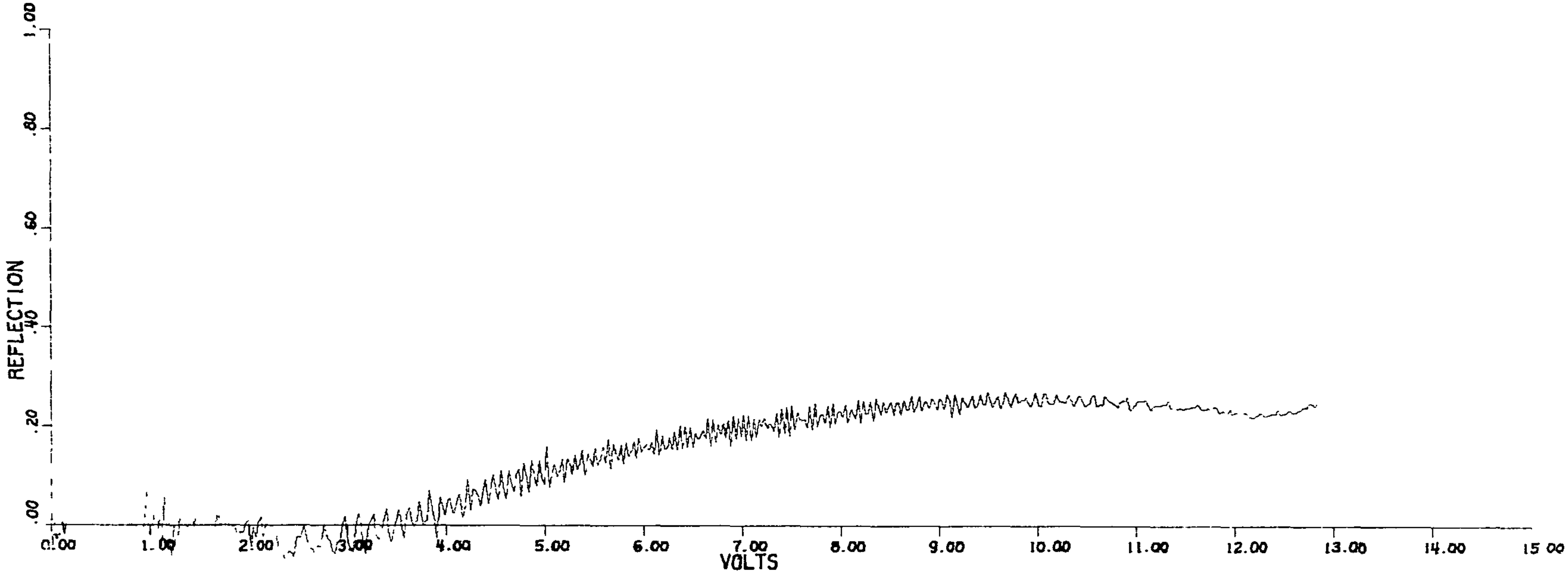

Fig. 5.7 : ELECTRON REFLECTION COEFFICIENT vs. PROBE TO PLASMA POTENTIAL

FLIGHT 18.12 CURVE NO. 49

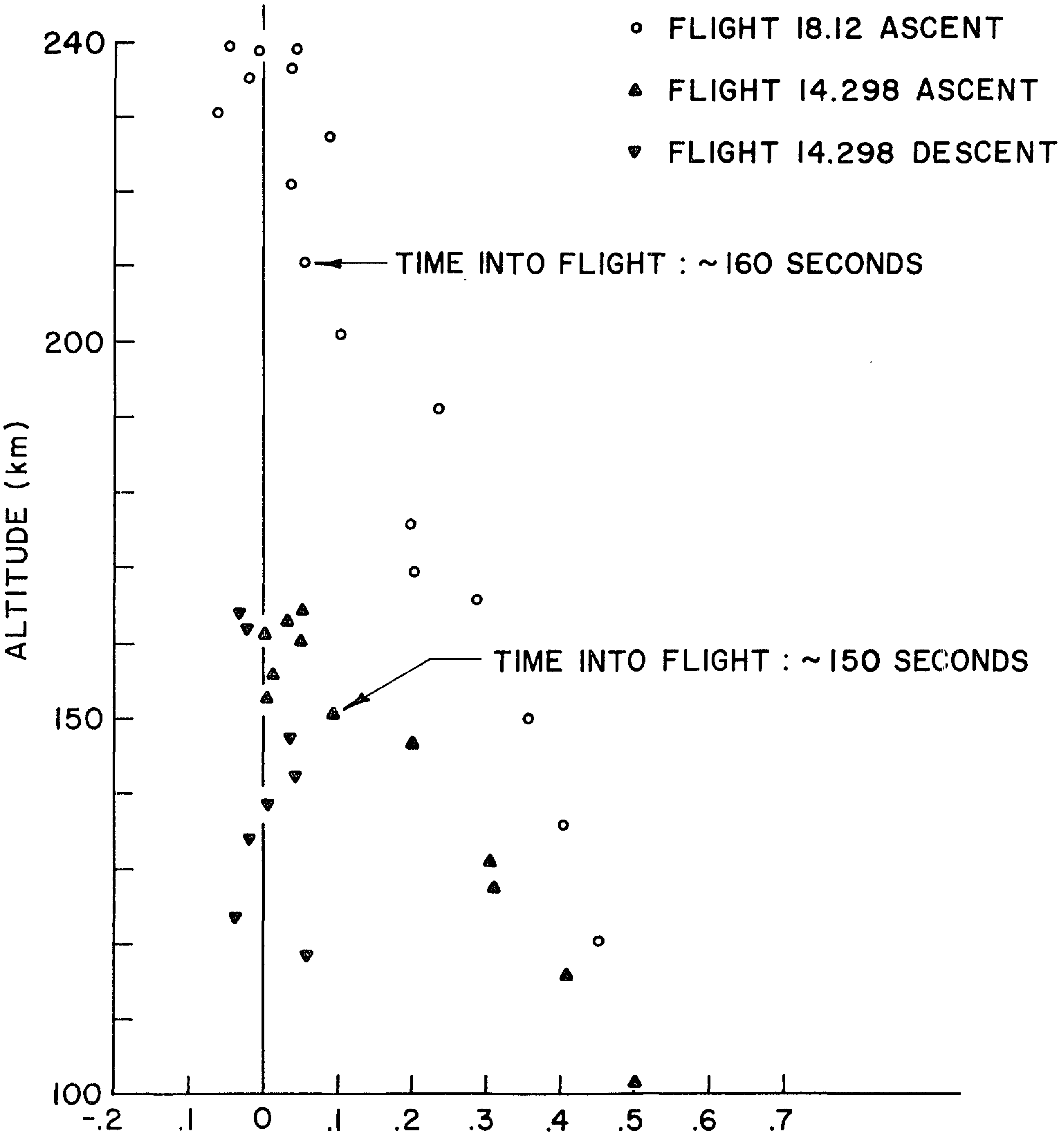

Fig. 5.7a APPROXIMATE MEAN ELECTRON REFLECTION COEFFICIENT IN THE INTERVAL 0.0 TO 3.0 V

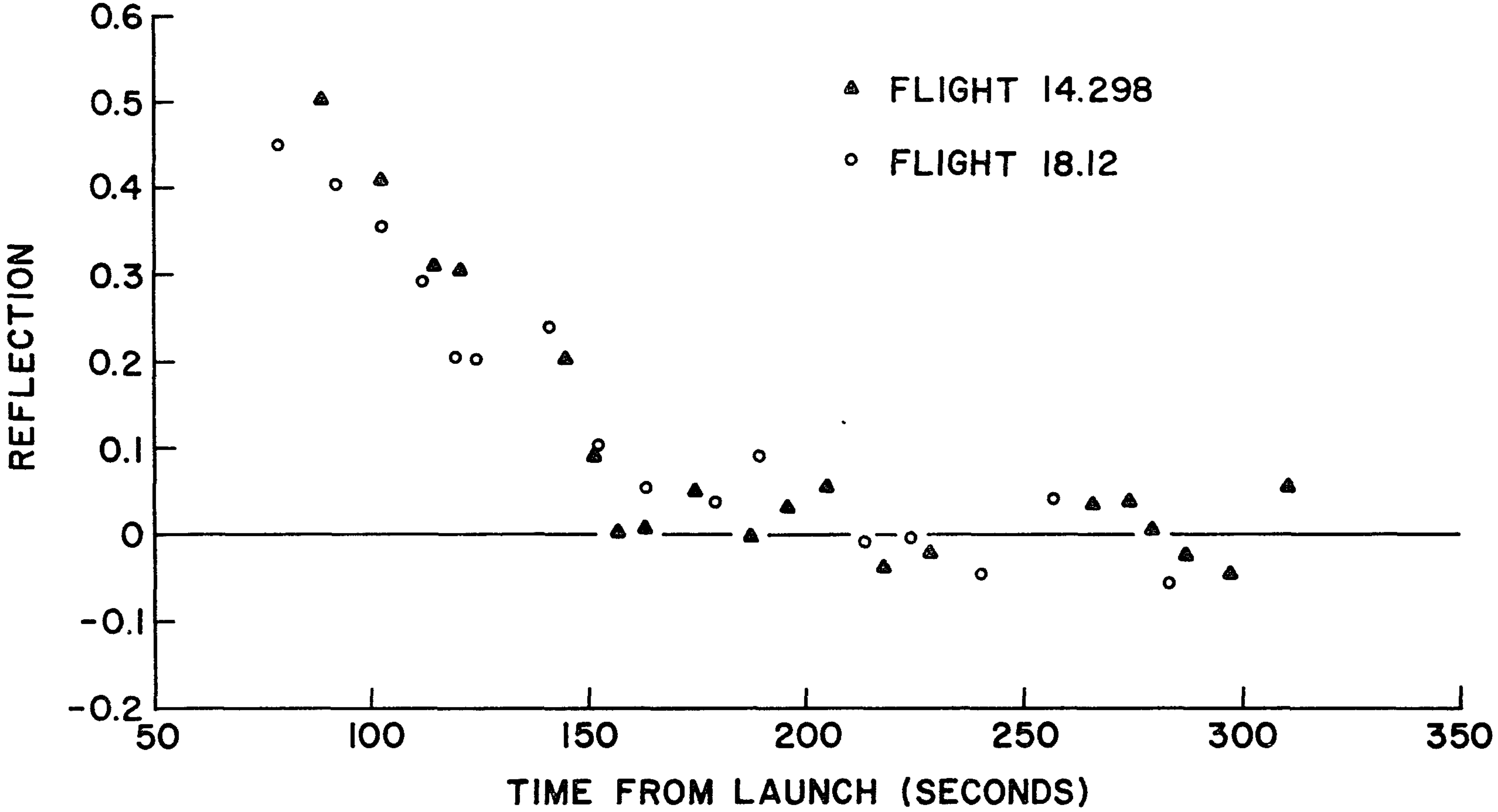

Fig. 5.7b AVERAGE ELECTRON REFLECTION COEFFICIENT FROM 0.0 TO 3.0 VOLTS vs. TIME FROM LAUNCH

and remained thus through the rest of the flight. (The regions where abnormal noise exists indicates a switch in electrometer sensitivity.) Most notable is that in Figure 5.7 the reflection coefficient has decreased to a near zero value for values of V between 0 and 3 volts. The behavior of R in this potential interval is plotted as a function of altitude in Figure (5.7a) and as a function of time from launch in Figure (5.7b). It can be seen that this decrease, as a function of time, is very similar for both flights, and that it is sustained throughout the remainder of Flight 14.298. This points to a corresponding decrease in the surface contaminants of the probe. (For Flight 18.12, we obtained no usable data on the downleg portion. For example, in the electron retarding region, there was obvious deviation from an exponential dependence, and a rough fit to this current gave temperatures well above 10,000°K. This failure was apparently isolated to the Langmuir probe section of the payload since the pulse probe continued to provide reasonable data throughout the flight, although we have not been able to identify the exact cause of the malfunction.)

In Section 3.D, we had briefly mentioned the nature of the reflection coefficients from laboratory experiments, which show a strong dependence on surface impurities and the crystalline structure of the surface itself. We have in our case the additional complication of the existence of an attracting probe potential. As Mott-Smith and Langmuir[6] have mentioned, electrons which are reflected inelastically need only lose a small part of their incident energy so as to be unable to escape back outside the sheath. Unfortunately, however, theoretical interpretations on the detailed nature of reflection as a function of incident energy have generally not been conclusive.

Although a decrease of surface contaminants would lower the percentage of reflected electrons, in order to justify the decrease of R to zero, it would be necessary that the electron reflection has also become sufficiently inelastic in the region of 0 to 3 volts so that the reflected electrons are not left with sufficient energy to escape the attractive probe potential. This, however, is strongly suggested by the similar behavior of the two flights and the consistency in the decent portion of Flight 14.298.

Finally, the similarity of our results for the electron accelerating region between the two flights would also confirm the validity of the sheath relation (3.23). For example, in Flight 14.298, where the probe radius is of the order 0.2 Debye lengths, the electron current is roughly .90 that of the limiting case of an infinite sheath. In Flight 18.12, the probe radius was slightly larger for an infinte sheath. Since the probe sizes were so different, the similarity between the electron reflection coefficients for the two flights is encouraging.

C. Summary and Discussion

Although much progress in ionospheric measurements have been made in the last decade, there are still discrepancies among the different experimental processes. This is underscored by attempted comparisons made among the results of different experimental methods. Detailed comparisons are, however, mostly precluded by diurnal, seasonal, geographical, and solar variations of ionospheric phenomena.

In our analysis, we have followed the steps discussed in Chapters III and IV and outlined at the end of Chapter IV. These included sheath sizes, patch effects, vehicle potential, electron reflection coefficients, and probe velocities. We have seen that the existence of patches causes a premature break and a general enhancement of the electron retarding current. If neglected, this would cause the overestimation of the electron density and temperature, although the difference would be only a few percent in the latter case. In light of the above considerations, it is unfeasible to directly estimate the degree of error and uncertainties of the results obtained here. We have, therefore, relied on empirical and consistency criteria for a measure of these errors. Specifically, we have compared different portions of a given volt-ampere curve and also the results between the different flights.

At the end of Chapter IV, we had outlined the methods used to obtain our results and the relationships between the different portions of a volt-ampere curve. The results show consistent agreement between the accelerating, retarding, and zero potential portions a volt-ampere characteristic. For example, at low altitudes, there is general accord between densities calculated from the ion section and the zero potential electron current (p.). At high altitudes, due to the smaller probe velocity, independent densities from the ion calculating region could not be obtained. On the other hand, at the high altitudes, the electron densities were used in the calculation of ion temperature and gave quite reasonable results. We have also seen that in the interval 0 to 3 volts of the electron accelerating region, the densities lead to a reflection coefficient of up to 0.5 which then decreased to approximately zero as the flights progressed. We have interpreted this as a corresponding decrease in probe surface contaminants since the zero reflection is sustained for the rest of Flight 14.298 (we had no usable descent data in Flight 18.12). This decrease in electron reflection coefficient is also compatible with the electron densities found from the ion accelerating region for low altitudes.

Finally, since the above results apply to both flights, and since the considerable difference in sheath of probe dimensions between the flights give corresponding differences in the accelerating regions, it would be very improbable that the internal consistency of a given volt-ampere curve be fortuitous.

In Figures 5.8 and 5.9 we have reproduced, for each flight, a representative curve showing the raw data along with a "reconstructed curve." These plots are semi-logarithmic and the units differ from amperes by a multiplicative factor. The portions shown correspond to the region CDH in Figure 4.1. The reconstructed curves were obtained from the results of electron density and temperature, and patch distribution. These results were substituted into equations 3.29 and 3.35 to obtain a consistency check with the data. In Flight 14.298 (Figure 5.8) the fit at the point marked D is not as clase as that in Figure 5.9. This stems from the fact that the point of break from an exponential could not be clearly pinpointed and thus a "compromise" was made. We have also extended the comparison to the electron accelerating region of the curve and may be seen in Figures 5.6 and 5.7. If we assume that at the higher altitudes, the net reflection is indeed zero (up to ∿ 3 volts), then our choice of zero potential is generally of the order of .02 volts in uncertainty. This was arrived at by varying the zero potential point for several representative curves and finding the value of best fit.

In the same figures, we have also shown the relative location of the ambient current which was defined in equation (3.8):

$$I_o = AN_e e\sqrt{\frac{kT_e}{2\pi m_e}} .$$

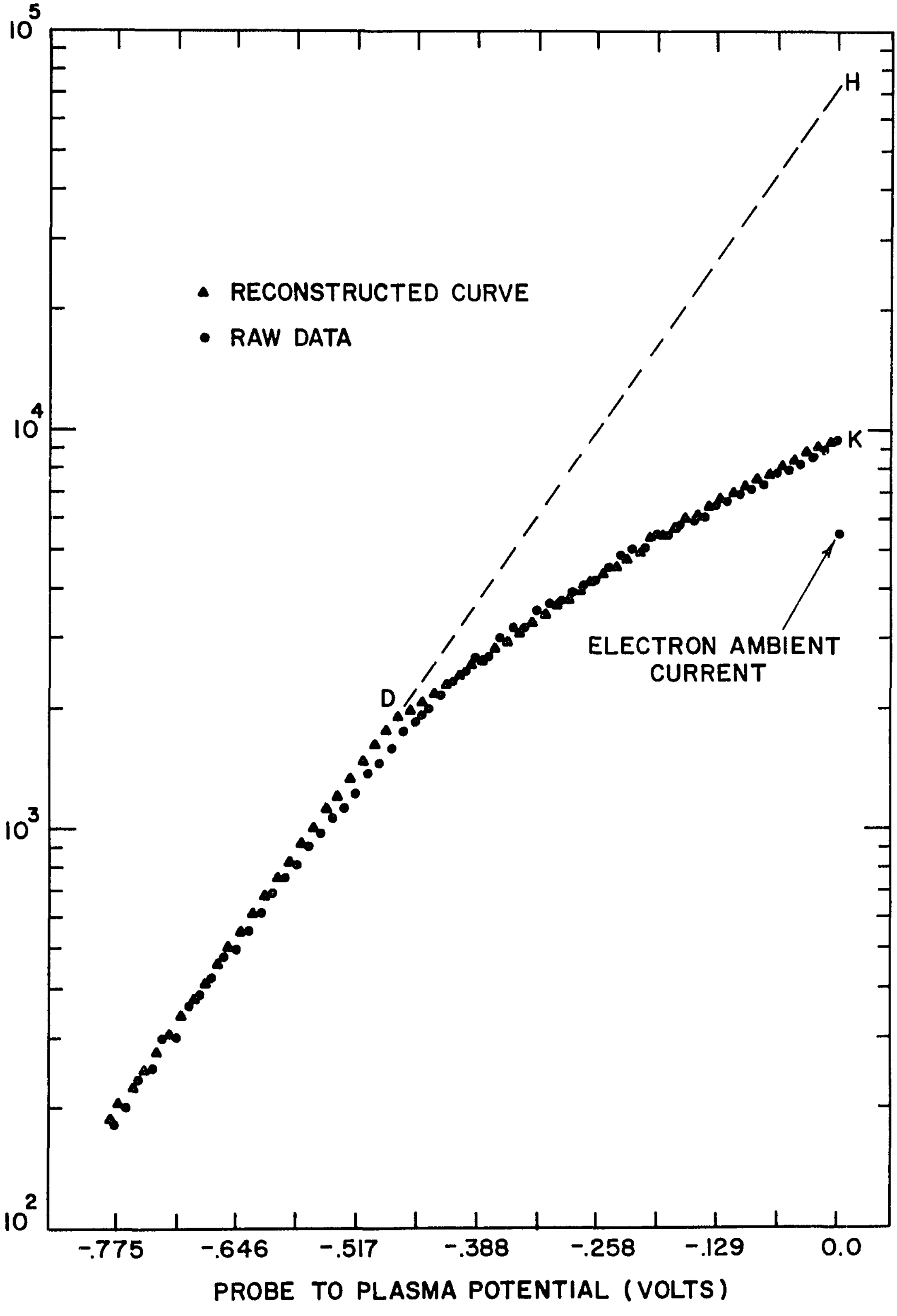

Fig. 5.8 LANGMUIR PROBE CURVE NO. 33, PLOT OF COUNTS vs. PROBE TO PLASMA POTENTIAL, CURRENT (AMPERES) = COUNTS × 2.1 × 10^{-12}, FLIGHT 14.298

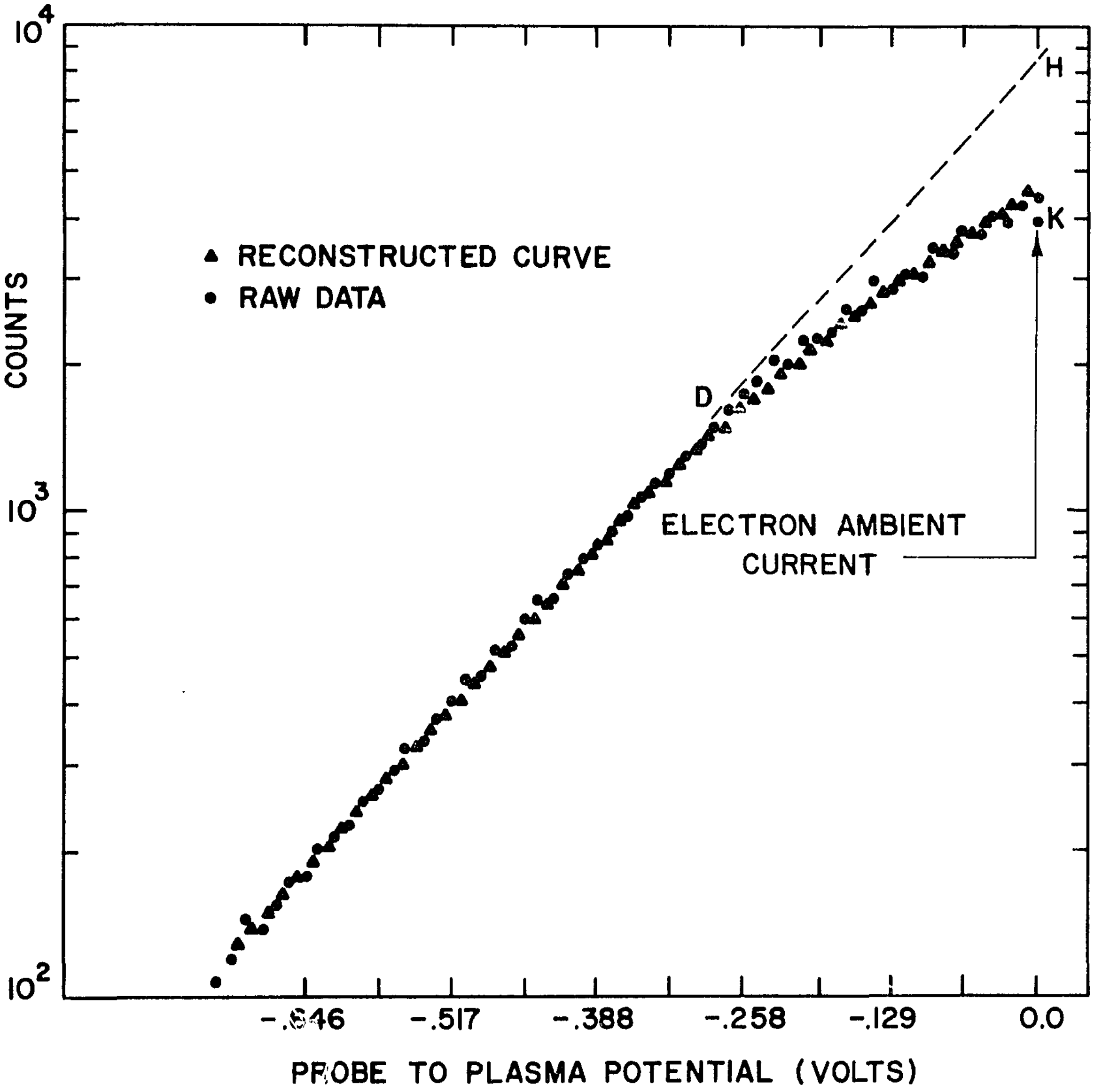

Fig. 5.9 LANGMUIR PROBE CURVE NO. 49, PLOT OF COUNTS vs. PROBE TO PLASMA POTENTIAL, CURRENT (AMPERES) = COUNTS × 2.4 × 10^{-10}, FLIGHT 18.12

This corresponds to I_o in Figure 4.1, and shows the enhancement in current due to patches. We had noted in Section 3.B. that we do not know exactly how quickly the patch fields decay. Thus, it would be worthwhile to make further measurements under different conditions for the sake of comparison. For example, in the case of planer geometry and accelerating potentials, the electron current collected cannot increase with potential. This is because the sheath area is equal to the probe and by current conservation, the current reaching the probe is the same as the thermal (or ambient) current crossing the sheath and cannot increase beyond that. Since some of the patches repel electrons, it is expected that the effect of the patches would depress rather than enhance the current collected by a planer probe in contrast to a spherical probe. In addition, a planer geometry would not be sensitive to sheath thickness nor to the exact behavior of the patch fields and it is expected that the depression in current would be of the order of 10 percent[21].

REFERENCES CITED

1) Dalgarno, A., McElroy, M.B., and Walker, J.C.G., "The Diurnal Variation of Ionospheric Temperatures," Planetary Space Sci. 12, 235-246 (1967)

2) Evans, J. V., "Cause of Mid-latitude Evening Increase in f_oF2," J. Geophys. Res. 70, 1175-1185 (1965)

3) King, J. W. and Newman, W.S. (eds.)(1967). Solar Terrestrial Physics, Academic Press, New York

4) Rishbeth, H. and Garriot, O.K., Introduction to Ionospheric Physics, Academic Press, New York (1969)

5) Hine, C.O., Paghis, I., Hartz, T.R., and Fijes, J.A., Physics of the Earth's Upper Atmosphere, Prentice Hall, New Jersey (1965)

6) Langmuir, I. and Mott Smith, H.M., "Theory of Collectors in Gaseous Discharges," Phys. Rev., 28 (4), 727 (1926)

7) Bettinger, R.T., "An In Situ Probe System for the Measurement of Ionospheric Parameters," Ph.D. Thesis, University of Maryland, Department of Physics and Astronomy, Tech. Rep. No. 277 (1964)

8) Huang, P.T., "Direct Measurements of Electron Energy Distributions in the Daytime Ionosphere," Ph.D. Thesis, University of Maryland, Department of Physics and Astronomy, Tech. Rep. No. 936 (1969)

9) Langmuir, I. and Tonks, L., "A General Theory of the Plasma of an Arc," Phys. Rev., 34, 876 (1929)

10) Bohm, D., Burhop, E., and Massey, H., In: Characteristics of Electrical Discharges in Magnetic Fields, Ed. Guthrie and Wakerling McGraw Hill, (1949)

11) Allen, J.E., Boyd, R.L.F., and Reynolds, P.,"The Collection of Positive Ions by a Probe Immersed in a Plasma," Proc. Phys. Soc. B., Vol. 70, p.297 (1957)

12) Bohm, D., In: Characteristics of Electrical Discharges in Magnetic Fields, Ed. Guthrie and Waherling, McGraw Hill, (1949)

13) Chen, F.F. , In: Plasma Diagnostic Techniques, Chapter IV, Ed. Huddlestone, R.H., and Leonard, S.L., Academic Press, N.Y. (1965)

14) Bernstein, I.B. and Rabinowitz, I.N., "Theory of Electrostatic Probes in a Low Density Plasma," Phys. of Fluids, 2 (2), 112, (1959)

15) Al'pert, Ya L., Gurevich, A.V., and Pitaevskii, L.P., Space Physics with Artificial Satellite, Consultants Bureau, New York (1965), Translated by H. H. Nickle

16) Laframboise, J.G., "Theory of Spherical and Cylindrical Langmuir Probes in a Collisionless Plasma at Rest," University of Toronto, Institute of Aerospace Studies Report No. 100,(June 1966)

17) Bettinger, R.T. and Walker, E.H., "Relationship for Plasma Sheaths about Langmuir Probes," Phys. of Fluids, 8, (4), 748 (1965)

18) Herring, C. and Nichols, M.H., "Thermionic Emission," Revs. of Mod. Phys. 21, (2), 185 (1949)

19) Haas, G.A. and Thomas, R.E., "Electron Beams Scanning Technique for Measuring Surface Work Function Variations," Surface Sci. 4, 64 (1966)

20) Haas, G.A. and Thomas, R.E., "Investigation of the Patch Effect in Uranium Carbide," J. of Appl. Phys. 34, (12), 3457 (1963)

21) Heil, H., "Electron Reflection Ceofficient at Zero Energy. Computer Experiments on the Reflection of Slow Electrons in the Electrostatic Field of Surface Patches," Phys. Rev., 164, (3), 887 (1967)

22) Heil, H., "Electron Reflection Coefficient at Zero Energy I. Experiments," Phys. Rev., 164, (3), 164 (1967)

23) Fowler, H.A. and Farnsworth, H.E., "Reflection of Very Slow Electrons," Phys. Rev., 111, (1), 103 (1958)

24) Kisluik, P., "Reflection of Slow Electron from Tungsten Single Crystals, Clean and with Adsorbed Monolayers," Phys. Rev., 122, (3), 405 (1960)

25) Armstrong, R.A., "Reflection of Slow Electron By Hydrogen-Covered Single Crystals of Tungsten," Canadian J. of Phys., 44, 1753 (1966)

26) Bettinger, R.T., "Wing Slope Techniques for the Analysis of Langmuir Probe Characteristics," JAP, 38, 2523-2527 (May 1967)

27) Smiddy, M. and Stuart, R.P., "An Analysis of the Behavior of a Multi-Grid Spherical Sensor in a Drifting Maxwellian Plasma," Air Force Cambridge Research Laboratories, Physical Sciences Research Papers, No. 364 (1969)

28) Shea, J.J. and Carpenter, K.H., "Investigation of Current Voltage Characteristics of Spacecraft Mounted Spherical Electrostatic Analyzers," Air Force Cambridge Research Labs., No. AFCRL-63-0588

29) Scarborough, J.B., Numerical Mathematical Analysis (6th ed.), John Hopkins Press, Baltimore (1966)

30) Ralston, A., "Methods for Numerical Quadrature," In: Mathematical Methods for Digital Computers, Ralston, A., and Wilf. H.S., eds., Part VI, John Wiley and Sons (1967)

31) Wright, J.W. and Wescott, L., Private Communication

32) Taylor, H.A. and Brinton, H.C., "Atmospheric Ion Composition Measured Above Wallops Island, Virginia," J. of Geophys. Res., 66, (8), 2587 (1961)

33) Evans, J.V., "Ground Based Measurements of Atmospheric and Ionospheric Particle Temperatures," In: Solar-Terrestrial Physics, Chapter IX, Eds. J.W. King and W.S. Newman, Academic Press, New York (1967)

34) Spencer, N.W., Brace, L.H., Carignan, G.R., Taeusch, D.R. and Niemann, H. J., "Electron and Molecular Nitrogen Temperature and Density in the Thermosphere," J. of Geophys. Res., 70 (11), 2665 (1965)

35) Fejer, J.A. "Scattering of Radio Waves by an IOnized Gas in Thermal Equilibrium." Can. J. Phys. 38, 1114-1133, 1960.

36) Dougherty, J.P., and Farley, D.T. " A Theory of Incident Scattering of Radio Waves by a Plasma." Proc. Royal Soc. (London) A259, 79-99, 1960.

Appendix A

List of Main Computer Programs Used (Section 4.E)

Program Number I: A(I) in this program correspond to the coefficients of the polynomial fit. AW(I) corresponds to the coefficients of a linear fit to the log of the current in the electron retarding region.

```
C      N10 =  10* THE NUMBER OF RECORDS TO BE READ
C   MA IS THE NUMBER CF SUBTRACTIONS TC GET ELECTRCN CURRENT FROM TCTAL
C MA1 IS  THE NUMBER CF SUBTRACTICNS TC GET ELECTRCN CURRENT FROM TOTAL
C  AFTER ZERO SWEEP IS REACHED
C  MA2 IS THE NUMBER OF FITS IN THE EXPOTENTIAL SECTION
C   MA3 IS THE THE NUMBER OF ELECTRCN CATA PRINTED OUT AFTER THE ION
C SECTION
C    JN1, JN2, ...,JN6  ARE THE INDECIES FOR AVERAGING IN SWEEP CAL
C      NW  IS ORDER OF FIT FOR SWEEP
C    NY  IS ORDER OF FIT FOR ION SECTICN
C  NF  IS THE RECORD BEFORE THE FIRST RECORC TO BE USED
C     NOI=NO. IN EACH OF THE TEN MATRICES
C     NK=DIMENSION OF EACH OF TEN MATRICES
C     JA IS INDEX FOR BEGINNING OF ION FIT
C      JB  IS INDEX FCR END OF THE ION FIT
C   MA6 IS NUMBER OF PCINTS AFTER EXTENSION CF ION PART TO START
C     SATURATION AVERAGE
C                       MA7 IS NUMBER OF PTS IN AVERAGE FOR SATURATION
C   MA8  IS  LCWER LIMIT FOR ION SATURATION
C   MA9  IS  UPPER LIMIT FOR ION SATURATION
C   MA10 IS LOWER   LIMIT FOR  ZERO CURRENT
C   MA11 IS UPPER   LIMIT FOR  ZERC CURRENT
C   MA12/5 IS THE NUMBER ADDED TO JB TC GET FIT TO SWEEP
      DIMENSION    A1(11)
      DIMENSION    A2(11)
      DIMENSION    IA1( 765),    S( 765),    C(3825),
     I   M6( 5),  M7( 5),  M8( 5),  JA( 5),  JB( 5),  MY( 5)
      COMMON  C ,   CZERO,   ICO,
     I   NF,   N10,
     I JN1, JN2, JN3, JN4, JN5, JN6,
     I  MY,
     I  JA,
     I  JB,
     I  M6,
     I  M7,
     I  M8,
     I MA, MA1, MA2, MA3, MA4, MA5,
     I      MA6,  MA7,  MA8,  MA9,  MA10,  MA11
     I  ,  S
      NW=1
      NY=1
      READ  (5,4)  NF, N10,
     I JN1, JN2, JN3, JN4, JN5, JN6,
     I  MY,
     I  JA,
     I  JB,
     I  M6,
     I  M7,
     I  M8,
     I MA, MA1, MA2, MA3, MA4, MA5,
     I      MA6,  MA7,  MA8,  MA9,  MA10,  MA11
     I  ,  MA12
      WRITE (6,4)  NF, N10,
     T JN1, JN2, JN3, JN4, JN5, JN6,
     T  MY,
```

```
     I   JA,
     I   JB,
     I   M6,
     I   M7,
     I   M8,
     I MA, MA1, MA2, MA3, MA4, MA5,
     I       MA6,  MA7,  MA8,  MA9,  MA10,  MA11
     I   ,   MA12
   4 FORMAT  (2I6/6I6/5I6/5I6/5I6/5I6/5I6/5I6/6I6/6I6/1I6)
     DO 906  I=1,NF
     CALL READ (IA1)
 906 CONTINUE
     CALL  ORDER  (0)
     WRITE  (6,161)     ( S(IB),IB=1,765,40)
     DO   902  I=1,N10
     M8I=M8(I)
     DO  20   MX=1,M8I
     CALL  READ(IA1)
  20 CONTINUE
     M6I=M6(I)
     M7I=M7(I)
     CALL ORDER   ( 2)
     CALL ZERO   (M6I,M7I)
     MYI=MY(I)
     DO 21  MX=1,MYI
     CALL   READ(IA1)
  21 CONTINUE
     CALL ORDER   ( 2)
     JAI=JA(I)
     JBI=JB(I)
     JB2=JB(I)+MA12
     WRITE  (6,161)     ( S(IB),IB=1,765,40)
 161 FORMAT  (  10X,10F7.2)
     CALL FIT (           S,    JAI,   JB2, NW,    1,  A1,   A2)
     DO 82 LC=1,11
     A2(LC)=A1(LC)
  82 CONTINUE
     CALL FIT (           S,    JAI,   JBI, NY,    0,  A2,   A1)
     CALL YFIT  (     JAI,   JBI,   A1,   A2,  1)
 902 CONTINUE
     STOP
     END
```

The following is the list of subroutine READ of program number I

```
   HUANG              205/04/104
      ASSEMBLED TEXT.

                        $TEXT  CDC160

                                                          ENTRY  READ

BINARY CARD ID. CDC10002
       00000   1 00000 0 00005   10001   READ     SAVE     1,2,4
       00001   0774 00 2 00000   10000
       00002   0774 00 1 00000   10000
       00003   0774 00 4 00000   10000
       00004   0020 00 4 00001   10000
       00005   0634 00 4 11000   10011
       00006   0634 00 4 00513   10001
       00007   0634 00 4 00003   10001
       00010   0634 00 1 00002   10001
       00011   0634 00 2 00001   10001
       00012   0500 00 4 00003   10000            CLA      3,4
       00013   0621 00 0 00034   10001            STA      A1
       00014   0621 00 0 00041   10001            STA      A2
       00015   0621 00 0 00045   10001            STA      A3
       00016   0600 00 0 00052   10001            STZ      EOFF
       00017   0074 00 4 12000   10011            TSX      RCSBIN,4
       00020   0020 00 0 01004   10011            TRA      *+4
       00021   0 00000 0 00000   10000            PZE
       00022   2 00010 0 00000   10000            TIX      0,0,8

BINARY CARD ID. CDC10003
       00023   2 00000 1 00462   10001            TIX      IOC,1,0
       00024   2 00461 1 00460   10101            TIX      EOFX,1,EOFX+1
       00025   0520 00 0 00052   10001            ZET      EOFF
       00026   0020 00 0 00051   10001            TRA      OUT
       00027   0774 00 1 00000   10000            AXT      0,1
       00030   0774 00 2 00000   10000            AXT      0,2
       00031   4500 00 1 00054   10001   L1       CAL      B,1
       00032   4320 00 0 00515   10001            ANA      =O777700000000
       00033   0771 00 0 00030   10000            ARS      24
       00034   0601 00 2 00000   10000   A1       STC      **,2
       00035   1 77777 2 01001   10011            TXI      *+1,2,-1
       00036   4500 00 1 00054   10001            CAL      B,1
       00037   4320 00 0 00516   10001            ANA      =O77770000
       00040   0771 00 0 00014   10000            ARS      12
       00041   0601 00 2 00000   10000   A2       STC      **,2
       00042   1 77777 2 01001   10011            TXI      *+1,2,-1
       00043   4500 00 1 00054   10001            CAL      B,1
       00044   4320 00 0 00517   10001            ANA      =O7777
       00045   0601 00 2 00000   10000   A3       STC      **,2

BINARY CARD ID. CDC10004
       00046   1 77777 2 01001   10011            TXI      *+1,2,-1
       00047   1 77777 1 01001   10011            TXI      *+1,1,-1
       00050   3 77401 1 00031   10001            TXH      L1,1,-255
                         00051            OUT      RETURN   READ
       00052   000000000000      10000   EOFF     OCT      0
       00053   200000000001      00001   ID       BSS      1
       00054   200000000404      00001   B        BSS      260
       00460   4625 00 0 00052   10001   EOFX     STL      EOFF
       00461   0020 00 4 00001   10000            TRA      1,4
```

```
        00462  3 00400 0 00053  10001  IOC    IORT    IC,C,256
                                              ENTRY   REWIND
        00463  1 00000 0 00466  10001  REWIND SAVE
        00464  0774 00 4 00000  10000
        00465  0020 00 4 00001  10000
        00466  0634 00 4 11000  10011
        00467  0634 00 4 00513  10001
        00470  0634 00 4 00464  10001
        00471  0074 00 4 13000  10011         TSX     REWTAP,4
        00472  0020 00 0 01003  10011         TRA     *+3
        00473  0 00000 0 00000  10000         PZE     **

BINARY CARD ID. CDC10005
        00474  2 00010 0 00000  10000         TIX     0,0,8
                         00475                RETURN  REWIND
                                              ENTRY   EOF
        00476  0500 00 0 00052  10001  EOF    CLA     EOFF
        00477  0020 00 4 00001  10000         TRA     1,4
                                              ENTRY   BKSPAC
        00500  1 00000 0 00503  10001  BKSPAC SAVE
        00501  0774 00 4 00000  10000
        00502  0020 00 4 00001  10000
        00503  0634 00 4 11000  10011
        00504  0634 00 4 00513  10001
        00505  0634 00 4 00501  10001
        00506  0074 00 4 14000  10011         TSX     BSRTAP,4
        00507  0020 00 0 01003  10011         TRA     *+3
        00510  0 00000 0 00000  10000         PZE
        00511  2 00010 0 00000  10000         TIX     0,0,8
                         00512                RETURN  BSRTAP
        00513  000000000000     10000         *LDIR
        00514  232423010600     10000
        00515  777700000000     10000         *LORG
        00516  000077770000     10000

BINARY CARD ID. CDC10006
        00517  000000007777     10000
                         00000  01111         END
```

The following is the list of subroutine ORDER for program number I

```
      SUBROUTINE   ORDER  (K1)
C     SCAN FOR MISSING CHANNELS
C     EACH OF TEN MATRICES STANC FOR TIME,CURRENT, SWEEP,ETC.
C     NOE=RANGE OF DC LOOP IN SCAN FOR FIRST EVEN NUMBER
C     ND=NUMBER OF ELEMENTS IN IA
      DIMENSION     CAL1(3),     CAL2(3)
      DIMENSION IA1(  765),IA2(  765),IA3(765),    IA4(  765),
     TIA5(  765),   IA6(  765),IA7(  765),IA8(  765),IA9(765),
     TIA10(  765)
      EQUIVALENCE    (IA1(1), IA(    1))
      EQUIVALENCE    (IA2(1), IA( 766))
      EQUIVALENCE    (IA3(1), IA(1531))
      EQUIVALENCE    (IA4(1), IA(2296))
      EQUIVALENCE    (IA5(1), IA(3061))
      EQUIVALENCE    (IA6(1), IA(3826))
      EQUIVALENCE    (IA7(1), IA(4591))
      EQUIVALENCE    (IA8(1), IA(5356))
      EQUIVALENCE    (IA9(1), IA(6121))
      EQUIVALENCE    (IA10(1),IA(6886))
      DIMENSION  IA(  7650),     T(    765),      C(  3825),     S(    765),
     T                V1(    765),                       V2(    765),
     T             G(    765)
      DIMENSION  M6( 5), M7( 5), M8( 5), JA( 5), JB( 5), MY( 5)
      COMMON  C ,   CZERO,   ICO,
     T   NF,   N10,
     T JN1, JN2, JN3, JN4, JN5, JN6,
     T  MY,
     T  JA,
     T  JB,
     T  M6,
     T  M7,
     T  M8,
     T MA, MA1, MA2, MA3, MA4, MA5,
     T     MA6,  MA7,  MA8,  MA9,  MA10,  MA11
     T  ,  S
      NT1=0
      NCI=765
      NK=765
      NOE=1000
      ND=7650
      NK5=  5*NK
      DO  1006   I=1,NK5
      C(I)   =0.0
 1006 CONTINUE
      DO 1100   I=1,NK
       T(I)=0
       S(I) =0
       V1(I)=0
       V2(I)=0
       G(I)=0
 1100 CONTINUE
      CALL READ   (IA1 )
      CALL READ   (IA2 )
      CALL READ   (IA3 )
      CALL READ   (IA4 )
```

```
      CALL READ   (IA5 )
      CALL READ   (IA6 )
      CALL READ   (IA7 )
      CALL READ   (IA8 )
      CALL READ   (IA9 )
      CALL READ   (IA10)
C     SCAN FOR FIRST EVEN NUMBER
      DO 409 I=1,NOE
      IF  (I.EQ.NOE)  GO TO 1004
      N=IA(I)
      M=MOD(N,2)
      IF (M.EQ.0) GO TO 1001
      GO TO 409
 1001 K=I+60
      DO 1002   J=I,K,10
      N=IA(J)
      M=MOD(N,2)
      IF(M.NE.0)  GO TO 409
      IF  (J.EQ.K)  GO TO 1003
 1002 CONTINUE
  409 CONTINUE
 1003 KI=I
      GO TO 1900
 1004 WRITE (6,1005)  NOE
      GO TO 1200
 1900 CONTINUE
      NT=0
      IP=0
      DO 100   I=1,NOI
      I1=I-1
      I10=I1*10
  101 J1=I10+KI+1+IP
      NO=ND-J1
      NO=NO-10
      IF (NO.LT.0) GO TO 505
      J2=I10+KI+2+IP
      J3=I10+KI+3+IP
      J4=I10+KI+4+IP
      J5=I10+KI+5+IP
      J6=I10+KI+6+IP
      J7=I10+KI+7+IP
      J8=I10+KI+8+IP
      J9=I10+KI+9+IP
      J10=I10+KI+10+IP
      IB1  =  I1*  5  +1
      IB2  =  I1*  5  +2
      IB3  =  I1*  5  +3
      IB4  =  I1*  5  +4
      IB5  =  I1*  5  +5
       T(I)=IA(J1)
       C(IB1) =IA(J2)
       S(I) =IA(J3)
      C(IB2)=IA(J4)
       V1(I)=IA(J5)
      C(IB3)=IA(J6)
       V2(I)=IA(J7)
```

```
      C(IB4)=IA(J8)
       G(I)=IA(J9)
      C(IB5)=IA(J10)
      IF  (I.EQ.1)   GO TO 100
      N=    C(IB5)
      M=MOD (N,2)
      IF (M.NE.0) GO TO 201
      N=    G(I)
      M=MOD(N,2)
      IF (M.EQ.0)   GO TO 901
      II= T(I)- T(I1)
      II=IABS(II)
      NT2= 3*(NT1+1)
      IF (II.GT.30 )GO TO 201
      NT1=0
      GO TO 100
901   IP=IP+9
      NT=NT+1
      NT1=NT
      S(I)   =0.0
      C(IB1)    =0.0
      C(IB2) =   0.0
      C(IB3) =   0.0
      C(IB4)   =   0.0
      C(IB5)   =   0.0
      T(I)   =T(I1)
      G(I)   =    G(I1)
      GO TO 100
201   DO 301  L=1,10
      JL=J10-L
      N=IA(JL)
      M=MOD(N,2)
      IF (M.NE.0)  GO TO 301
401   JL=JL-1
      N=IA(JL)
      M=MOD(N,2)
      IF (M.EQ.0)  GO TO 402
      IL=10-L
      IF  (IL.LT.1)  GO TO100
      GO TO 403
301   CONTINUE
      GO TO 100
402   IL=10-L-1
      IF (IL.LT.1) GO TO 510
403   IP=IP+IL
      NT=NT+1
      NT1=NT
      S(I)   =0.0
      C(IB1)    =0.0
      C(IB2) =   0.0
      C(IB3) =   0.0
      C(IB4)   =   0.0
      C(IB5)   =   0.0
      T(I)   =T(I1)
      G(I)   =    G(I1)
      GO TO 100
```

```
 510 IP=IP+10
     NT=NT+1
     NT1=NT
     S(I)  =0.0
     C(I,1)   =0.0
     C(I,2) =  0.0
     C(I,3) =  0.0
     C(I,4)  =  0.0
     C(I,5)  =  0.0
     T(I)  =T(I1)
     G(I)  =   G(I1)
     GO TO 100
 100 CONTINUE
 505 CONTINUE
     WRITE (6,506)  NT,  I,  IP
 506 FORMAT((17H NUMBER OF SKIPS=,I5),  (6X,I6)  ,  (6X,I6))
1200 CONTINUE
1005 FORMAT   (13H NO ANSWER TO,I10)
     IF (K1.GT.1)   GO TO   911
     SUM=0.0
     SUM2=0.0
     IU=0
     DO   931   L=JN1,JN2
     IF  (S(L).EQ.0.0)  GO TO 56
     SUM=SUM+    S(L)
     GO TO   931
  56 IU=IU+1
 931 CONTINUE
     FN=JN2-JN1+1-IU
     CAL1(1)=SUM/FN
     SUM=0.0
     IU=0
     DO  932  L=JN3,JN4
     IF  (S(L).EQ.0.0)  GO TO 57
     SUM=SUM+    S(L)
     GO TO   932
  57 IU=IU+1
 932 CONTINUE
     FN=JN4-JN3+1-IU
     CAL1(2)=SUM/FN
     SUM=0.0
     IU=0
     DO 933 L=JN5,JN6
     IF  (S(L).EQ.0.0)  GO TO 58
     SUM=SUM+    S(L)
     GO TO   933
  58 IU=IU+1
 933 CONTINUE
     FN=JN6-JN5+1-IU
     CAL1(3)=SUM/FN
     DO  999  L=1,3
 955 FORMAT      ((9H CAL1(L)=,E12.5), ( 9H CAL2(L)=,F12.5)  )
     WRITE  (6,955)   CAL1(L),   CAL2(L)
 999 CONTINUE
     D1C1=CAL1(2)-CAL1(1)
     D2C1=CAL1(3)-CAL1(2)
```

```
      D1C1=ABS(D1C1)
      D2C1=ABS(D2C1)
      DCAL1= (D2C1+D1C1)/2.0
  911 CONTINUE
      NS=765-NT
      DO 951  J=1,NS
      IF  (S(J).EQ.0.0)  GO TO 951
       S(J)=  ( 2.5/D2C1 )*    (S(J)        -CAL1(2))
  951 CONTINUE
      RETURN
      END
```

The following is the list of subroutine XFIT of program number I

```
      SUBROUTINE   FIT (     Y, NA, NB,      N,    MQ,  A,   A1)
C     DIMENSION OF D IS N+1
C     DIMENSION OF SMX IS  2*N
C     DIMENSION SMXY IS N
C     DIMENSION OF  A IS N+1
C     DIMENSIONS OF B ARE  N+1 BY N+1
C     DIMENSIONS OF X AND Y ARE M
C     N=ORDER OF POLYNOMIAL
C     M=NUMBER OF DATA POINTS
C     Y=ORDINATE, X=ABSCISSA
C     SMX DENOTES SUM OF X
C     A(I)=COEFF'S OF POLYNOMIALS TO BE DETERMINED
      DIMENSION    D(     11)
      DIMENSION C1(3825)
      DIMENSION    SMX(  20),SMXY(  11), A(   11)  ,  B(   11 ,  11)
      DIMENSION    X(    765),  Y(   765)
      DIMENSION A1(11)
      DIMENSION  M6( 5), M7( 5), M8( 5), JA( 5), JB( 5), MY( 5)
      COMMON  C1,   CZERO,   ICO,
     1   NF,   N10,
     1 JN1, JN2, JN3, JN4, JN5, JN6,
     1  MY,
     1  JA,
     1  JB,
     1  M6,
     1  M7,
     1  M8,
     1 MA, MA1, MA2, MA3, MA4, MA5,
     1      MA6,  MA7,  MA8,   MA9,  MA10,   MA11
      DO    78  IZ=1,2
      N50  =NA/5
      N503  =NB/5
      WRITE (6,162)        N50,  N503
  162 FORMAT   ( I5,     I5)
       N2=2*N
      NP1=N+1
      NP2=N+2
      IF  (MQ.NE.1)   GO TO  25
      DO    160    IO  =  N50,N503
      X(IO)  =  IO
  160 CONTINUE
      DO 50    I=1,N2
      SMX(I)=0.0
   50 CONTINUE
      DO    51    I=1,N
      SMXY(I)=   0.0
   51 CONTINUE
      DO    100    I=1,N2
      DO    101    J=N50,N503
      IF   (Y(J).EQ.0.0)  GO TO 101
      SMX(I)    =   SMX(I)   +   X(J)**I
  101 CONTINUE
  100 CONTINUE
      DO    102    I=1,N
      DO    103    J=N50,N503
```

```
      IF  (Y(J).EQ.0.0)  GO TO 103
      SMXY(I)     =     SMXY(I)   +   Y(J)*X(J)**I
  103 CONTINUE
  102 CONTINUE
      SMY =0.0
      DO    104    I=N50,N503
      IF  (Y(I).EQ.0.0)   GO TO 104
      SMY     =SMY    +    Y(I)
  104 CONTINUE
      IU=0
      DO 113      IW=N50,N503
      IF   ( Y(IW).NE.0.0)   GO TO 113
      IU=IU+1
  113 CONTINUE
      GO TO 200
   25 CONTINUE
      N50   =   NA
      N503   =   NB
      DO 350    I=1,N2
      SMX(I)=0.0
  350 CONTINUE
      DO 351        I=1,N
      SMXY(I)=    0.0
  351 CONTINUE
      T0=FLOAT(N50)/5.0
      V0 = A1(1)  +A1(2)*T0
      DV    =  A1(2)*0.2
      DO   3100     I=1,N2
      V   =   V0
      DO    3101      J=N50,N503
      X1   =   V
      IF   (C1(J).EQ.0.0)    GO TO    105
      SMX(I)     =    SMX(I)    +    X1   **I
  105 V =V+DV
 3101 CONTINUE
 3100 CONTINUE
      T0=FLOAT(N50)/5.0
      V0 = A1(1)   +A1(2)*T0
      DV    =  A1(2)*0.2
      DO   3102    I=1,N
      V   =  V0
      DO    3103     J=N50,N503
      X1   =  V
      IF   (C1(J).EQ.0.0)    GO TO  106
      Y1  =     C1  (J)
      SMXY(I)     =      SMXY(I)    +    Y1   *X1   **I
  106 V=V+DV
 3103 CONTINUE
 3102 CONTINUE
      SMY =0.0
      DO    3104    I=N50,N503
      IF  (C1(I).EQ.0.0)  GO TO 3104
      Y1 = C1  (I)
      SMY     =SMY    +     Y1
 3104 CONTINUE
      IU=0
```

```
      DO 114  IW=N50,N503
      IF  (C1(IW).NE.0.0)   GO TO 114
      IU=IU+1
  114 CONTINUE
C     NORMAL EQS. ARE  N+1 EQS. IN N+1 UNKNOWNS
C     UNKNOWNS ARE COEFF'S A(I), KNOWNS ARE SMX(I),SMXY(I),SMY
  200 CONTINUE
      NP1=N+1
      DO 110    I=2,NP1
      I1=I-1
      D(I)=SMXY(I1)
  110 CONTINUE
      D(1)=SMY
      NP1=N+1
      DO 111      I=1,NP1
      DO 112       J=1,NP1
      I1=I-1
      J1=J-1
      K=I1+J1
      IF (I1.NE.0)    GO TO 150
      IF    (J1.EQ.0)   GO TO 112
  150 B(I,J)    =SMX(K)
  112 CONTINUE
  111 CONTINUE
      B(1,1) = N503- N50   +1 -   IU
      N1=N+1
C     CROUT'S METHOD
      NP1=N+1
      DO 500     I=1,  NP1
      DO 501    J=I,NP1
      IF (B(I,J).NE.0.)  GO TO 512
  501 CONTINUE
      WRITE    (6,2)   N
    2 FORMAT   (15H NO SOLUTION TO,I3)
      GO TO 140
  512 IF (I.EQ.J)  GO TO 590
  590 F=B(I,I)
      D(I)=D(I)/F
      B(I,I)=1.0
      IP1=I+1
      DO 505    J=IP1,NP1
      B(I,J)=B(I,J)/F
  505 CONTINUE
      DO 506    J=IP1,NP1
      F1=B(J,I)
      B(J,I)=0.0
      DO 507  K=IP1,NP1
      B(J,K)=B(J,K)   -F1*B(I,K)
  507 CONTINUE
      D(J)=D(J)  - F1*D(I)
  506 CONTINUE
  500 CONTINUE
C     SOLVIMG THE REDUCED EQ'S
      A(NP1)=D(NP1)
      DO   510  I=1,N
      J=NP1-I
```

```
    JP1=J+1
    A(J)=0.0
    DO   511   K=JP1,NP1
    A(J)=  A(J)+B(J,K)*A(K)
511 CONTINUE
    A(J)=D(J)-A(J)
510 CONTINUE
    IF  (MQ.NE.1)   GO TO 55
    WRITE   (6,57)
 57 FORMAT   (40H THE FOLLOWING COEFF'S ARE FOR THE SWEEP,)
    WRITE (6,958)   A
958 FORMAT ((3H A=,6E12.5))
    IF   (MQ.EQ.1)   GO TO 58
 55 CONTINUE
    WRITE  (6,56)
 56 FORMAT   (46H THE FOLLOWING COEFF'S ARE FOR THE ION SECTION,)
    WRITE  (6,958)   A
 58 CONTINUE
    NP1  =N+1
    IF  (MQ.NE.1)   GO TO  135
    SIGMA  =  0.0
    DO  121  L2=N50,   N503
    CC=0.0
    DO  120  L=1,   NP1
    L1=L-1
    CC   = CC+  A(L) * X(L2) **L1
120 CONTINUE
    IF   (Y(L2).EQ.0.0)   GO TO 121
    DELTA =  (  CC   - Y(L2))**2
    SIGMA   =    SIGMA   +  DELTA
121 CONTINUE
    FM  =  N503 - N50 - ID
    SIGMA   =   SQRT  (SIGMA/FM)
    WRITE  (6,171)     SIGMA
171 FORMAT  (7H SIGMA=,F10.2)
    SIGM5=5.0*SIGMA
    DO   81  L2=N50,   N503
    CC=0.0
    DO   80  L=1,   NP1
    L1=L-1
    CC   = CC+  A(L) * X(L2) **L1
 80 CONTINUE
    IF   (Y(L2).EQ.0.0)   GO TO  81
    DIFF=ABS(CC-Y(L2))
    IF   (DIFF.GT.SIGM5) Y(L2)=0.0
 81 CONTINUE
    GO TO 140
135 CONTINUE
    TO=FLOAT(N50)/5.0
    VO=      A1(1)  +  A1(2)*TO
    DV   =   A1(2)*0.2
    V=VO
    SIGMA  =  0.0
    DO  141  L2=N50,   N503
    CW = 0.0
    DO  144  L=1,   NP1
```

```
      L1=L-1
      X1=V
      CW=  CW +   A(L) * X1**L1
  144 CONTINUE
      IF  (C1(L2).EQ.0.0)  GO TO 146
      DELTA =  (CW  -  C1(L2))**2
      SIGMA   =    SIGMA   +  DELTA
  146 V=V+DV
  141 CONTINUE
      FM  =  N503 - N50 - IU
      SIGMA   =   SQRT  (SIGMA/FM)
      WRITE  (6,171)     SIGMA
      SIGM5=5.0*SIGMA
      TO=FLOAT(N50)/5.0
      VO=      A1(1)  +  A1(2)*TO
      DV  =    A1(2)*0.2
      V=VO
      DO   71  L2=N50,   N503
      CW = 0.0
      DO   74  L=1,    NP1
      L1=L-1
      X1=V
      CW=  CW +   A(L) * X1**L1
   74 CONTINUE
      IF  (C1(L2).EQ.0.0)  GO TO  76
      DIFF  =  ABS(CW- C1(L2))
      IF  (DIFF.GT.SIGM5)   C1(L2)=0.0
   76 V=V+DV
   71 CONTINUE
      IF  (IZ.LT.2)   GO TO 78
      N400=N503+MA
      TO=FLOAT(N50)/5.0
      VO=      A1(1)  +  A1(2)*TO
      DV  =    A1(2)*0.2
      V=VO
      DO  131  L2=N50,   N400
      CW = 0.0
      DO  130  L=1,    NP1
      L1=L-1
      X1=V
      CW=  CW +   A(L) * X1**L1
  130 CONTINUE
      V=    V   +DV
      C3=ABS(C1(L2)-CW)
      IF  (C1(L2).EQ.0.0)   C3=0.0
      C1(L2)=C3
      IF     (CW.GT.CZERO)   GO TO 151
  131 CONTINUE
  151 CONTINUE
      ICO=L2
      VZERO = V - DV
      L21=L2+1
      L20=L2+MA1
      IF  (L20.GT.3825)   L20 =3825
      DO  231  L3=L21,  L20
      CW = 0.0
```

```
      DO  230  L=1,    NF1
      L1=L-1
      X1=V
      CW=  CW +   A(L) * X1**L1
  230 CONTINUE
      V=    V  +DV
      C3=ABS(C1(L3)-CW)
      IF  (C1(L3).EQ.0.0)   C3=0.0
      C1(L3)=C3
  231 CONTINUE
C    MA6 IS NUMBER OF POINTS AFTER EXTENSION OF ION PART TO START
      L30=  L20+MA6
      L40=L30+MA7
      DO 38 K13=1,2
      SMC1=0.0
      IU1=0
      DO 31  K12=L30,L40
      ICK=C1(K12)
      IF (C1(K12).EQ.0.0)   GO TO 32
      IF   (ICK.LT.MA8)   GO TO 32
      IF   (ICK.GT.MA9)   GO TO 32
      SMC1=SMC1+C1(K12)
      GO TO 31
   32 IU1=IU1+1
   31 CONTINUE
      FN=L40-L30+1-IU1
      SMC1=SMC1/FN
      CSA1=SMC1
      AD=0.0
      IU1=0
      DELTA=0.0
      DO   33  K14=L30,L40
      ICK=C1(K14)
      IF (C1(K14).EQ.0.0)       GO TO  34
      IF   (ICK.LT.MA8)   GO TO 34
      IF   (ICK.GT.MA9)   GO TO 34
      DELTA  = ABS(SMC1-C1(K14))
      AD=AD+DELTA
      GO TO 33
   34 IU1=IU1+1
   33 CONTINUE
      FN=L40-L30+1-IU1
      AD=AD/FN
      IF   (K13.GT.1)   GO TO 35
      DO   36  K16=L30,L40
      DELTA  =   ABS(SMC1-C1(K16))
      AD5=AD*5.0
      IF  (DELTA.GT.AD5)     C1(K16)  =0.0
   36 CONTINUE
   38 CONTINUE
   35 CONTINUE
      T0=FLOAT(N50)/5.0
      TF=FLOAT(N503)/5.0
      V0=      A1(1)  +  A1(2)*T0
      VF=      A1(1)  +  A1(2)*TF
      CW1=0.0
```

```
      CW = 0.0
      DO  143  L=1,   NP1
      L1=L-1
      CW=  CW +   A(L) * VO**L1
      CW1= CW1+   A(L) * VF**L1
  143 CONTINUE
      WRITE  (6,145)   CW,   CW1,  CZERO,  VZERO,  ICO ,  AD, CSAT
  145 FORMAT      (F10.2,    F10.2, (11H ZERO CURR=,F10.2),
     T  (10H ZERO POT=,F10.2), I10, F10.2,  (10H SAT CURR=,F10.2))
  140 CONTINUE
   78 CONTINUE
      RETURN
      END
```

The following is the subroutine YFIT of program I

```
      SUBROUTINE YFIT  (       NA,    NB, A1, A2, N )
C     N=ORDER OF POLYNOMIAL
C     A(I)=COEFF'S OF POLYNOMIALS TO BE DETERMINED
      DIMENSION     D(     11)
      DIMENSION     SMX( 20), SMXY( 11) ,  A(    11),  B(    11,   11)
      DIMENSION  A2(11)
      DIMENSION     A1(11)
      DIMENSION    DW(11),           SMYYX(20), SMXYYY(11), BW(11,11)
      DIMENSION    AW(11)
      DIMENSION  C2(3825)
      DIMENSION  M6( 5), M7( 5), M8( 5), JA( 5), JB( 5), MY( 5)
      COMMON  C2,   CZERO,    ICO,
     1   NF,    N10,
     1 JN1, JN2, JN3, JN4, JN5, JN6,
     1  MY,
     1  JA,
     1  JB,
     1  M6,
     1  M7,
     1  M8,
     1 MA, MA1, MA2, MA3, MA4, MA5,
     1     MA6,  MA7,  MA8,  MA9,  MA10,  MA11
      N50=NA
      N503=NB
      N50=N503
      N503=N503+MA4
       N2=2*N
      NP1=N+1
      NP2=N+2
      N400=N503+MA3
      WRITE  (6,52)    (C2(I),I=N50,N400)
   52 FORMAT   (10X,10F10.1)
      ICN=ICO-NB+100
      I4=ICN/4
      DO  132   MZ=1,MA2
      N503=N503+MA5
      N50=N50+MA5
      DO 50     I=1,N2
      SMX(I)=0.0
      SMYYX(I)=0.0
   50 CONTINUE
      DO      51     I=1,N
      SMXY(I)=    0.0
      SMXYYY(I)=0.0
   51 CONTINUE
      T0=FLOAT(N50)/5.0
      V0=      A1(1)   +  A1(2)*T0
      DV   =   A1(2)*0.2
      DO   100     I=1,N2
      V=V0
      DO     101     J=N50,N503
      X=V
      IF  (C2(J).EQ.0.0)   GO TO 105
      Y  =  C2(J)
      SMX(I)    =    SMX(I)    +   X    **I
```

```
      SMYYX(I) = SMYYX(I)  +   Y    *Y    *X    **I
  105 V=V+DV
  101 CONTINUE
  100 CONTINUE
      T0=FLOAT(N50)/5.0
      V0=      A1(1)  +  A1(2)*T0
      DV  =    A1(2)*0.2
      DO   102   I=1,N
      V=V0
      DO    103    J=N50,N503
      X=V
      IF  (C2(J).EQ.0.0)   GO TO 106
      Y  =  ABS(C2(J))
      YL =    ALOG(Y    )
      SMXY(I)     =     SMXY(I)    +  C2(J)*X    **I
      SMXYYY(I)=   SMXYYY(I)  +   YL * (Y   **2) *(X   **I)
  106 V=V+DV
  103 CONTINUE
  102 CONTINUE
      SMY =0.0
      SMYY=0.0
      SMYYY=0.0
      DO    104    I=N50,N503
      IF  (C2(I).EQ.0.0)   GO TO 104
      Y  =  ABS(C2(I))
      YL =    ALOG(Y    )
      SMYY=  SMYY+Y   **2
      SMY    =SMY   +   C2(I)
      SMYYY  =  SMYYY  +    YL *(Y   **2)
  104 CONTINUE
      NP1=N+1
      DO 110   I=2,NP1
      I1=I-1
      DW(I)=   SMXYYY(I1)
      D(I)=SMXY(I1)
  110 CONTINUE
      DW(1)  =SMYYY
      D(1)=SMY
      NP1=N+1
      DO 111    I=1,NP1
      DO 112     J=1,NP1
      I1=I-1
      J1=J-1
      K=I1+J1
      IF (I1.NE.0)   GO TO 150
      IF   (J1.EQ.0)  GO TO 112
  150 BW(I,J)   =   SMYYX(K)
      B(I,J)   =SMX(K)
  112 CONTINUE
  111 CONTINUE
      IU=0
      DO 113     IW=N50,N503
      IF  (C2(IW).NE.0.0)   GO TO 113
      IU=IU+1
  113 CONTINUE
      BW(1,1)   =SMYY
```

```
      B(1,1) = N505- N50  +1 -  IU
      N1=N+1
      NP1=N+1
      DO 500    I=1,  NP1
      DO 501   J=I,NP1
      IF(BW(I,J).NE.0.)  GO TO 512
      IF (B(I,J).NE.0.)  GO TO 512
  501 CONTINUE
      WRITE   (6,2)  N
    2 FORMAT  (15H NO SOLUTION TO,I3)
      GO TO 132
  512 IF (I.EQ.J)  GO TO 590
  590 FW=BW(I,I)
      F=B(I,I)
      DW(I)    =DW(I)/FW
      D(I)=D(I)/F
      BW(I,I)    =1.0
      B(I,I)=1.0
      IP1=I+1
      DO 505   J=IP1,NP1
      BW(I,J)=  BW(I,J)/FW
      B(I,J)=B(I,J)/F
  505 CONTINUE
      DO 506   J=IP1,NP1
      FW1=BW(J,I)
      F1=B(J,I)
      BW(J,I)=0.0
      B(J,I)=0.0
      DO 507  K=IP1,NP1
      BW(J,K)    =  BW(J,K)    -   FW1   *BW(I,K)
      B(J,K)=B(J,K)  -F1*B(I,K)
  507 CONTINUE
      DW(J)    =   DW(J)   - FW1 * DW(I)
      D(J)=D(J) - F1*D(I)
  506 CONTINUE
  500 CONTINUE
C     SOLVIMG THE REDUCED EQ'S
      AW(NP1)    =    DW(NP1)
      A(NP1)=D(NP1)
      DO   510  I=1,N
      J=NP1-I
      JP1=J+1
      AW(J)    =0.0
      A(J)=0.0
      DO    511   K=JP1,NP1
      AW(J)   =AW(J)   +   BW(J,K) * AW(K)
      A(J)=  A(J)+B(J,K)*A(K)
  511 CONTINUE
      AW(J)   = DW(J)    -AW(J)
      A(J)=D(J)-A(J)
  510 CONTINUE
      IF   (MZ.GT.1)   GO TO 91
      WRITE  (6,55)
   55 FORMAT (46H THE FOLLOWING COEFF'S ARE FOR THE EXP SECTION,)
   91 CONTINUE
      WRITE (6,958)  (AW(ID),ID=1,3)
```

```
  958 FORMAT ((4H AW=,3E12.5))
      IF   (MZ.GT.1)    GO TO 95
      WRITE  (6,93)
   93 FORMAT   (27H COEFF'S FOR LIN FIT TO EXP,)
   95 CONTINUE
      WRITE  (6,92)    (A(ID),ID=1,3)
   92 FORMAT   ((3H A=,3E12.5))
      NP1   =N+1
      T0=FLOAT(N50)/5.0
      V0=       A1(1)   +   A1(2)*T0
      DV   =    A1(2)*0.2
      V=V0
      SIGMA   =   0.0
      DO   121   L2=N50,    N503
      Cw  = 0.0
      DO   120   L=1,    NP1
      L1=L-1
      X=V
      Cw=   Cw +   AW(L) * X **L1
  120 CONTINUE
      IF   (C2(L2).EQ.0.0)    GO TO 122
      DELTA =   (EXP(CW) -      (C2(L2)))**2
      SIGMA    =     SIGMA    +  DELTA
  122 V=V+DV
  121 CONTINUE
      FM   =   N503 - N50 - IU
      SIGMA    =    SQRT  (SIGMA/FM)
      WRITE   (6,171)       SIGMA,    C2(N50),   C2(N503)
  171 FORMAT ((7H SIGMA=,F10.2),    (23H END PTS OF CURRENT ARE,F10.2),
     1 (4H AND,F10.2))
  132 CONTINUE
      RETURN
      END
```

The following is subroutine XZERO of program number I

```
       SUBROUTINE   ZERO  (M6I,  M7I)
       DIMENSION    C(3825),
      I   M6( 5),  M7( 5),  M8( 5),  JA( 5),  JB( 5),  MY( 5)
       COMMON  C ,   CZERO,   ICO,
      I   NF,   M10,
      I JN1, JN2, JN3, JN4, JN5, JN6,
      I  MY,
      I  JA,
      I  JB,
      I  M6,
      I  M7,
      I  M8,
      I MA, MA1, MA2, MA3, MA4, MA5,
      I     MA6,  MA7,  MA8,  MA9,  MA10,  MA11
       DO 38 K13=1,2
       IU=0
       SMC=0.0
       DO 52   M1=M6I,M7I
       IF  (C(M1).EQ.0.0)    GO TO 54
       ICK=C(M1)
       IF   (ICK.LT.MA10)   GO TO 54
       IF   (ICK.GT.MA11)   GO TO 54
       SMC = SMC  +C(M1)
       GO TO  52
    54 IU=IU+1
    52 CONTINUE
       FN=M7I-M6I+1-IU
       CZERO=SMC/FN
       AD=0.0
       IU=0
       DELTA=0.0
       DO   33  K14=M6I,M7I
       ICK=C(K14)
       IF  (C(K14).EQ.0.0)      GO TO   34
       IF   (ICK.LT.MA10)   GO TO 34
       IF   (ICK.GT.MA11)   GO TO 34
       DELTA  = ABS(SMC-C(K14))
       AD=AD+DELTA
       GO TO 33
    34 IU=IU+1
    33 CONTINUE
       FN=M7I-M6I+1-IU
       AD=AD/FN
       IF   (K13.GT.1)   GO TO 35
       DO  36  K16=M6I,M7I
       DELTA  =   ABS(SMC-C(K16))
       AD5=AD*5.0
       IF  (DELTA.GT.AD5)      C(K16)  =0.0
    36 CONTINUE
    38 CONTINUE
    35 CONTINUE
       RETURN
       END
```

The following is the list for program number II

The notation of the program which corresponds to the notation of the text (chapter IV) is as follows:

Computer Program Notation	Text Notation
TE, T	T_e
DDS	Estimate of the brackets in eq. 4.16
AI1	K (equation 4.16)
AI2	D (equation 4.16)
CB	Initial electron density estimate
EI3	W
DEN	Calculated electron density
SIGMA	Calculated patch standard deviation

```
      DIMENSION     DDS(50),  CB(50),  AI1(50),   AI2(50)
      DIMENSION   EI( 300),   EI1( 300), EI2( 300)
      DIMENSION      DV0(50)
      DIMENSION   TE(50)
      DIMENSION   EI3( 300)
      DIMENSION   EI4(300),    EI5(300)
      COMMON  T, V,  E2, SIGMA,  DEN,  R
      READ   (5,1)  V0, DV, S0,DS,T, DT,DEN,R,  GAMMA
      WRITE  (6,1)  V0, DV, S0,DS,T, DT,DEN,R,  GAMMA
    1 FORMAT   (5E12.5/4E12.5)
      READ   (5,28)   TE
      WRITE  (6,28)   TE
   28 FORMAT    (5E12.5/5E12.5)
      READ  (5,28)   DDS
      READ  (5,28)   AI1
      READ  (5,28)   AI2
      READ  (5,28)   CB
      READ      (5,28)   DV0
      WRITE   (6,28)   DDS
      WRITE   (6,28)   AI1
      WRITE   (6,28)   AI2
      WRITE   (6,28)   CB
      WRITE    (6,28)   DV0
      READ  (5,20)   N1,  N2,  N3
      WRITE (6,20)   N1,  N2,  N3
   20 FORMAT   (3I6)
      A1=1.0
      Z=1.0
      BK=1.38E-23
      PI=3.1416
      SPI=SQRT(PI)
      S2=SQRT(2.0)
      AR= 2.0*PI*R*R
      EM=9.1E-31
      ECH=1.6E-19
      DO  21  L1=1,N3
      T=TE(L1)
      IF   (T.EQ.0.0)   GO TO 27
      WRITE  (6,60) T
   60 FORMAT   (3H T=,E12.5)
      CA=CB(L1)
      RA=   AI1(L1)/AI2(L1)
      EI0=ECH*SQRT((BK*T)/(2.0*PI*EM))*AR
      DEN=CA*GAMMA/EI0
      SIGMA=S0
      DO   51   J1=1,15
      F1=1.0
      DO  16   L=1,N1
      V=V0
      DV=-DV0(L1)
      ALPHA=ECH/(BK*T)
      BETA=1.0/(2.0*SIGMA*SIGMA)
      B=SQRT(BETA)
      Y3=BK*T/(2.0*PI*EM)
      A=ALPHA*(SIGMA/S2)
```

```
      RHO=ALPHA*ALPHA/(4.0*BETA)
      DO  2   J=1,N2
      PSI=RHO-ALPHA*V
    5 CONTINUE
      CALL INTEG
      EI1(J)=E2
      PSI1=RHO+ALPHA*V
      Y1=A+B*V
      C3=        EXP(PSI1)/2.0
      EI4(J)=    EXP(PSI1)
    8 EI2(J) = C3*(1.0  -  ERF(Y1))
    9 CONTINUE
      V=V+DV
    2 CONTINUE
      DO  15   I=1,N2
      EI3(I)=EI1(I)+EI2(I)
      EI5(I)=EI4(I)/EI3(I)
   15 CONTINUE
      EI5(1)=EI3(1)/EI3(2)
      IF   (F1.LE.0.001)   GO TO 52
      F         =  SIGMA-(EI5(1)    -RA)/COS(L1)
      F1   =    ABS(SIGMA-F)
      SIGMA=F
      WRITE   (6,53)  SIGMA
   53 FORMAT        (7H SIGMA=,E12.5)
   16 CONTINUE
   52 CONTINUE
      BETA=1.0/(2.0*SIGMA*SIGMA)
      RHO=ALPHA*ALPHA/(4.0*BETA)
      RATIO=EXP(RHO)
      F2=AI1(L1)/EI3(1)
      F3=ABS(F2-CA)
      CA=F2
      DEN=CA*GAMMA/EI0
      WRITE   (6,54)       CA,   DEN
   54 FORMAT     ((4H CA=,E12.5),  (5H DEN=,E12.5))
      IF        (F3.LE.25.0)   GO TO 21
   51 CONTINUE
   21 CONTINUE
   27 CONTINUE
      STOP
      END
```

The following is the list of subroutine INTEG of program II

```
      SUBROUTINE INTEG
C   V1   IS THE APPLIED POTENTIAL
C    V  IS THE TOTAL POTENTIAL
C    PHI   IS THE  DEVIATION FROM THE APPLIED POTENTIAL
      DIMENSION   C1(400),  E(400)
      DIMENSION    A(10),   B(10)
      COMMON  T, V1,  SUM,  SIGMA,  DEN,  R
      BK=1.38E-23
      ECH=1.6E-19
      PHI0=0.0
      N=200
      NM1=N-1
      SIG5=2.0
      DPHI=0.01
      PI=3.141596
      PI2=SQRT(PI)/2.0
      PI3=SQRT(2.0*PI)
      M1=1
      DO  11   I=1,1
      D=DEN/(1.0E+6)
      H=6.91*SQRT(T/D)
      H=H*0.01
      Y1=R/H
      A(I)=0.689/(Y1**1.33)
      B(I)=(1.66/0.689)*(Y1**0.667)
   11 CONTINUE
      WRITE   (6,15)    Y1
   15 FORMAT    (4H Y1=,E12.5)
      DO  12   J=1,M1
      PHI=PHI0
      DO 1   I=1,N
      V=V1+PHI
      IF  ( PHI.LT.-V1)   C1(I)=0.0
      IF  ( PHI.LT.-V1)   GO TO 2
      IF(V.EQ.0.0)   C1(I)=1.0
      IF(V.EQ.0.0)   GO TO 2
      PSI    =  (ECH*V)/(BK*T)
      PSI1      =SQRT(PSI    )
      AL    =1.0/(A(J)*(PSI    +B(J)*PSI1    ))
      A8    =A(J)*(1.0+B(J)/(2.0*PSI1    ) )
      A11    =EXP(-PSI    *AL    )
      C1(I)=(1.0/AL    )*(1.0-A11    )    +1.0
      E(I)    =   (1.0/(SIGMA*PI3))*EXP(-PHI*PHI/(2.0*SIGMA*SIGMA))
    2 PHI=PHI+DPHI
    1 CONTINUE
      SUM=0.0
      DO   3  I=2,NM1
      SUM   =    SUM   +   (C1(I)*E(I)*2.0)
    3 CONTINUE
      SUM    =    (SUM+ (C1(1)*E(1))   +   C1(N)*E(N))*DPHI/2.0
   12 CONTINUE
      RETURN
      END
```

The following is the list for program number III. The subroutines READ and INTEG are the same as in programs I and II respectively and are therefore not listed.

```
C     ONLY    EIGHT RECORDS ARE READ AT A TIME  IN SUBROUTINE ORDER
C      M  IS SUCH THAT EVERY M6 TH PT. IS PLOTTED.  M6MUST BE .GE. 2
C    N5R(I) IS THE NO. OF RECORDS TO REACH 10-5 RANGE
C    N6R(I) IS THE NO. OF RECORDS TO REACH 10-6 RANGE
C    N(I) IS THE INDEX OF THE 10-5 RANGE WHICH MATCHES 10-6 RANGE
C    M(I) IS THE INDEX OF THE 10-6 RANGE WHICH MATCHES 10-5 RANGE
C    FOR [illegible] MATRIX IS REVERSED
C     N6V (I) IS THE INDEX FOR 10-6 RANGE FOR ZERO POTENTIAL
C    FOR [illegible] MATRIX IS REVERSED
C     NOC(I) IS THE CURVE NUMBER
        DIMENSION     N5R(20), N6R(20), N(20), M(20), N6VU(20), NOC(20)
        DIMENSION      IA1(768)
        DIMENSION      SIGMA(20),   T(20),   AMBC(20)
        DIMENSION      C(3060)
        DIMENSION      C1(3060)
        DIMENSION     Y(1530), X1(1530)
        DIMENSION     CO(20)
        DIMENSION     D(1000)
        COMMON       C,    Y,   X1
        READ        (5,11)    NID
        WRITE       (6,11)    NID
   11 FORMAT       (I  )
        READ        (5,20)    G,U,Z,DV,PK, GAMMA
        WRITE       (6,20)    G,U,Z,DV ,PK,  GAMMA
   20 FORMAT        (E12.5,  E12.5,   E12.5,   E12.5,  E12.5,  E12.5)
        READ        (5,10)       N5R
        WRITE       (6,10)       N5R
        READ        (5,10)       N6R
        WRITE       (6,10)       N6R
        READ        (5,10)       N
        WRITE       (6,10)       N
        READ        (5,10)       M
        WRITE       (6,10)       M
        READ        (5,10)       N6V
        WRITE       (6,10)       N6V
        READ        (5,10)       NOC
        WRITE       (6,10)       NOC
   10 FORMAT        (10I6/10I6)
        READ     (5,25)     SIGMA
        READ     (5,25)     T
        READ     (5,25)     AMBC
        WRITE     (6,25)    SIGMA
        WRITE     (6,25)    T
        WRITE     (6,25)    AMBC
        READ   (5,25)   CO
        WRITE     (6,25)     CO
   25 FORMAT     (5E12.5/5E12.5/5E12.5/5E12.5)
        READ   (5,53)     M1, N1, M2, M3, M4, M5 , M6
        WRITE  (6,53)     M1, N1, M2, M3, M4, M5    ,   M6
        READ     (5,54)     AL5,     AL6,   D1,D2,D3, D4, D5, D6,D7
        WRITE    (6,54)     AL5,     AL6,   D1,D2,D3, D4, D5, D6,D7
        READ     (5,54) D8, D9, D10,  D11
        WRITE    (6,54) D8, D9, D10,  D11
   53 FORMAT   (7I6)
   54 FORMAT   ([illegible])
```

```
   55 FORMAT (4F[illegible].2)
      UV1=UV*FLOAT(NC)
      I2=[illegible]
      L[illegible]=N1-[illegible]
      I[illegible]=[illegible]-1
      [illegible]=1.[illegible]-[illegible]
      PI=3.14[illegible]
      SPI=[illegible](PI)
      S[illegible]=SQRT([illegible].[illegible])
      [illegible]=[illegible].[illegible]PI*[illegible]
      [illegible]=[illegible].1[illegible]-3[illegible]
      [illegible]=[illegible].[illegible]-1[illegible]
      CALL PLOTS ([illegible],1[illegible])
      CALL PLOT ([illegible].[illegible],-11.[illegible],-[illegible])
      DO [illegible] J=1,[illegible]
      N[illegible]=[illegible](J)
      DO [illegible] I=1,[illegible]
      CALL [illegible](I[illegible])
    2 CONTINUE
      CALL [illegible]([illegible])
      DO 3 I=1,[illegible]
      C1(I)=(C(I)-C[illegible](J))*[illegible]
      IF (C(I).[illegible].[illegible]) C1(I)=0.
    3 CONTINUE
      I[illegible]=N[illegible](J)
      IF ([illegible].[illegible].[illegible]) GO TO 22
      [illegible] I=1,[illegible]
      CALL [illegible](I[illegible])
    4 CONTINUE
   22 CONTINUE
      CALL [illegible]([illegible])
      K=N[illegible]V[illegible](J)/2
      K1=IABS([illegible](J)-[illegible]V[illegible](J))
      DO 5 I=1,K
      I1=NOV[illegible](J)+1-I
      W=(C(I)-C[illegible](J))*[illegible]
      IF (C(I).[illegible].[illegible]) W=0.0
      C(I)=(C(I1)-C[illegible](J))*[illegible]
      IF (C(I1).[illegible].[illegible]) C(I)=0.0
      C(I1)=W
    5 CONTINUE
      DO 6 L=[illegible]1,L2
      L1=[illegible](J)-K1+1
      IF (L1.GT.L2) GO TO 14
      C(L)=C1(L1)
    6 CONTINUE
      GO TO 32
   14 CONTINUE
      I[illegible]=L-2
      DO 40 I[illegible]=I[illegible],L2
      C(I[illegible])=[illegible].[illegible]
   40 CONTINUE
   32 CONTINUE
      IF (J.GT.3) GO TO 1001
 1000 FORMAT ([illegible]F12.5/[illegible]12.[illegible])
      WRITE (7,1000) (C(JJ),JJ=1,[illegible])
```

```
      WRITE  (6,1000)      (C(JJ),JJ=1,500)
 1001 CONTINUE
      ALPHA=ECH/(BK*T(J))
      BETA=1.0/(2.0*SIGMA(J)*SIGMA(J))
      B=SQRT(BETA)
      Y3=BK*T(J)/(2.0*PI*EM)
      A=ALPHA*(SIGMA(J)/S2)
      RE0=ALPHA*ALPHA/(4.0*BETA)
      AR=AMRC(J)
      A1=AMPC(J)
      EI0=ECH*SQRT((BK*T(J))/(2.0*PI*EM))*AR
      GAM=A1*GAMMA/EI0
      U1=EI0/(1.E+6)
      U2=0.01*SQRT(T(J)/U1)
      U2=U2*1.01
      U3=2/U2
      U4   =0.683/(U3**1.33)
      U5   =(1.66/0.689)*(U3**0.667)
      V=0.
      DO    26    I=1,L2,M6
      IF   (V.LT.2.0)  GO  TO   70
      PHI     =    (ECH*V)/(BK*T(J))
      PHI1         =SQRT(PHI      )
      AL       =1.0/(U4    *(PHI     +U5    *PHI1      ))
      A11      = EXP(-PHI      *AL      )
      EI1=  ((1.0/AL      )*(1.0-A11      )       +1.0  )*A1
      GO   TO   71
   70 CALL  [illegible]   (T(J), V, L2, SIGMA(J), A1, R,GAMMA, I)
      EI1=R0*A1
   71 CONTINUE
      PSI1=RE0+ALPHA*V
      Y1=A+B*V
      A5=ERF(Y1)
      A7=1.0-A5
      IF  (A7.LE.0.0)   EI2=0.0
      IF  (A7.LE.0.0)   GO  TO  51
      A4=ALOG(1.0-A5)
      EI2=A1*EXP(A4+PSI1)/2.0
   51 CONTINUE
      IF    (C(I).EQ.0.0)    GO  TO  60
      C(I)=    1.0-    C(I)/(EI1+EI2)
   60 CONTINUE
      C1(I)=EI1+EI2
      V=V+DV1
   26 CONTINUE
      L22=L2/M6
      DO    21   I=1,L22
      F=(I-1)*M6
      I12=(I-1)*M6+1
      X1(I)=C(I12)
      X(I)=F*DV
   21 CONTINUE
      CALL  PLOTS    (AL5,AL6,-3)
      CALL  SCALE  (X1,D1,        L3,M1)
      CALL  SCALE   (X,D2,        L3,M2)
      X(L4)=0.0
```

```
  X(N1)=1.0
  X1(L4)=0.0
  X1(N1)=0.0
  CALL LINE   (X,X1,      L3,M3,M4,M5)
  CALL AXIS   (D3,D4,  10HREFLECTION,10,D5,D6,  X1(      L4),
 6    X1(        N1))
  CALL AXIS   (D7,D8,  5HVOLTS,-5,D9,D10,  X(      L4),X(          N1))
  AL6=0.0
  AL5=N1
1 CONTINUE
  CALL PLOTC   (0,0,999)
  CALL REWIND
  CALL EXIT
  STOP
  END
```

The following is the list for program IV.

The correspondence between computer program and text notation is as follows:

Computer Program	Text
H	Altitude of Payload
DEN	Electron (ion) density
DEN1	Percentage Density of Atomic Oxygen Ions
DL	Electron Debye Length
U	Speed of Probe
TEL	Electron Temperature
DOT	Derivitive of eq. 4.1 with respect to probe to plasma potential

```
C  H(I)  IS THE ALTITUDE OF THE  ITH CURVE IN METERS
C  SOPE(I)  IS THE SLOPE OF THE ITH CURVE
C  U(I) IS THE PROBE VELOCITY FOR THE ITH CURVE
C  DEN(I)  IS YHE DENSITY  FOR THE ITH CURVE
      DIMENSION     DEN1(30)
      DIMENSION     DEN2(30)
      DIMENSION  DL(30)
      DIMENSION  H(30)
      DIMENSION   U(30)
      DIMENSION   DEN(30)
      DIMENSION   SLOPE(30)
      DIMENSION TEL(30)
      READ    (5,30)   GAMMA, R,  U0,  H1 ,  FN,  FM
      WRITE   (6,30)   GAMMA, R,  U0,  H1, FN,  FM
   30 FORMAT    (6F12.5)
      READ    (5,3)      SLOPE
      WRITE   (6,3)      SLOPE
      READ    (5,3)    H
      WRITE   (6,3)    H
      READ    (5,3)    DEN
      WRITE   (6,3)    DEN
      READ     (5,3)    DEN1
      WRITE    (6,3)    DEN1
      READ    (5,3)    DL
      WRITE   (6,3)    DL
      READ    (5,3)   TEL
      WRITE   (6,3)   TEL
    3 FORMAT      (5E12.5/5E12.5)
      DT=25.0
      N=FN
      M=FM
      EM=9.1E-31
      ECH=1.6E-19
      BK=1.38E-23
      PI=3.14159
      SPI=SQRT(PI)
      PI2=SQRT(PI)/2.0
      S2=SQRT(2.0)
      HM=1.67E-27
      OM=HM*16.0
      HE=6.378E+6
      H0=HE+H1
      AR= 2.0*PI*R*R
      DV=0.5
      V01=SQRT(2.0*BK/OM)
      V02=V01/S2
      V03=SQRT(BK/(2.0*PI*OM))
      DO  14  I=1,N
      DEN1(I)=DEN1(I)*DEN(I)
      DEN2(I)=DEN(I)-DEN1(I)
      H(I)=H(I)+HE
      G=9.8*(HE/H0)*(HE/H0)
      SQ=      2.0*G*H0*(H0/H(I)-1.0)+U0*U0
      U(I)=SQRT(SQ)
   14 CONTINUE
```

```
      DO  32  I=1,N
      TE=TEL(I)
      Y1=PL(I)
      WRITE  (6,35)     U(I)
   35 FORMAT     (3H U=,E12.5)
      V=2.0
      DO  36  IJ=1,1
      WRITE   (6,37)  V
   37 FORMAT     (24H PRCBE TO PLASMA POT IS=,E12.5)
      T=100.0
      DO  33   J=1,M
      ST=SQRT(T)
      GA=U(I)/(V01*ST)
      GB=U(I)/(V02*ST)
      A    =0.689/(Y1**1.33)
      B    =(1.66/0.689)*(Y1**0.667)
      PSI    =   (ECH*V)/(BK*T)
      PSII   =   (ECH*V)/(BK*TE)
      PSI1      =SQRT(PSI)
      PSII1     =SQRT(PSII)
      AL   =1.0/(A    *(PSII   +B    *PSII1   ))
      BL=AL
      A8    =A    *(1.0+B    /(2.0*PSII1   ) )
      B8=A8
      X    =SQRT(AL    *PSI    )
      A9    =(ERF(X    +GA   )-ERF(X    -GA   ))
      B9    =(ERF(X    +GB   )-ERF(X    -GB   ))
      A11    =EXP(-PSI    *AL    )
      AA=(1.0/AL    )+1.0
      C1    =(PI2*(1.0+2.0*GA    *GA    )*ERF(GA    )+GA    *EXP(-GA    *GA    ))*AA
      C2    =(PI2*(1.0+2.0*GB    *GB    )*ERF(GB    )+GB    *EXP(-GB    *GB    ))*AA
      A3    =PI2*(0.5+GA   *GA    -X    *X    )*A9
      B3    =PI2*(0.5+GB   *GB    -X    *X    )*B9
      A1    =0.5*(X    +GA   )*EXP(-(X    -GA   )**2)
      B1    =0.5*(X    +GB   )*EXP(-(X    -GB   )**2)
      A2    =0.5*(X    -GA   )*EXP(-(X    +GA   )**2)
      B2    =0.5*(X    -GB   )*EXP(-(X    +GB   )**2)
      F     =A3    +A1    -A2
      W     =B3    +B1    -B2
      A5    =F    /AL
      B5    =W    /BL
      CA   =(C1       -A5       )/(2.0*GA    )
      CB   =(C2       -B5       )/(2.0*GB    )
      A7    =(C1    /AA)-F
      B7    =(C2    /AA)-W
      A10    =(1.0-X    *X    *A8    )*A9    *PI2
      B10    =(1.0-X    *X    *B8    )*B9    *PI2
      D1DV    =(A8    *A7    +A10    )/(2.0*GA    )
      D2DV    =(B8    *B7    +B10    )/(2.0*GB    )
      AC=DEN1(I)*ECH*ECH*V03
      AC1=DEN2(I)*ECH*ECH*V03/S2
      D01=(AC /(ST*BK))*D1DV
      D02=(AC1/(ST*BK))*D2DV
      D01=D01*AR/GAMMA
      D02=D02*AR/GAMMA
      DOT=D01+D02
```

```
   V04=V01*ST
   WRITE  (6,34)   DC1,  D02 , T    , V04,  DOT
34 FORMAT   (E12.5,  E12.5,  E12.5,  E12.5,  E12.5)
   T=T+DT
33 CONTINUE
   V=V+DV
36 CONTINUE
32 CONTINUE
   WRITE  (6,3)    U
   WRITE   (6,3)   DEN2
   STOP
   END
```

VITA

Name: Frank Tsung-chien Huang

Permanent Address: 9206 Springhill Lane, Greenbelt, Maryland

Degree and Date to be conferred: Doctor of Philosophy, 1970

Date of Birth: July 18, 1941

Place of Birth: Peking, China

Secondary Education: Forest Hills High School, New York, New York, 1958

Collegiate Institutions Attended	Dates	Degree	Date of Degree
Brandeis University, Waltham Massachusetts	1958-1962	B.A.	1962
University of Maryland, College Park, Maryland	1962-1970	Ph.D.	1970

Major: Physics

Minor: Astronomy

Publications: "Ionospheric Parameters from Langmuir Probes," with R. T. Bettinger, AGU Transactions, 50 (4), 271 (April 1969)

Positions Held: Research Assistant, Department of Physics and Astronomy University of Maryland, 1964 - Present

Teaching Assistant, Department of Physics and Astronomy, University of Maryland, 1962 - 1964.